

**NAVAL POSTGRADUATE SCHOOL**  
**Monterey, California**



**THESIS**

**A MODELING STUDY OF THE COASTAL  
EASTERN BOUNDARY CURRENT SYSTEM OFF  
IBERIA AND MOROCCO**

by

Johnny R. Martinez

March 1999

Thesis Advisor:

Mary L. Batteen

**Approved for public release; distribution is unlimited.**

DTIC QUALITY INSPECTED 4

19990419 059

# REPORT DOCUMENTATION PAGE

Form Approved OMB No. 0704-0188

Public reporting burden for this collection of information is estimated to average 1 hour per response, including the time for reviewing instruction, searching existing data sources, gathering and maintaining the data needed, and completing and reviewing the collection of information. Send comments regarding this burden estimate or any other aspect of this collection of information, including suggestions for reducing this burden, to Washington Headquarters Services, Directorate for Information Operations and Reports, 1215 Jefferson Davis Highway, Suite 1204, Arlington, VA 22202-4302, and to the Office of Management and Budget, Paperwork Reduction Project (0704-0188) Washington DC 20503.

1. AGENCY USE ONLY (Leave blank)	2. REPORT DATE March 1999	3. REPORT TYPE AND DATES COVERED Master's Thesis	
4. TITLE AND SUBTITLE Title A Modeling Study Of the Coastal Eastern Boundary Current System Off Iberia and Morocco		5. FUNDING NUMBERS	
6. AUTHOR(S) Johnny R. Martinez		8. PERFORMING ORGANIZATION REPORT NUMBER N/A	
7. PERFORMING ORGANIZATION NAME(S) AND ADDRESS(ES) Naval Postgraduate School Monterey, CA 93943-5000		10. SPONSORING/MONITORING AGENCY REPORT NUMBER	
9. SPONSORING/MONITORING AGENCY NAME(S) AND ADDRESS(ES) Office of Naval Research 800 N. Quincy Street, Arlington, VA 22217		11. SUPPLEMENTARY NOTES The views expressed in this thesis are those of the author and do not reflect the official policy or position of the Department of Defense or the U.S. Government.	
12a. DISTRIBUTION/AVAILABILITY STATEMENT Approved for public release; distribution is unlimited.		12b. DISTRIBUTION CODE	
13. ABSTRACT (maximum 200 words) To investigate the northern Canary Current system (NCCS), results from four numerical experiments of increasing complexity are examined. Experiment 1, which uses seasonal wind forcing only, shows that, as expected, wind forcing is the key generative mechanism for the current, upwelling, meander, eddy, and filament structures. Experiments 2 and 3 have the addition of an irregular coastline. These two experiments show that capes are areas for enhanced upwelling, extensive filaments, maximum current velocities, and enhanced growth of cyclonic meanders and eddies. Also, an embayment like the Gulf of Cadiz is a primary region for anticyclonic meander and eddy development. A fourth experiment has the additional effects of thermohaline gradients and Mediterranean Outflow. This complex regime has features similar to NCCS observations, including the generation of Meddies.			
SUBJECT TERMS Canary Current, eastern boundary currents, meanders, eddies, filaments, Mediterranean Outflow			15. NUMBER OF PAGES 98
17. SECURITY CLASSIFICATION OF REPORT Unclassified			16. PRICE CODE
18. SECURITY CLASSIFICATION OF THIS PAGE Unclassified	19. SECURITY CLASSIFICATION OF ABSTRACT Unclassified	20. LIMITATION OF ABSTRACT UL	



Approved for public release; distribution is unlimited.

**A MODELING STUDY OF THE COASTAL EASTERN BOUNDARY  
CURRENT SYSTEM OFF IBERIA AND MOROCCO**

Johnny R. Martinez  
Lieutenant, United States Navy  
B.S., University of New Mexico, 1992

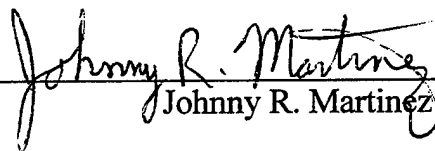
Submitted in partial fulfillment  
of the requirements for the degree of

**MASTER OF SCIENCE IN PHYSICAL OCEANOGRAPHY**

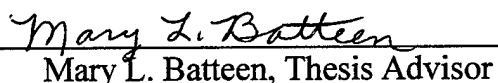
from the

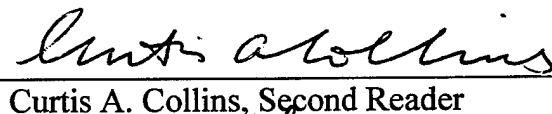
**NAVAL POSTGRADUATE SCHOOL  
March 1999**

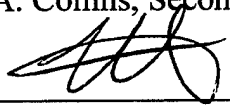
Author:

  
\_\_\_\_\_  
Johnny R. Martinez

Approved by:

  
\_\_\_\_\_  
Mary L. Batteen, Thesis Advisor

  
\_\_\_\_\_  
Curtis A. Collins, Second Reader

  
\_\_\_\_\_  
Roland W. Garwood, Chairman  
Department of Oceanography



## ABSTRACT

To investigate the northern Canary Current system (NCCS), results from four numerical experiments of increasing complexity are examined. Experiment 1, which uses seasonal wind forcing only, shows that, as expected, wind forcing is the key generative mechanism for the current, upwelling, meander, eddy, and filament structures. Experiments 2 and 3 have the addition of an irregular coastline. These two experiments show that capes are areas for enhanced upwelling, extensive filaments, maximum current velocities, and enhanced growth of cyclonic meanders and eddies. Also, an embayment like the Gulf of Cadiz is a primary region for anticyclonic meander and eddy development. A fourth experiment has the additional effects of thermohaline gradients and Mediterranean Outflow. This complex regime has features similar to NCCS observations, including the generation of Meddies.



## TABLE OF CONTENTS

I.	INTRODUCTION.....	1
II.	MODEL DESCRIPTION.....	5
	A. MODEL EQUATIONS.....	5
	B. FORCING CONDITIONS AND EXPERIMENTAL DESIGN.....	7
III.	RESULTS FROM THE WIND-FORCED MODEL SIMULATIONS.....	11
	A. EXPERIMENT 1 – EFFECTS OF STRAIGHT COASTLINE GEOMETRY	
	1. Spin-up Phase.....	11
	2. Quasi-equilibrium Phase.....	13
	B. EXPERIMENT 2 – EFFECTS OF IDEALIZED IRREGULAR COASTLINE GEOMETRY	
	1. Spin-up Phase.....	14
	2. Quasi-equilibrium Phase.....	15
	C. EXPERIMENT 3 – EFFECTS OF REALISTIC IRREGULAR COASTLINE GEOMETRY	
	1. Spin-up Phase.....	16
	2. Quasi-equilibrium Phase.....	17



D. EXPERIMENT 4 - ADDITIONAL EFFECTS OF THERMOHALINE FORCING AND MEDITERRANEAN OUTFLOW

- 1. Spin-up Phase.....19
- 2. Quasi-equilibrium Phase.....20
- 3. Comparison of Model Results with Observations.....21

IV. SUMMARY.....25

LIST OF REFERENCES.....75

INITIAL DISTRIBUTION LIST.....81

## LIST OF FIGURES

1. The model domain for the northern Canary Current system (NCCS) is bounded by 30°N to 42.5 N, 5 W to 17.5 W. The cross-shore (alongshore) resolution is 9 km (11 km). Geographic locations and prominent features are labeled.....27
2. Climatological (1980-1989) ECMWF winds in m/s for: (a) February, (b), July, (c) September, and (d) November. Maximum wind vector is 10 m/s.....28
3. Times series plots of monthly temperature and salinity fields used as seasonal forcing in the basic simulation. The '\*' symbol represents data at 30° N, 17.5° W, while the '+' symbol represents data at 42.5° N, 17.5° W for 30 m depth.....33
4. Temperature contours and velocity vectors for Experiment 1 at 30 m depth at days (a) 210, (b) 270, (c) 330 and (d) 621. The contour interval is 1°C. To avoid clutter, the velocity vectors are plotted every third grid point in the cross-shore direction and every fourth grid point in the along-shore direction. Maximum current velocity is 100 cm/s.....34
5. Cross-shore sections of meridional velocity (v) for Experiment 1 on day 210 at 35.5 ° N. Solid lines indicate poleward flow, while dashed lines indicate equatorward flow. The contour interval is 2.5 cm/s for poleward flow and 5 cm/s for equatorward flow.....38
6. Temperature contours (a,b) and velocity vectors (a-c) at 30 m depth in the third year of Experiment 1 of the model simulation time-averaged over the months of (a) April, (b) August, (c) December. The contour interval is 1° C. Maximum current velocity is 100 cm/s.....39
7. Time-averaged plots (Experiment 1) for the peak upwelling season (July-September) of a cross-shore section of mean meridional velocity(v) in (a) at 38° N, and velocity vectors (b) at 1226 m. In (a) solid lines indicate poleward flow, while dashed lines indicate equatorward flow. The contour interval for poleward flow is 2.5 cm/s. The contour interval for equatorward flow is 5 cm/s in (a). The maximum current velocity is 20 cm/s in (b).....42
8. Temperature contours and velocity vectors for Experiment 2 at 30 m depth at day 270. Maximum current velocity is 100 cm/sec.....44
9. Time-averaged plots (Experiment 2) of temperature (b) and velocity vectors (a-c) at 30m in the third year for April (a), August (b), December (c). The contour interval is 1° C. The maximum current velocity is 100 cm/s.....45

10. Temperature contours and velocity vectors for Experiment 3 at 30 m depth at days (a) 210 and (b) 285. The contour interval is 1°C. Maximum current velocity is 100 cm/s. The abbreviations used to denote the different capes are as follows: CR (Cabo da Roca), CS (Cabo de Sines), CSV (Cabo de Sao Vincente), CSM (Cabo de Santa Maria, CB (Cape Beddouzza), CG (Cape Ghir).....48
11. Cross-shore sections of meridional velocity (v) for Experiment 3 on day 240 at 39.5° N (a) and at 35.5° N (b). Solid lines indicate poleward flow, while dashed lines indicate equatorward flow. The contour interval is 2.5 cm/s for poleward flow and 5 cm/s for equator ward flow.....50
12. Time-averaged plot of temperature contours and velocity vectors for Experiment 3 at 30 m in the third year for August. The contour interval is 1° C. The maximum current velocity is 100 cm/s.....52
13. Time-averaged plots (Experiment 3) for cross-shore sections of mean meridional flow velocity in August at 37.5° N (a) and in January at 39.4° N (b). Solid lines indicate poleward, while dashed lines indicate equatorward flow. The contour interval is 2.5 cm/s for poleward flow and 5 cm/s for equatorward flow.....53
14. Temperature contours (a,b) and velocity vectors (a-c) for Experiment 4 at 30 m depth on day (a) 30, (b) 255, (c) 363. The contour interval is 1° C. Maximum velocity is 100 cm/s in (a,b) and 20 cm/s in (c).....55
15. Cross-shore sections of meridional velocity (v) (a-b) and salinity (S) (c) for Experiment 4 on day 210 at 37.5° N (a), and on day 363 at 41.5° N (b-c). The contour interval for v is 2.5 cm/s for the poleward flow in (a,b), and 5 cm/s for equatorward flow in (a) and 2 cm/s in (b). The contour interval for S is 0.01 (0.05) above (below) 1400 m depth.....58
16. Time-averaged plot of temperature contours and velocity vectors for Experiment 4 at 30 m in the third year for August. The contour interval is 1° C. The maximum current velocity is 100 cm/s.....61
17. Time-averaged plot for Experiment 4 of cross-shore sections of meridional velocity (v) in the third year for December. The contour interval is 2.5 cm/s for poleward flow and 1 cm/s for equatorward flow.....62

18. Cross-shore sections for Experiment 4 for day 999 (end of September) at 38° N of meridional velocity ( $v$ ) (a), and salinity ( $S$ ) (b). The contour interval for  $v$  is 1 cm/s for poleward flow and 5 cm/s for equatorward flow. The contour interval for  $S$  is 0.01 (0.05) above (below) 1300 m depth.....63
  
19. Time-averaged plots of velocity vectors for Experiment 4 at 1226 m depth in the third year of the model for September (a) and November (b). Maximum current velocity is 20 cm/s.....65
  
20. Cross-shore sections for Experiment 4 on day 1059 (end of November) at 36° N of meridional velocity ( $v$ ) (a), temperature ( $T$ ) (b), and salinity ( $S$ ) (c). The contour interval is 2.5 cm/s for poleward flow and 5 cm/s for equatorward flow. The contour interval for  $T$  is 0.1 (1.0) above (below) 600 m depth. The contour interval for  $S$  is 0.01 (0.05) above (below) 1300 m depth.....67



## LIST OF TABLES

1. Summary of specific experimental design.....	71
2. Values of Constants Used in the Model.....	72
3. Salinity profiles .....	73



## ACKNOWLEDGEMENT

I would like to thank Dr. Mary L. Batteen, my advisor, for her outstanding professional guidance, considerable knowledge, and patience which made this study possible. Thanks to Pete Braccio and Mike Cook for FORTRAN, FERRET and MATLAB assistance. Special thanks to Dr. Curtis Collins for the advice he provided as second reader.

I would like to thank my wife, Lori, and son, Aaron, for their support. Their understanding allowed me to pursue and meet my educational goals at the Naval Postgraduate School. Finally, I would like to thank my dad for teaching me at a young age the importance of getting an education. Thanks to all.





## I. INTRODUCTION

The eastern boundary current (EBC) system off the coasts of Iberia and Morocco is on the northern fringe of the Canary Current coastal upwelling system, which starts at  $\sim 10^\circ$  N, south of Dakar (Parrish *et al.*, 1981; Bakun and Nelson 1991). Like other EBCs, the mean Canary Current (CC) is a broad ( $\sim 1000$  km), relatively slow ( $\sim 10$ - $30$  cm/s), equatorward, yearlong surface flow extending to an average depth of  $\sim 500$  m (Wooster *et al.*, 1976). The portion of the CC which lies off the Iberian west coast is sometimes called the Portugal Current (e.g., Tomczak and Godfrey, 1994).

Below  $\sim 100$ - $300$  m depth near the coast, a poleward undercurrent is present (e.g., Meincke *et al.*, 1975; Fiuza 1982). In winter the undercurrent shoals to the north, occasionally reaching the surface, to form a third flow component. This current, known as the Iberian Current (Haynes and Barton, 1990), is a narrow ( $\sim 25$ - $40$  km), relatively weak (less than  $\sim 20$  cm/s) coastal, seasonal surface poleward current (Fiuza, 1982; Frouin *et al.*, 1990; Haynes and Barton, 1990). Geographically, the Iberian Current is usually found north of Cabo da Roca (see Figure 1 for locations), but it has also been seen as far south as Cabo de Sao Vincente.

Off Portugal the undercurrent can transport water from the Mediterranean Sea between  $\sim 500$  and  $1500$  m depth, and water from a subtropical origin in the upper layers (Fiuza, 1982). Off the southwestern coast of Portugal, the water from the Mediterranean Sea can be as shallow as  $\sim 300$  m depth (Ambar, 1982).

Ambar and Howe (1979) and Ambar (1982) have documented the separation of the Mediterranean Outflow (MO) into two distinct cores at  $\sim 7^\circ$  W: a shallow core above  $\sim 900$  m depth and a deeper core at  $\sim 1200$  m depth. Both cores flow westward along the northern coast of the Gulf of Cadiz and turn poleward around Cabo de Sao Vincente. A third shallower (above  $\sim 700$  m depth) core of MO (distinct from the two main cores) has been traced from the vicinity of the Strait of Gibraltar northward to  $\sim 38.5^\circ$  N, off western Portugal, following the coast of Iberia (Ambar, 1982).

The northern Canary Current system (NCCS) is influenced predominantly by equatorward, upwelling favorable winds produced by the Azores High. As described in Nelson (1977), the Azores High, located in the northern part of the Atlantic Ocean, is a semi-permanent subtropical high pressure system similar in nature and behavior to the North Pacific Subtropical High. The center of the Azores High migrates meridionally with the seasons, reaching  $\sim 27^\circ$  N, its southernmost extent, in March and ridging north to  $\sim 33^\circ$  N by August. This migration causes maximum wind stress values that vary temporally at given locations. The summer mean east-west pressure contrast between Portugal and the center of the Azores High is  $\sim 8$  mb; however, in the winter, the contrast weakens to  $\sim 1$  mb. This pressure difference results in considerably stronger northerly to northwesterly winds during the summer. In the winter the winds become weaker northwesterly to even slight southerly winds off Iberia. The shift of maximum wind stress also causes the upwelling favorable winds to shift from  $\sim 27^\circ$  N near the Canary Islands in January, to  $\sim 43^\circ$  N off Iberia by July (Fiuza, 1982).

Recent observations have shown highly energetic, mesoscale features such as jet-like surface currents, meanders, eddies, and filaments superimposed on the broad, climatological mean flow of the CC and other EBCs. Satellite images of sea surface temperatures have shown several filaments extending off Portugal's coast and northwest Spain (Fiuza and Sousa, 1989), as well as off Cape Ghir in northwest Africa (Van Camp *et al.*, 1991; Hagen *et al.*, 1996). Other observations have also shown anticyclonic and cyclonic pairs of mesoscale eddies on the order of 100 km off the coast of Iberia (Fiuza, 1984). These features have been observed during periods of predominantly equatorward, upwelling favorable winds and seem to be located near prominent coastline features such as capes. These observations provide evidence that wind forcing and coastline irregularities could be important mechanisms in the formation and sustainment of many of the mesoscale features found in EBC regions.

Over the past few decades numerous wind forcing models of EBCs have been conducted, particularly for the California Current system, the classical EBC system. Early studies included steady wind stress (Pedlosky, 1974) and transient wind forcing (Philander and Yoon, 1982). The response of reduced gravity models to realistic coastal

winds was investigated by Carton (1984) and Carton and Philander (1984). A series of experiments were also conducted by McCreary *et al.* (1987) using a linear model with both transient and steady wind forcing in the California Current system. These previous models produced weak currents (5-10 cm/s) and no eddies or filaments developed.

In the last decade, modeling studies have focused on the driving mechanisms of complex features, such as filaments and eddies observed in EBC regions. While Ikeda *et al.* (1984a, b) and Haidvogel *et al.* (1991) studied baroclinic and barotropic instability, coastline irregularities, and bottom topography as possible mechanisms, Batteen *et al.* (1989), McCreary *et al.* (1991), Pares-Sierra *et al.* (1993), and Batteen (1997) studied wind forcing as a possible generative mechanism. Recently, Batteen (1997) used a multilevel primitive equation (PE) model of the California Current system from 35° N to 47.5° N to study the effects of seasonal winds and coastline irregularities. Batteen and Vance (1998) studied the additional effects of thermohaline gradients. In a more recent study Batteen *et al.* (1998) studied the contribution of seasonal wind forcing, thermohaline gradients and irregular coastline geometry to the generation of eddies and filaments for the entire California Current system (22.5° N to 47.5° N). The results showed that wind forcing was the dominant process responsible for many of the observed features of the California Current system.

In contrast to the California Current system, coastal modeling studies of the NCCS have been scarce. McClain *et al.* (1986) performed the first limited modeling study in the region, using ship-derived winds to produce a large negative wind stress curl off the northwest coast of Iberia. This resulted in opposing equatorward and poleward surface currents. Batteen *et al.* (1992) used an eddy resolving PE model with both uniform and variable wind stress, the latter computed from synoptic surface pressure analyses, to produce realistic currents as well as mesoscale eddies. Both studies, however, only covered a limited region of the NCCS (i.e., the northwest coast of Iberia) and had a straight coast in their model domains.

While the predominantly wind-driven NCCS would be expected to produce similar features as in a classical EBC system, the NCCS has several distinguishing EBC features. It has the unique geographical feature of the relatively large embayment known

as the Gulf of Cadiz. It also has the MO, which spreads saltier waters outward from the Gulf of Cadiz, and is a source region for Meddies.

The objective of this process-oriented study is to use a multilevel PE model to investigate the roles of classical as well as unique features in the NCCS. Toward this end, results from several numerical experiments of increasing complexity (see Table 1) are systematically examined. The results of a classical wind-driven EBC system along a straight coastline are first presented in Experiment 1. The additional effects of irregular coastline geometry, which includes the Gulf of Cadiz and coastline promontories, such as capes, are presented in Experiments 2 and 3. Lastly, in Experiment 4, the additional effects of thermohaline gradients and the MO are explored.

## II. MODEL DESCRIPTION

### A. MODEL EQUATIONS

This study uses the eddy-resolving, limited-area EBC model of Batteen (1997) with open northern, western, and southern boundaries. The model is multi-level, uses non-adiabatic primitive equations on a beta-plane, and has both baroclinic and barotropic velocity components. It is based on the hydrostatic, Boussinesq, and rigid lid approximations. Equations governing the model are as follows:

$$\frac{du}{dt} = \frac{-1}{\rho_0} \frac{\partial p}{\partial x} + fv - A_M \nabla^4 u + K_M \frac{\partial^2 u}{\partial z^2} \quad (1)$$

$$\frac{dv}{dt} = \frac{-1}{\rho_0} \frac{\partial p}{\partial y} - fu - A_M \nabla^4 v + K_M \frac{\partial^2 v}{\partial z^2} \quad (2)$$

$$\frac{\partial u}{\partial x} + \frac{\partial v}{\partial y} + \frac{\partial w}{\partial z} = 0 \quad (3)$$

$$\frac{\partial p}{\partial z} = -\rho g \quad (4)$$

$$\rho = \rho_0 [1 - \alpha(T - T_0) + \beta(S - S_0)] \quad (5)$$

$$\frac{dT}{dt} = -A_H \nabla^4 T + K_H \frac{\partial^2 T}{\partial z^2} \quad (6)$$

$$\frac{dS}{dt} = -A_H \nabla^4 S + K_H \frac{\partial^2 S}{\partial z^2} \quad (7)$$

In the above equations,  $t$  is time,  $T$  is temperature,  $S$  is salinity,  $\rho$  is density, and  $p$  is pressure. A right-handed Cartesian coordinate system  $(x, y, z)$  is used where  $x$  points toward shore,  $y$  alongshore, and  $z$  upward. The corresponding velocity components are  $(u, v, w)$ . Table 2 provides a list of symbols found in the model equations, as well as values of constants used throughout the study.

A space-staggered B-scheme (Arakawa and Lamb, 1977) is used for the horizontal finite differencing. Batteen and Han (1981) have shown this scheme to be appropriate when the grid spacing is approximately on the same order as, or less than, the Rossby radius of deformation. The horizontal grid spacing is 9 km in the east-west direction and

11 km in the north-south direction, while the internal Rossby radius of deformation is ~30 km. The model uses ten vertical layers, with constant z-levels, at depths of 10, 30, 75, 150, 250, 400, 600, 1226, 2283, and 3656 m. This vertical spacing scheme of the model concentrates more layers above the thermocline, which is in the dynamically active portion of the ocean.

The model domain (Figure 1) encompasses the west coasts of Iberia and Morocco, from 30° N to 42.5° N (1408 km alongshore), and from 5° W to 17.5° W (1152 km cross-shore). The coastal boundaries of the model domain are closed, and have both the tangential and normal components of velocity set to zero. Bottom topography has been omitted to focus on the roles of climatological wind forcing, thermohaline gradients, and of the MO. The eastern boundary is modeled as a vertical wall. The constant depth used in the model is 4500 m.

The northern, southern, and western borders are open boundaries, which use a modified version of the radiation boundary conditions of Camerlengo and O'Brien (1980). Biharmonic lateral heat and momentum diffusion is used in the model with the same choice of coefficients (i.e.,  $2.0 \times 10^{17} \text{ cm}^4/\text{s}$ ) as in Batteen (1997). Holland (1978) showed that highly scale-selective biharmonic diffusion acts predominantly on submesoscales, while Holland and Batteen (1986) found that baroclinic mesoscale processes can be damped by Laplacian lateral heat diffusion. As a result, the use of biharmonic lateral diffusion should allow mesoscale eddy generation via barotropic (horizontal shear) and/or baroclinic (vertical shear) instability mechanisms. Batteen (1997) used weak ( $0.5 \text{ cm}^2/\text{s}$ ) vertical eddy viscosities and conductivities. Bottom stress is parameterized by a simplified quadratic drag law (Weatherly, 1972), as in Batteen (1997).

The method of solution is straightforward with the rigid lid and flat bottom assumptions because the vertically integrated horizontal velocity is subsequently nondivergent. The vertical mean flow can be described by a streamfunction which can be predicted from the vorticity equation, while the vertical shear currents can be predicted after the vertical mean flow is subtracted from the original equations. The other

variables, i.e. temperature, density, salinity, vertical velocity, and pressure, can be explicitly obtained from the thermodynamic energy equation (6), equation of state (5), salinity equation (7), continuity equation (3), and hydrostatic equation (4), respectively (For more complete details on the method of solution, see Batteen, 1997).

## **B. FORCING CONDITIONS AND EXPERIMENTAL DESIGN**

To explain the effects of seasonal wind, the model is forced from rest with climatological wind fields from a  $2.5^\circ$  by  $2.5^\circ$  grid of the European Centre for Medium Range Weather Forecasts (ECMWF) near-surface wind analyses (Trenberth et al., 1990). The monthly mean stresses based on twice daily wind analyses from 1980-1989 have been interpolated spatially to the 9 by 11 km model resolution and temporally to daily wind values. Sample wind fields used can be seen in Figure 2, which shows the annual migration of the Azores Subtropical High from the south in the winter (e.g., Figure 2a) to its most northern extent in the summer (e.g., Figure 2d). The atmospheric pressure pattern for November (not shown) and December (Figure 2a) depicts a low to the north and the Azores High to the south. This results in a wind divergence with weakly poleward winds north of  $\sim 40^\circ$  N and equatorward winds to the south. During January (not shown) and February (Figure 2b) the divergence in the wind field migrates poleward. By March (not shown) and April (Figure 2c) an equatorward component in the wind field is observed along the entire domain. The strongest equatorward winds are discernible from July (not shown) through August (Figure 2d). In September (not shown) and October (Figure 2e) the winds start to weaken throughout the domain, and divergence in the wind field is observed in the north by October (Figure 2e). By November (not shown) the wind divergence returns to  $\sim 40^\circ$  N.

Table 1 summarizes the design of the four experiments. Note that in all the experiments the model is forced from rest with seasonal ECMWF winds. The model is then allowed to reach a quasi-equilibrium state by running each experiment for three years.



As Table 1 shows, in Experiment 1, to isolate the response to seasonal wind forcing from coastline variations, a straight coastline is used throughout the entire domain (e.g., see Figure 4a from Experiment 1). The initial mean stratification used are annual climatological temperature fields based on Levitus and Boyer (1994). The temperatures ( $^{\circ}\text{C}$ ) used for the ten levels from the surface to 4500 m are 17.5, 17.3, 16.5, 15.0, 13.7, 12.5, 11.0, 8.52, 3.59, and 2.09, respectively, while a salinity constant of 34.7 is used for all levels.

To examine the additional effects of irregular coastline geometry, two additional cases are run. In Experiment 2 an idealized “straightened” coastline is used with two prominent capes (i.e., Cabo de Sao Vicente and Cape Ghir), and an embayment representing the Gulf of Cadiz (e.g., see Figure 8 from Experiment 2). In Experiment 3, a coastline with extensive coastline irregularities (e.g., see Figure 10a from Experiment 3) is used to investigate the additional effects of more realistic capes on the formation and sustainment of the features found in the NCCS.

Finally, in Experiment 4, the additional effects of the MO and of thermohaline gradients on the NCCS are explored. The salinity at each level for the MO is input as a constant value for five grid points at  $\sim 36^{\circ}\text{N}$  every time step with the values given in Table 3 (from Levitus *et al.*, 1994).

Seasonal temperature and salinity climatological conditions for the upper seven levels from Levitus and Boyer (1994) and from Levitus *et al.* (1994) are used to initialize the model, and, every third day, to force the model at the western boundary at  $17.0^{\circ}\text{W}$ . The seasonal temperature and salinity forcing conditions, which are initially assumed to be zonally homogeneous, are shown for one of the seven levels in Figure 3 for the northern ( $42.5^{\circ}\text{N}$ ) and southern ( $30^{\circ}\text{N}$ ) boundaries of the model domain. Since the lower three levels do not exhibit much horizontal variation, they are assumed to be constant for each level. The temperature values used for levels 8-10 are  $8.52^{\circ}\text{C}$ ,  $3.59^{\circ}\text{C}$ , and  $2.09^{\circ}\text{C}$ . The salinity constant used for the lower three levels is 34.7 psu.

While the temperatures to the south are warmer than those to the north above 1000m depth, only the upper level temperature conditions (e.g., Figure 3) show significant seasonal variability with a temperature maximum in September and a

temperature minimum in February throughout the whole region. Below around 150m depth (not shown), both the seasonal temperature fluctuations and the temperature gradient weaken, as expected. In contrast, the salinity conditions above 1000m (e.g., Figure 3), which in the upper levels show less (more) saline water to the north (south), have no significant seasonal cycle.



### III. RESULTS FROM THE WIND-FORCED MODEL SIMULATIONS

#### A. EXPERIMENT 1 – EFFECTS OF STRAIGHT COASTLINE GEOMETRY

##### 1. Spin-up Phase

In response to the predominantly equatorward winds over the model domain, a coastal equatorward surface current develops. The current develops initially in the southern end of the domain in response to the stronger equatorward winds associated with the southerly position of the Azores High. By summer (e.g., Figure 4a) there is generally equatorward flow throughout the domain. In addition, a poleward undercurrent has also developed, initially, in the southern end of the domain and then extending along the entire coast (not shown).

A cross-section of meridional velocity (e.g., Figure 5) shows the typical vertical structure of the equatorward coastal jet and poleward undercurrent during the upwelling season. The coastal jet core remains within  $\sim 50$  km of the coast and extends from  $\sim 200$  m depth near the coast to  $\sim 300 - 600$  m depth offshore. The core velocities range from  $\sim 30 - 40$  cm/s. Below the equatorward jet, a weaker undercurrent with a core velocity of  $\sim 5$  cm/s at 600 m depth is also seen. The offshore extent of the undercurrent core is confined to  $\sim 50$  km off the coast. Typical core velocities for the undercurrent range from  $\sim 3$  to 10 cm/s.

As the wind becomes equatorward over the entire domain and increases in intensity, increased stress is exerted on the ocean surface creating Ekman transport offshore. This results in upwelling of cooler water along the coast. In the spring the upwelling is confined to the south where the stronger winds exist, while in summer, it is present all along the coast (e.g., Figure 4a).

As the coastal jet and undercurrent become fully established (for example, see Figure 5, which shows the structure of the currents just prior to meander formation), the currents become unstable, due to strong vertical and horizontal shear instabilities between

the equatorward jet and poleward undercurrent, and form meanders. This first occurs in the equatorward end of the model domain where there has been more time for the strong equatorward winds to act on the ocean surface. As the meanders intensify, cold, upwelling filaments and eddies develop (e.g., Figure 4b). These eddies are predominantly cold core and cyclonic,  $O(100 \text{ km})$  in diameter, and extend  $\sim 50 - 150 \text{ km}$  from the coast. Throughout the summer, which corresponds to the period of maximum equatorward wind stress (e.g., Figure 2d), meanders, filaments, and eddies continue to develop equatorward of  $\sim 37^\circ \text{ N}$ .

In the fall, the currents begin to weaken with the slacking winds. The upwelling also ends, first in the poleward end of the domain and then progressively equatorward until by  $\sim$  day 330 all upwelling has ceased. By day 315 a surface coastal poleward current appears north of  $\sim 38^\circ \text{ N}$  in response to the weak poleward winds present off the northwestern coast of Portugal in November and December. The current persists in the northern portion of the domain throughout the winter (e.g., Figure 4c). South of  $\sim 38^\circ \text{ N}$ , the equatorward surface current, embedded with cyclonic eddies, has taken the form of a meandering jet (e.g., Figure 4c), which continues to meander downstream throughout the winter.

During the second year, in the spring, with the return of the Azores High along the west coast, upwelling of cooler water along the coast redevelops (not shown). Throughout the upwelling season, cold, upwelling filaments develop inshore of cyclonic meanders of the equatorward jet (e.g., Figure 4d). Cold, cyclonic eddies also tend to form offshore of the filaments, while warm, anticyclonic eddies tend to develop downstream of the filaments in regions where the equatorward jet meanders anticyclonically (e.g., Figure 4d shows an anticyclonic eddy centered at  $\sim 13^\circ \text{ W}$ ,  $\sim 33.5^\circ \text{ N}$ ). In the fall, as expected, the filaments and cold, upwelled water near the coast disappear. A surface poleward current reappears in the poleward end of the model domain, while to the south, the meandering, equatorward jet, embedded with eddies, persists throughout the fall and winter.

## 2. Quasi-equilibrium Phase

By year three, the system has reached a quasi-equilibrium state. To see the seasonal structures of the features of the NCCS, the model output fields are time-averaged every month.

In the spring (e.g., Figure 6a), a relatively strong (~20-30 cm/s) coastal, equatorward current develops. In addition a relatively strong (~35 cm/s) equatorward jet is present ~200-250 km off the coast. Both the equatorward current and jet meander downstream until ~37° N where they join offshore of a cyclonic eddy to the south. Both the current and jet continue to meander downstream. Both cyclonic and anticyclonic eddies of O(100 km) diameter are discernible both offshore and inshore of the meandering current and jet.

In summer (e.g., Figure 6b), upwelling of cooler water is present all along the coast, and reaches a maximum off Portugal in August. Evidence of cold offshore flowing, upwelling filaments south of ~35° N is also found. There is both a relatively strong coastal equatorward flow present along the coast and an offshore equatorward jet. Below the coastal equatorward current there is a poleward undercurrent (Figure 7a) which is present all along the coast (Figure 7b). The undercurrent meanders within ~100 km of the coast. Offshore of the undercurrent are both cyclonic and anticyclonic eddies of O(100 km) diameter.

By fall (not shown), upwelling has weakened along the entire coast. Winter results (e.g., Figure 6c) show a meandering equatorward surface jet, embedded with eddies, all along the coast.

## B. EXPERIMENT 2 – EFFECTS OF IDEALIZED IRREGULAR COASTLINE GEOMETRY

In Experiment 1, a straight coastline was used. In Experiment 2, to examine the additional effects of irregular coastline geometry, the idealized “straightened” coastline shown in Figure 8 is used with two prominent capes and an embayment (representing the Gulf of Cadiz). All other parameters are the same as in Experiment 1.

### 1. Spin-up Phase

North of the Gulf of Cadiz (i.e., north of  $\sim 37^\circ$  N), the current and temperature patterns in Experiment 2 are expected to show many of the same basic features that exist in Experiment 1. South of  $\sim 37^\circ$  N, the change in coastline orientation from a north-south to an east-west orientation and the presence of the relatively large embayment representing the Gulf of Cadiz, are expected to play significant roles in the generation of meanders and eddies in the NCCS.

As in the spin-up phase in Experiment 1, an equatorward surface current develops first in the south and then in the north as the equatorward wind forcing migrates north with the Azores High. While the upwelling in Experiment 1 develops fairly uniformly along the coast, first in the south and progressively to the north, the upwelling in Experiment 2 is relatively patchy and is most intense in the southern part of the domain (e.g., Figure 8). The upwelling is generally weaker along the south coast of Portugal and the west coast of the Gulf of Cadiz. In addition, a poleward undercurrent (not shown) also develops, initially in the southern end of the domain and then extending along the entire coast. As in Experiment 1, the undercurrent has a typical core speed of  $\sim 5$  cm/s at  $\sim 600$  m depth (not shown).

Once the coastal jet and the undercurrent become fully established, the currents become unstable and form meanders. The meanders and cold, cyclonic eddies in Experiment 2 are generally much more pronounced and more intense than in Experiment 1 (e.g., compare Figures 4b and 8), and can be “anchored” to coastal promontories. Of particular interest is the presence of two cold cyclonic eddies which develop north and

south of the Gulf of Cadiz at coastal promontories. The southern side of the cyclonic eddy (at  $\sim 36.5^\circ$  N,  $9^\circ$  W) on the south coast of Portugal and the northern side of the cyclonic eddy (at  $\sim 34.5^\circ$  N,  $8.5^\circ$  W) entrain the large anticyclonic meander in the Gulf of Cadiz with the result that an anticyclonic eddy develops in the Gulf of Cadiz.

## 2. Quasi-equilibrium Phase

To see the seasonal structures of the features of the NCCS, the model output fields are time-averaged every month. In the spring (e.g., Figure 9a), a relatively strong coastal equatorward jet of  $\sim 25$  cm/s and a weaker offshore ( $\sim 250$  km) equatorward current of  $\sim 10$  cm/s exist off the coast of Portugal. The coastal jet has a meandering pattern. North and south of the Gulf of Cadiz, it meanders cyclonically, while in the Gulf of Cadiz it meanders anticyclonically.

By summer (e.g., Figure 9b), upwelling is present all along the coast and in August reaches a maximum. Beneath the surface (not shown), a core of poleward flow with a speed of  $\sim 5$  cm/s at  $\sim 600$  m depth, is discernible. Since the coastal jet and undercurrent are fully established by summer, the currents become unstable, and form meanders. The coastal jet flows alongshore off Portugal until  $\sim 39^\circ$  N, where it develops a cyclonic meander. Off Cabo de Sao Vincente, the coastal jet veers offshore again to form a second cyclonic meander. The coastal jet then meanders anticyclonically into the Gulf of Cadiz. At  $\sim 34^\circ$  N it forms a third cyclonic meander. The largest meanders and eddies occur to the south in response to the stronger currents. As the strengthened currents flow offshore in the regions of the developed meanders, the current advects cold upwelled water offshore.

In fall (not shown), upwelling has weakened along the entire coast. By winter (Figure 9c), a weak meandering equatorward flow is discernible. Embedded in this flow are numerous jets and relatively large cyclonic and anticyclonic eddies south of Cabo de Sao Vincente.



## C. EXPERIMENT 3 – EFFECTS OF REALISTIC IRREGULAR COASTLINE GEOMETRY

In Experiment 2, an idealized “straightened” coastline was used with two prominent capes (i.e., Cabo de Sao Vicente and Cape Ghir) and an embayment representing the Gulf of Cadiz. In Experiment 3, a more realistic coastline with extensive coastline irregularities (e.g., Figure 10a) is used to investigate the additional effects of more realistic capes on the formation and sustainment of the features found in the NCCS. All other parameters are the same as in Experiments 1 and 2.

### 1. Spin-up Phase

As in the previous experiments, the current and temperature patterns in Experiment 3 show many of the same features. In response to predominantly equatorward winds, a coastal equatorward surface current develops in the southern end of the domain, and by day 60 extends along the entire coast (not shown).

When the Azores High migrates north in the spring, the wind intensifies and transitions to equatorward flow over the entire domain. Upwelling first occurs in the south where the stronger winds exist (not shown). While the upwelling in Experiment 2 was intensified on the west coast in the southern part of the domain (e.g., Figure 8), upwelling in Experiment 3 is also enhanced near prominent capes to the north on the west coast (e.g., off Cabo da Roca in Figure 10a). Since these capes are areas where the alongshore component of the wind stress is at a local maximum, the coastal current velocity is also at a maximum, which leads to enhanced upwelling (Batteen, 1997). In addition, local enhanced upwelling can occur south of Cabo de Sao Vicente and off Cabo de Santa Maria (e.g., Figure 10a), a feature not seen in Experiment 2 with the east-west orientation at  $\sim 37^\circ$  N.

Below the equatorward surface current, a poleward undercurrent develops first at the equatorward end of the domain and then extending all along the coast (not shown). A cross-section of the opposing currents (Figure 11) shows the typical structure of the currents off the west coasts. The coastal jet extends from  $\sim 200$  m depth near the coast to

~600 m depth offshore, and has a peak core velocity of ~35-40 cm/s (Figure 11a). Below the coastal jet along the west coasts of Portugal (e.g., Figure 11a), and Morocco (not shown), the undercurrent develops separate cores: one between ~200-600 m centered at ~400 m depth and one below ~1000 m depth centered at ~1200 m depth. Both cores have peak velocities of ~5-10 cm/s and remain within ~50 km of the coast. Off the west coast of the Gulf of Cadiz below ~400 m depth, there is a single undercurrent core with a peak velocity of ~5 cm/s (Figure 11b). As the coastal jet and the subsurface undercurrent become fully established, the flow becomes both barotropically and baroclinically unstable and leads to the formation of meanders and filaments.

In Experiment 2 the majority of features had no geographical preference, except for the features that appeared tied to the major geographical features depicted in the idealized coastline (e.g., the cyclonic eddy off Cabo de Sao Vicente, the anticyclonic flow through the Gulf of Cadiz, and the large filament off Cape Beddouzza). In contrast, Experiment 3 frequently shows additional eddies and filaments "anchored" off less prominent coastal features (e.g., off Cabo da Roca, Cabo de Santa Maria, and the Cape Beddouzza/Cape Ghir area shown in Figure 10b) that occur along the realistic irregular coastline. In addition, in Experiment 3 upwelling occurs earlier (~2-3 weeks) and with greater intensity off Portugal, where the largest differences occur between the idealized and realistic coastlines (e.g., compare Figure 8 with Figure 10b). Experiment 3 also develops more meanders in the vicinity of the additional capes (which also form earlier than those in Experiment 2). These meanders intensify and develop into predominantly cyclonic cold core eddies, which in time coalesce with other eddies to form larger cyclonic eddies on the order of ~100-300 km. Similar to Experiment 2, by the end of the upwelling season (not shown) the equatorward surface flow has taken the form of a meandering jet embedded with predominantly cyclonic eddies.

## **2. Quasi-equilibrium Phase**

Similar to previous experiments, the model reaches quasi-equilibrium by year three, and shows that most features continue to be generated and maintained. The model results show that in the spring (not shown) there is a mean equatorward jet embedded

with numerous eddies. The jet flows close to the coast off Portugal, but leaves the coast as it impinges on Cabo de Roca. It then continues to meander equatorward. By late April the coastal jet appears off the coast of Morocco and upwelling resumes.

In the summer (e.g., Figure 12) upwelling is visible along the western and southern coasts of Iberia, as well as along the coast of Morocco. Cyclonic and anticyclonic eddies are discernible over the entire domain. As the equatorward jet flows off Portugal, it is deflected offshore by the large capes (e.g., Cabo da Roca and Cabo de Sao Vicente), and advects the cold, upwelled water with it, resulting in the formation of filaments. Maximum upwelling occurs by late summer. Beneath the surface (Figure 13a), cores of poleward flow with speeds of  $\sim 5$ - $7.5$  cm/s at  $\sim 600$  and  $1200$  m depth are discernible. An additional narrow ( $< 20$  km wide) third core of poleward flow at  $\sim 250$  m depth with a speed of  $\sim 5$  cm/s is also seen off Portugal in the vicinity of  $\sim 37.5^\circ$  N (Figure 13a).

In the fall and winter, upwelling has weakened and a meandering equatorward current embedded with westward propagating, cyclonic eddies is discernible (not shown). In response to the weak poleward winds during November and December (Figure 2), a poleward flow develops north of  $\sim 40^\circ$  N (not shown). This flow, which has speeds of  $\sim 20$ - $25$  cm/s and extends to  $\sim 200$  m depth, lasts throughout the winter (e.g., Figure 13b). Beneath the surface cores of poleward flow at  $\sim 600$  and  $\sim 1200$  m depth with speeds of  $\sim 10$ - $17.5$  cm/s depth are also discernible. An additional narrow third core of poleward flow at  $\sim 250$  m depth with a speed of  $\sim 7.5$  cm/s is also shown.

#### **D. EXPERIMENT 4 – ADDITIONAL EFFECTS OF THERMOHALINE FORCING AND MEDITERRANEAN OUTFLOW**

In Experiment 3, a coastline with extensive coastline irregularities was used to investigate the effects of realistic capes. In Experiment 4 the additional effects of thermohaline gradients and of the MO on the NCCS are explored.

## 1. Spin-up Phase

Due to the combination of thermohaline gradients and wind forcing, different oceanic responses are expected depending on the season. As expected, when the temperature decreases poleward (Figure 3), resulting in an increase of density poleward, the pressure gradient due to the temperature (density) gradient establishes an onshore geostrophic inflow from the interior ocean. In the winter (e.g., Figure 14a), in the poleward end of the model domain, the large pressure gradient and poleward wind stress result in onshore geostrophic and Ekman flow. As the flow approaches the coast, it turns and forms a poleward boundary current. In the equatorward end of the model domain, the smaller pressure gradient and equatorward wind stress result in weak onshore geostrophic flow, offshore Ekman flow, and a coastal equatorward surface current.

During the peak upwelling season (July through September), the combination of a weakened pressure gradient and increased equatorward winds over the entire model domain lead to a strengthening of equatorward flow all along the coast and a weakening (strengthening) of onshore (offshore) flow. Upwelling can be seen along the coast, but the coldest water is found near coastal promontories (e.g., off Cape Ghir and Cape Beddouzza in Figure 14b). A typical cross-section (Figure 15a) of the currents shows that there is a surface coastal equatorward jet which extends to ~180 m depth near the coast and ~800 m depth offshore. The surface current is within ~100 km of the coast and has core velocities of ~20-25 cm/s. Below the equatorward current is a poleward undercurrent within ~50 km of the coast which has a core velocity of ~5 cm/s at ~1200 m depth.

In the fall, as expected, the surface poleward flow strengthens in the coastal poleward end of the model domain in response to both the strengthening of the pressure gradient and the return of poleward wind stress in the region. A typical cross-section of the currents in the poleward end of the model domain north of ~41° N (e.g., Figure 15b) shows that the coastal poleward surface current has a core velocity of ~10 cm/s and is within ~100 km of the coast. To the west of the current is the year-round equatorward current with a core velocity of ~25-30 cm/s.

At depth, a relatively narrow (< 50 km wide) coastal equatorward undercurrent is discernible. The undercurrent is within ~30km of the coast, extends from ~400-1000 m depth, and has a core velocity of ~2 cm/s.

The equatorward flow to the west of the poleward undercurrent below ~900 m depth is the inshore branch of an anticyclonic eddy (Figure 14c), which is relatively salty (Figure 15c). It has a core velocity of ~ 3 cm/s at ~ 1200 m depth (not shown), and forms at ~ 41° N on the inshore side of the poleward undercurrent (Figure 14c). Other anticyclonic eddies at ~ 1200 m depth are also discernible in Figure 14c near the coast of Portugal at ~39.5° N, and at ~37.5° N. The salty characteristics of these anticyclonic eddies are consistent with Meddies which have been found at ~1200 m depth in these regions (e.g., Richardson and Tychensky, 1998).

## **2. Quasi-equilibrium Phase**

Longer run times (~3 years) of the model simulation show that while many of the features simulated in the previous experiment are also seen in Experiment 4, there are some notable differences. A comparison of the temperature and currents for Experiments 3 (Figures 12) and Experiment 4 (Figure 16) during the upwelling season show similar results, except for a tighter temperature gradient all along the coast in Experiment 4.

In the winter, in the poleward end of the model domain north of ~41° N, an equatorward undercurrent, a feature not present in previous experiments, is discernible (e.g., Figure 17). This undercurrent is within ~30 km of the coast, extends from ~1000-1800 m depth, and has a core velocity of ~3 cm/s. Consistent with previous experiments, a surface poleward current with a core velocity of ~17.5 cm/s is also present.

To clarify whether the tighter temperature gradient and equatorward undercurrent are due to the effect of thermohaline gradients, or to the MO, or to a combination of the two, a sensitivity experiment was run which was the same as Experiment 4, but without the effect of the MO. Model results (not shown) showed that both features were still present so that these features must be due to onshore geostrophic flow resulting from the alongshore pressure gradient.

Of particular note is the subsurface spreading of MO, which at  $\sim 36^\circ$  N,  $6.5^\circ$  W in the Gulf of Cadiz, splits into two cores, one at  $\sim 600$  m depth and the other at  $\sim 1200$  m depth (not shown), consistent with the observations of Ambar and Howe (1979) and Ambar (1982). The two cores follow the northern coast of the Gulf of Cadiz. When the cores reach Cabo de Sao Vincente, they turn poleward. A cross-section shows that the two deeper cores at 600 and 1200 m depth (Figure 18a) have core velocities of  $\sim 4-7$  cm/s and are relatively salty (Figure 18b) compared to the fresher water above and below the cores (The fresher water with depth is due to the general decrease of salinity with depth in the region).

At  $\sim 38^\circ$  N a third shallower poleward core is also seen with a core velocity of  $\sim 4$  cm/s at  $\sim 400$  m depth (Figure 18a). Meddies occur as regular features in the vicinity of the southwest coast of Portugal. For example, Figure 19a shows Meddies of  $O(100$  km) at  $\sim 1200$  m depth at  $\sim 39^\circ$  N,  $12^\circ$  W and at  $\sim 38^\circ$  N,  $15^\circ$  W.

Meddies are also seen to the west of the Gulf of Cadiz. For example, Figure 19b shows Meddies of  $O(100$  km) at  $\sim 36^\circ$  N,  $11^\circ$  W, and at  $\sim 36^\circ$  N,  $15^\circ$  W. Cross-sections of meridional velocity (Figure 20a) and temperature (Figure 20b) at  $36^\circ$  N illustrate the anticyclonic rotation pattern for the Meddies. The corresponding cross-section of salinity (Figure 20c) shows the relatively salty signature of the Meddies at  $\sim 1200$  m depth.

In time the Meddies move in a predominantly westward direction with a propagation speed of  $\sim 2$  km/day (e.g., compare the position of the Meddies in Figure 19a from September with those in Figure 19b from November). The basic characteristics and speeds of the Meddies off the southwest coast of Portugal and to the west of the Gulf of Cadiz are consistent with the recent observations of Richardson and Tychensky (1998).

### **3. Comparisons of Model Results with Observations**

Since this experiment incorporated the most realistic features of the NCCS, it is useful to qualitatively compare the results of the model simulations with observational data. Since this is an idealized process-oriented study and not a model hindcast, we cannot make direct comparisons with data; however, we can investigate whether the

phenomenological model behavior is qualitatively similar to observational data in the NCCS. Overall, the results of this experiment's complex flow regime highlight the major characteristics of the NCCS with relatively close similarities to field observations.

#### **a. Comparison of Ocean Currents**

The major characteristics of the modeled currents off Portugal and Morocco are consistent with the few available field observations and studies. The model develops a mean, equatorward, yearlong surface flow (i.e., the CC) of ~10-30 cm/s throughout the model domain (e.g., Figure 16), consistent with Wooster and Reid (1963) and observations by DMAH/TC (1988). A surface equatorward jet with a mean velocity of ~20-35 cm/s also develops near the coast.

Below ~200 m depth near the coast, the model establishes a poleward undercurrent, consistent with Meincke *et al.* (1979). Off Iberia, the poleward undercurrent in Experiment 4 was shown to transport salty MO between ~500 and 1300 m depth (e.g., Figure 15c), consistent with Fiuza (1982).

In the experiments with extensive coastline irregularities i.e., Experiments 3 and 4, multiple cores (as many as three) in the undercurrent were generated, particularly off the southwestern coast of Iberia, consistent with the observations of Ambar and Howe (1979) and Ambar (1982). Since there were no multiple cores simulated in Experiments 1 and 2, this suggests that the coastline irregularities can play a role in the development of multiple cores. The simulated areas of the capes off southwestern Iberia were areas of enhanced upwelling (e.g., see Figure 10a for the west and south coasts). Since capes are areas where the alongshore component of the wind stress is at a local maximum, these areas also have maximum surface coastal current velocities (Batteen, 1997). From a continuity perspective, it is argued that enhanced subsurface current velocities should also be present in these regions. These subsurface velocities are seen as the multiple core signature in the undercurrent.

Consistent with Frouin *et al.* (1990) and Haynes and Barton (1990), our winter results show a coastal surface poleward current (i.e., the Iberian Current) ~25-40 km wide, which reaches speeds of ~17.5 cm/s north of 41° N (e.g., Figure 17).

Our winter results also suggest the presence of a relatively weak coastal equatorward undercurrent in the poleward part of the model domain (e.g., Figure 17). While there are no available observations in the NCCS to confirm this feature, it should be noted that an equatorward undercurrent (and also a coastal poleward surface current) with similar speeds has been observed by Hickey (1979, 1998) in the fall and winter off the coast of Washington, the poleward end of the California Current system.

#### **b. Comparison of Eddies**

The model's generation of numerous eddies on the order of 100 km throughout the NCCS is consistent with high resolution satellite imagery and observations by Fiuza (1984). Preferred locations of eddy generation occur offshore of prominent changes in coastline orientation, i.e., off Cabo da Roca, Cabo de São Vincent, the Gulf of Cadiz, and Cape Beddouzza and Cape Ghir. A comparison of the results of Fiuza (1984) with the results of the model simulations shows that the model generates eddies in similar locations.

The salty characteristics and structure of the anticyclonic eddies seen at ~1200 m depth in the model simulations (e.g., Figure 20) are consistent with observations of Meddies in the Canary Basin (e.g., Richardson *et al.*, 1989). The locations, propagation speeds, and propagation directions of the Meddies (e.g., Figure 19) are also consistent with the recent synthesis of observations in the Canary Basin of Meddies by Richardson and Tychensky (1998).

Like the previous experiments, the preferred locations for Meddy generation are in the vicinity of prominent changes in coastline orientation, i.e., off southwestern Portugal for the Meddies. It is suggested that the Meddies are generated by the same mechanism as in the previous experiments, i.e., due to the basic instability of the equatorward coastal jet and the poleward undercurrent. The major difference between the Meddies and the other eddies is that the Meddies are generated at depth rather than near the surface. This is likely due to the relatively salty MO core of the undercurrent below ~500 m depth which makes the water in the core saltier than the water above and below it. This could lead to a local baroclinic instability process, resulting in the production of



Meddies. This scenario is consistent with the results of Kase *et al.*, (1989), who observed eddies in the MO off Iberia and postulated that baroclinic instabilities generated by the undercurrent could lead to the generation of Meddies.

### c. Comparison of Upwelling and Filaments

Upwelling varies by season throughout the domain as a result of the seasonally oscillating winds seen in Figure 2. Observations show that upwelling appears first off Cape Ghir and Cape Beddouzza in early spring as seen in Van Camp *et al.* (1991), and then progressively to the north as the Azores High moves up the Moroccan coast. This progression of upwelling is well simulated in the model. Observed upwelling off the west coast of Portugal and along the southern coast of Iberia (Folkard *et al.*, 1997) is also well simulated by the model (e.g., Figure 16).

Several studies by Fiuza (1983), Barton (1986), and Fiuza and Sousa (1989) have confirmed the existence of cold filaments extending off the west coast of Portugal which is depicted by the model (e.g., off Cabo da Roca in Figure 16). While investigating the waters of southern Iberia in the Gulf of Cadiz, Folkard *et al.* (1997) observed cold, upwelled filaments extending southward from the coast. The model results simulate these filaments as well (e.g., south of Cabo de Sao Vincente in Figure 16).

To the south, satellite observations from Van Camp *et al.* (1991) and Hagen *et al.* (1996) show a filament of cold, upwelled water extending off Cape Ghir for ~200 km. They also show that the coastal jet and subsequent frontal zone caused by the advected cold water can result in the generation of a cyclonic (anticyclonic) meander or eddy on the southern (northern) side of the jet. Consistent with these observations, the model depicts a filament off Cape Ghir as an equatorward meandering coastal jet which transports cold, upwelled water offshore (Figure 16). The model results also show that, consistent with the observations, the jet at ~32.5° N has a cyclonic eddy (anticyclonic meander) to the south (north).

#### IV. SUMMARY

The objective of this process-oriented study was to use a multilevel PE model to investigate the roles of classical as well as unique features in the predominantly wind-driven NCCS. Toward this end, results from four numerical experiments of increasing complexity were examined. Similar to a classical EBC system, all of the experiments produced an offshore surface equatorward meandering current, a surface equatorward coastal jet, a surface poleward coastal current, a poleward undercurrent, upwelling, meanders, eddies, and filaments.

To isolate the response to seasonal wind forcing from coastline variations, Experiment 1 used seasonal wind forcing along a straight coastline. The results, as expected in a classical EBC system, showed that wind forcing was the key generative mechanism for the currents and upwelling as well as for the intense and complex meander, eddy, and filament structures in the NCCS.

To examine the additional effects of irregular coastline geometry, two additional experiments were run. Experiment 2 used an idealized "straightened" coastline with two prominent capes and an embayment representing the Gulf of Cadiz. Due to the presence of the Gulf of Cadiz, large anticyclonic meander and eddy formation in the Gulf of Cadiz were regular features. Due to the presence of the two prominent idealized capes (i.e., Cabo de Sao Vicente and Cape Ghir), cyclonic meanders and eddies tended to form in the vicinity of the capes.

The additional effects of using more realistic capes with extensive coastline irregularities in Experiment 3 showed that irregularities in the coastline geometry were key elements for enhanced growth of meanders and eddies, and for "anchoring" upwelling and filaments to geographical features. For example, upwelling was present in Experiment 3 south of Cabo de Sao Vicente and off Cabo de Santa Maria, which was not seen in Experiment 2 with the idealized east-west coastline orientation. Experiment 3 also showed that multiple cores of the undercurrent could be present in the vicinity of

capex, e.g., between Cape Ghir and Cape Beddouzza, and between Cabo de Sao Vicente and Cabo da Roca.

In Experiment 4, the additional effects of thermohaline gradients and the MO were used. Due to thermohaline gradients, there was an onshore geostrophic flow resulting in a tighter temperature gradient all along the coast, and the seasonal development of an equatorward undercurrent in the poleward end of the model domain.

The effects of the MO were seen between ~500 to 1300 m depth as relatively salty cores of the undercurrent which, west of  $\sim 7^\circ$  W, followed the south and west coasts of Iberia. At these depths, Meddies occurred as regular features in the vicinity of the west coast of the Gulf of Cadiz and off the southwest coast of Portugal. It was proposed that baroclinic instabilities of the undercurrent, which had saltier MO cores than the water above or below, was the generation mechanism for the Meddies.

A comparison of the currents, upwelling, meanders, eddies, jets, and filaments generated by the model with available observations showed that the model successfully simulated the location, size, and velocity of these features. Of the features generated, the cores of the poleward undercurrent are of particular interest. Until now, it has generally been accepted that multiple cores were the result of MO influence (e.g., Ambar, 1982). This study showed, however, that irregular coastline geometry, particularly capes, could play an important role in the generation of the subsurface cores.

In summary, the results from the complex flow regime of Experiment 4, which has the most realistic features, highlight the major characteristics and unique features of the NCCS with relatively close similarities to field observations. These results show that the model successfully captures the qualitative nature of the NCCS.

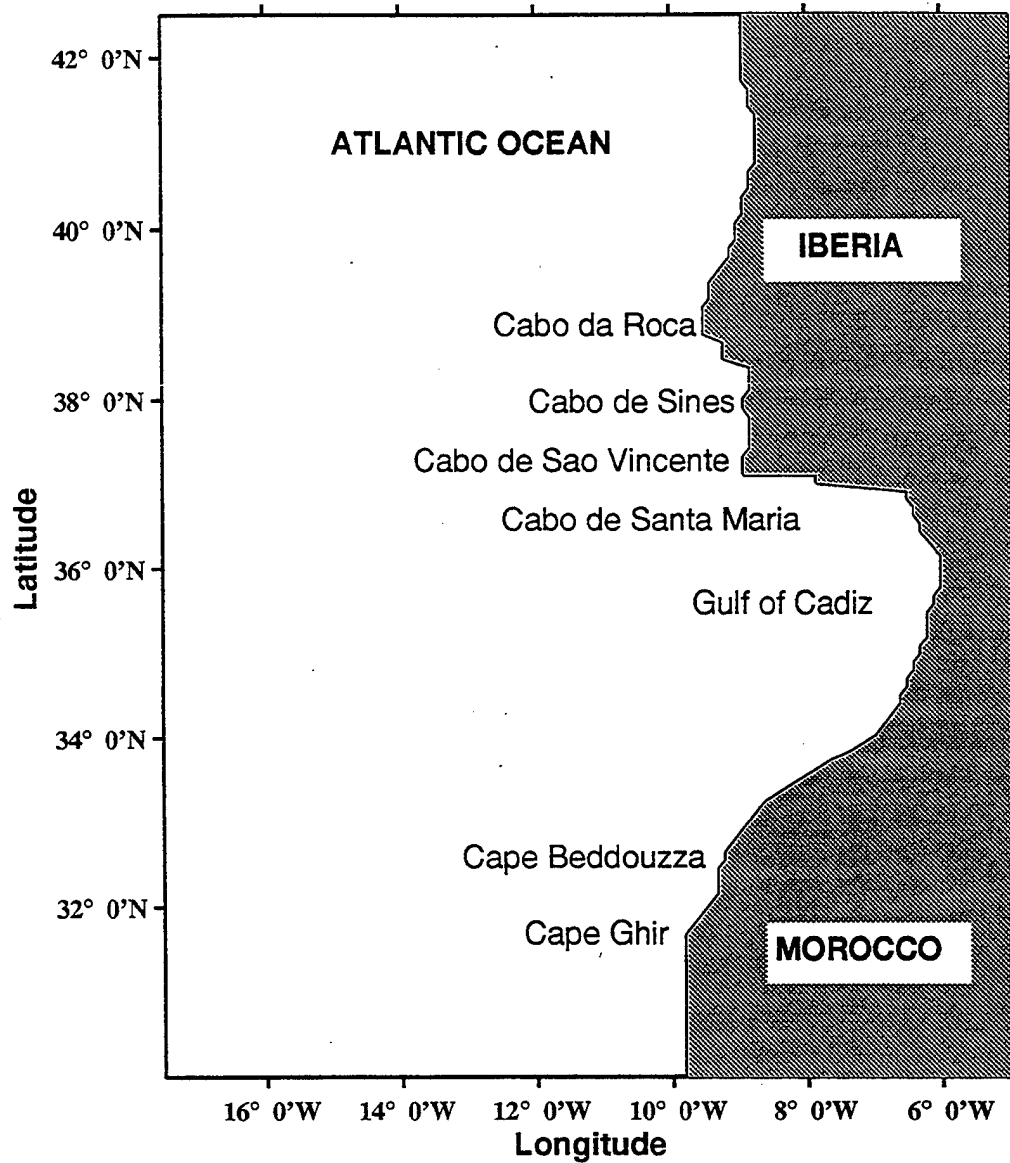
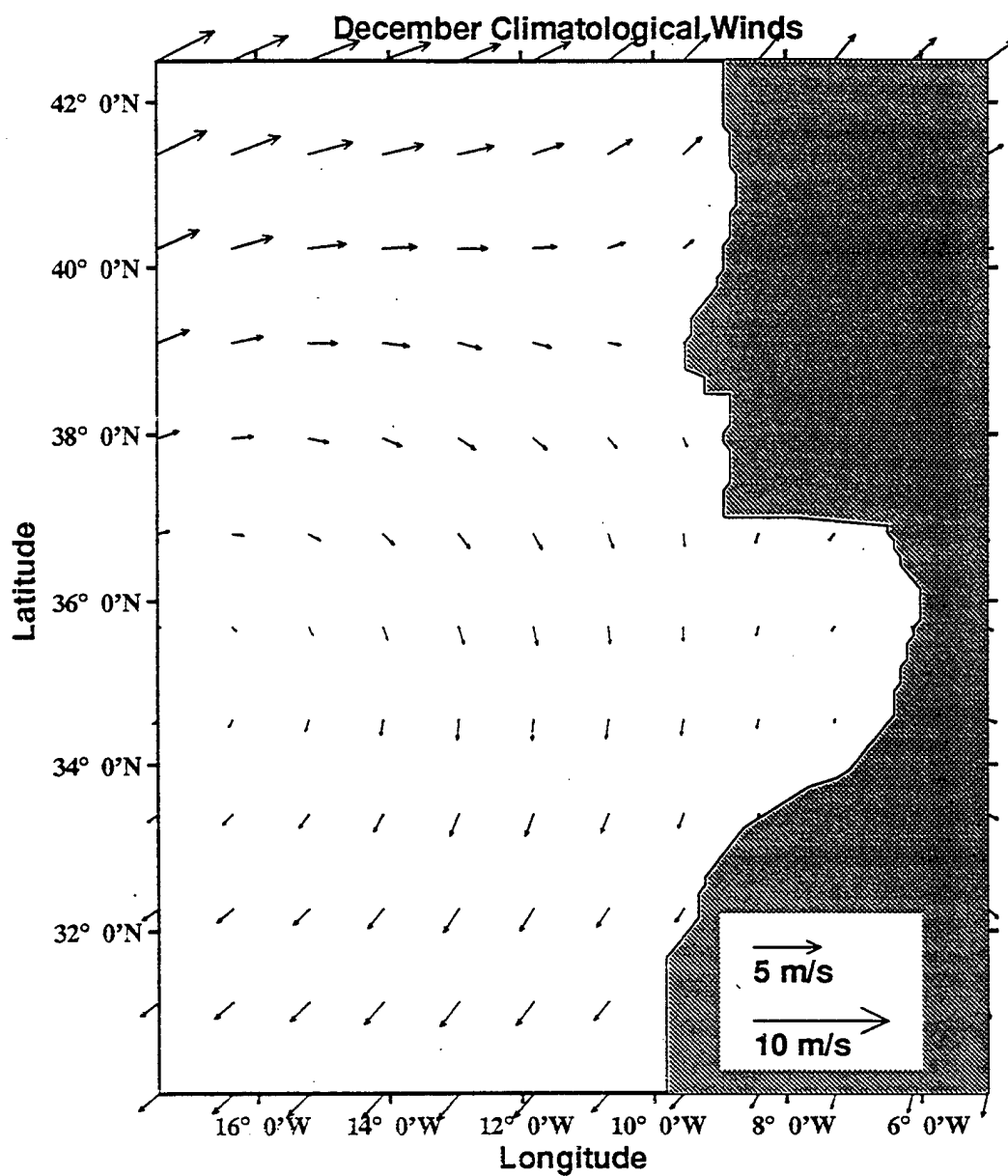
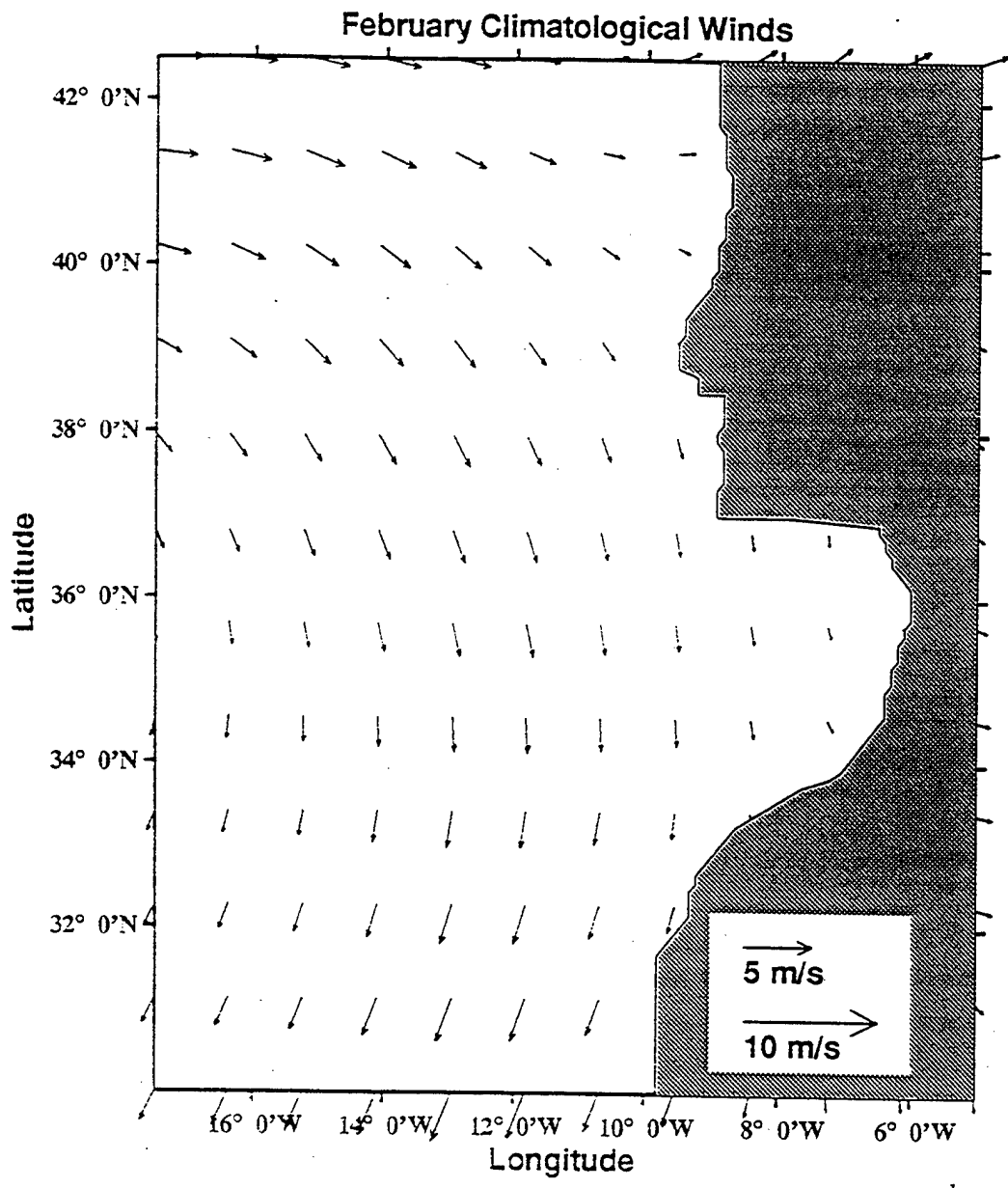


Figure 1. The model domain for the northern Canary Current System (NCCS) is bounded by 30° N to 42.5° N, 5° W to 17.5° W. The cross-shore (alongshore) resolution is 9 km (11 km). Geographic locations and prominent features are labeled.



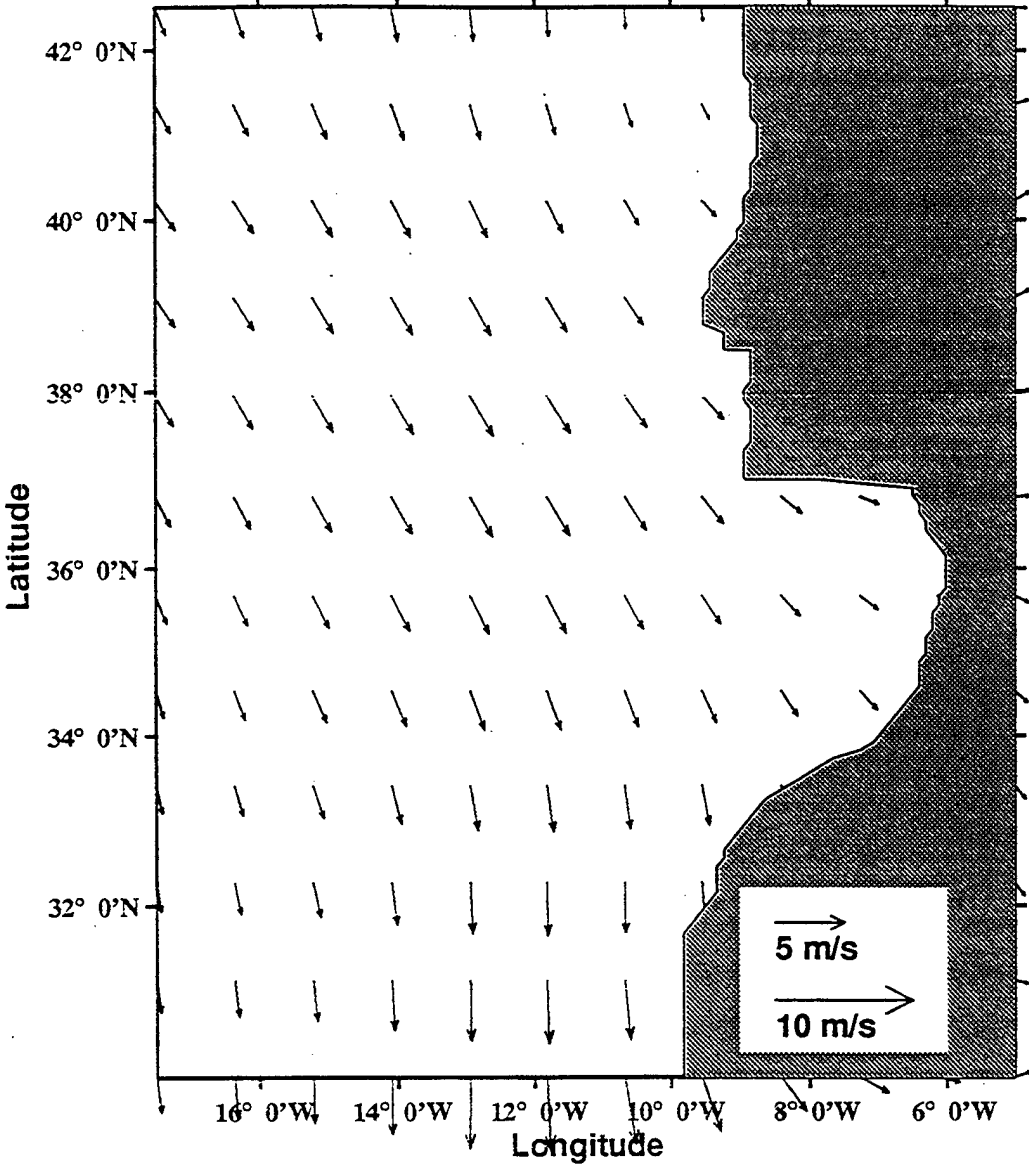
a.

Figure 2. Climatological (1980-1989) ECMWF winds in m/s for: (a) December, (b) February, (c) April, (d) August, and (e) October. Maximum wind vector is 10 m/s.



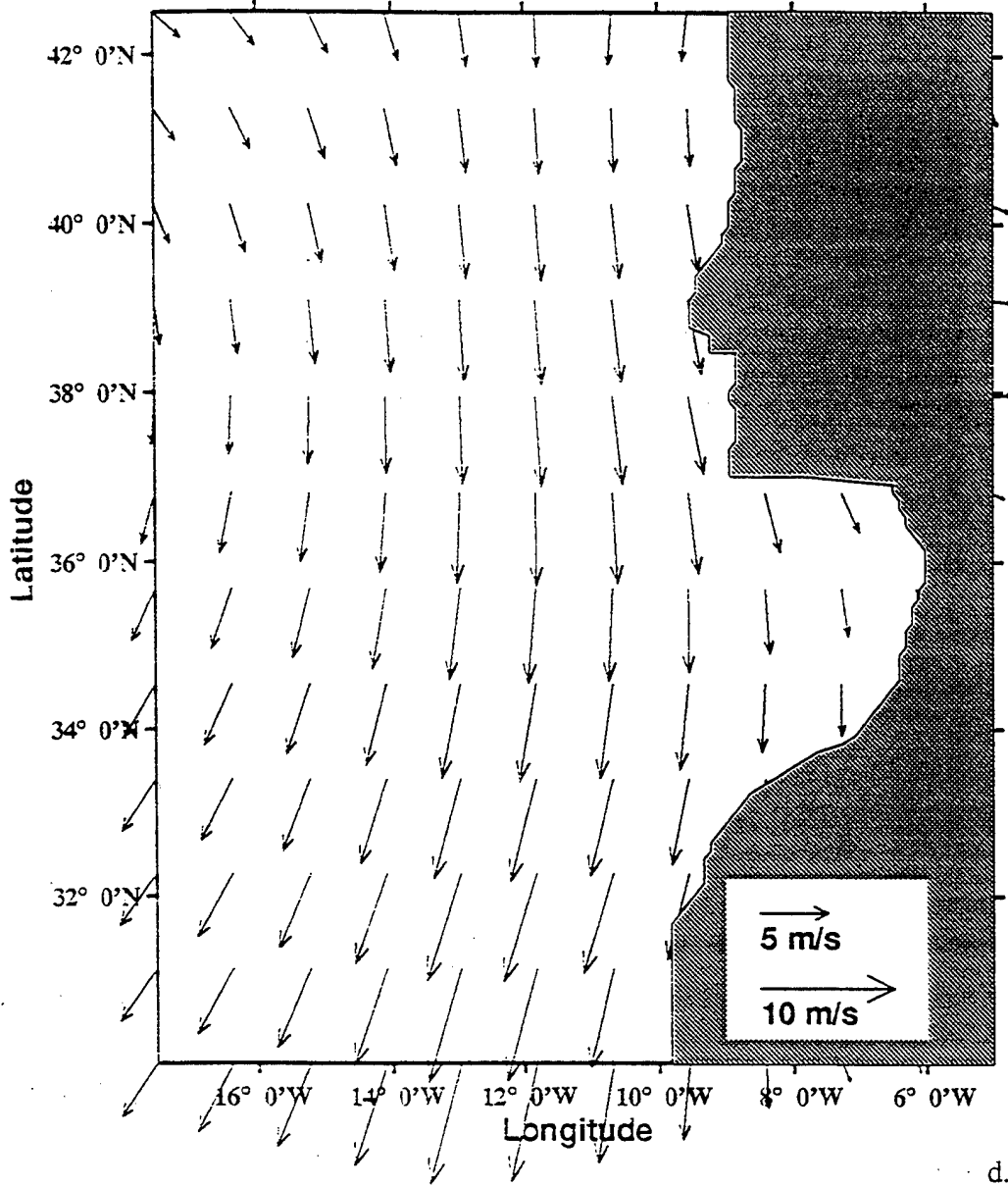
b.

April Climatological Winds



c.

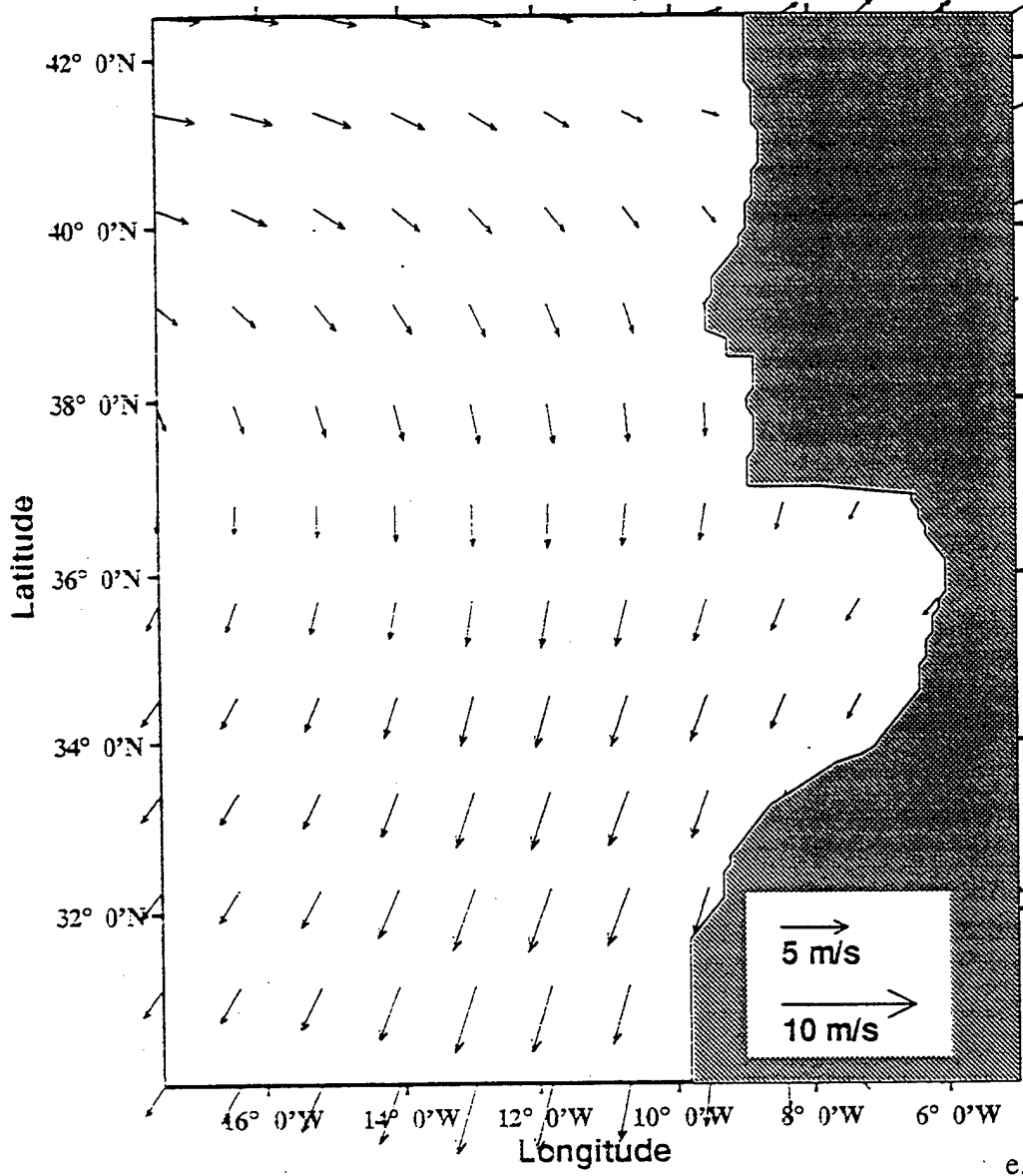
### August Climatological Winds



d.



### October Climatological Winds



e.

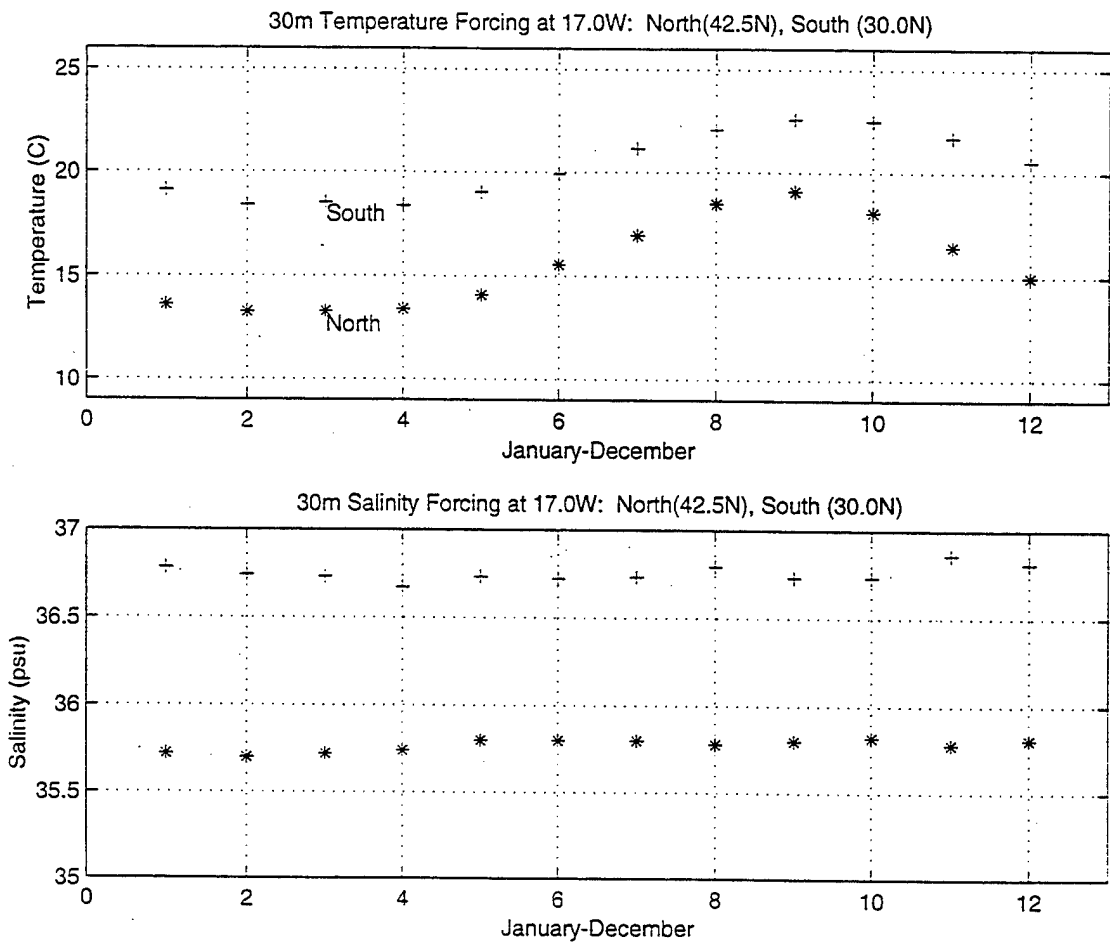


Figure 3. Times series plots of monthly temperature and salinity fields used as seasonal forcing in the basic simulation. The '\*' symbol represents data at 30° N, 17.5° W, while the '+' symbol represents data at 42.5° N, 17.5° W for 30 m depth.

DEPTH : 30m  
T : 210

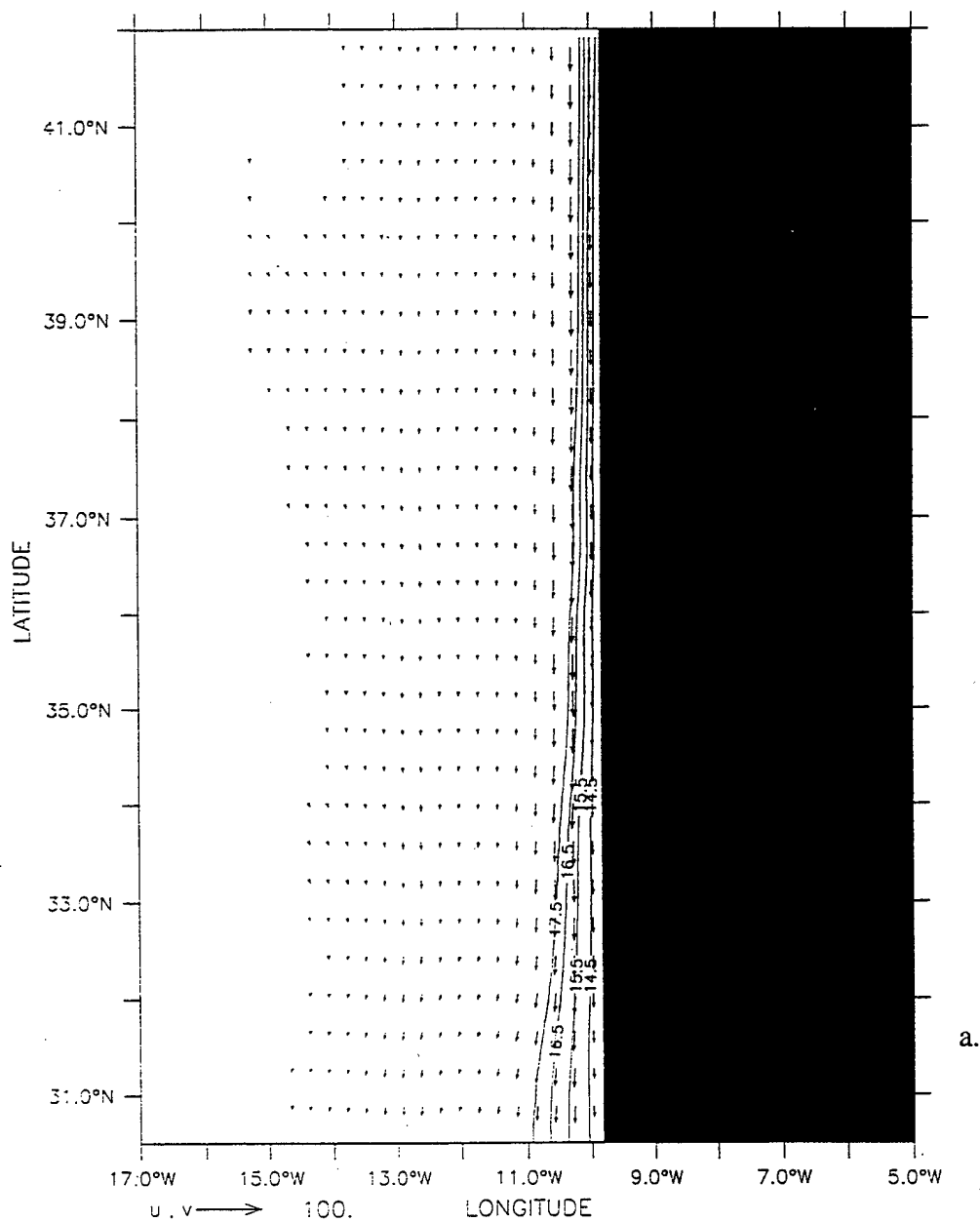
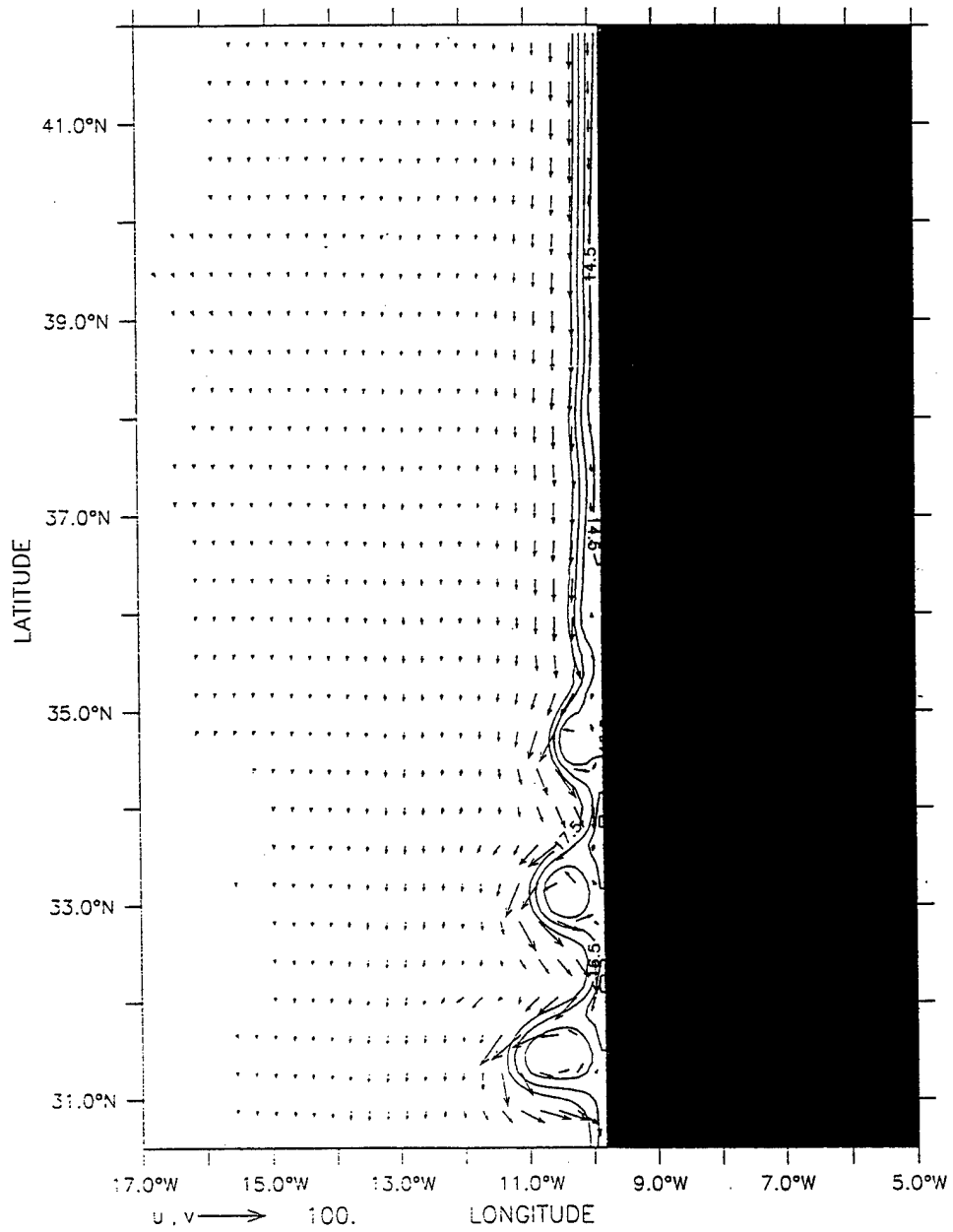


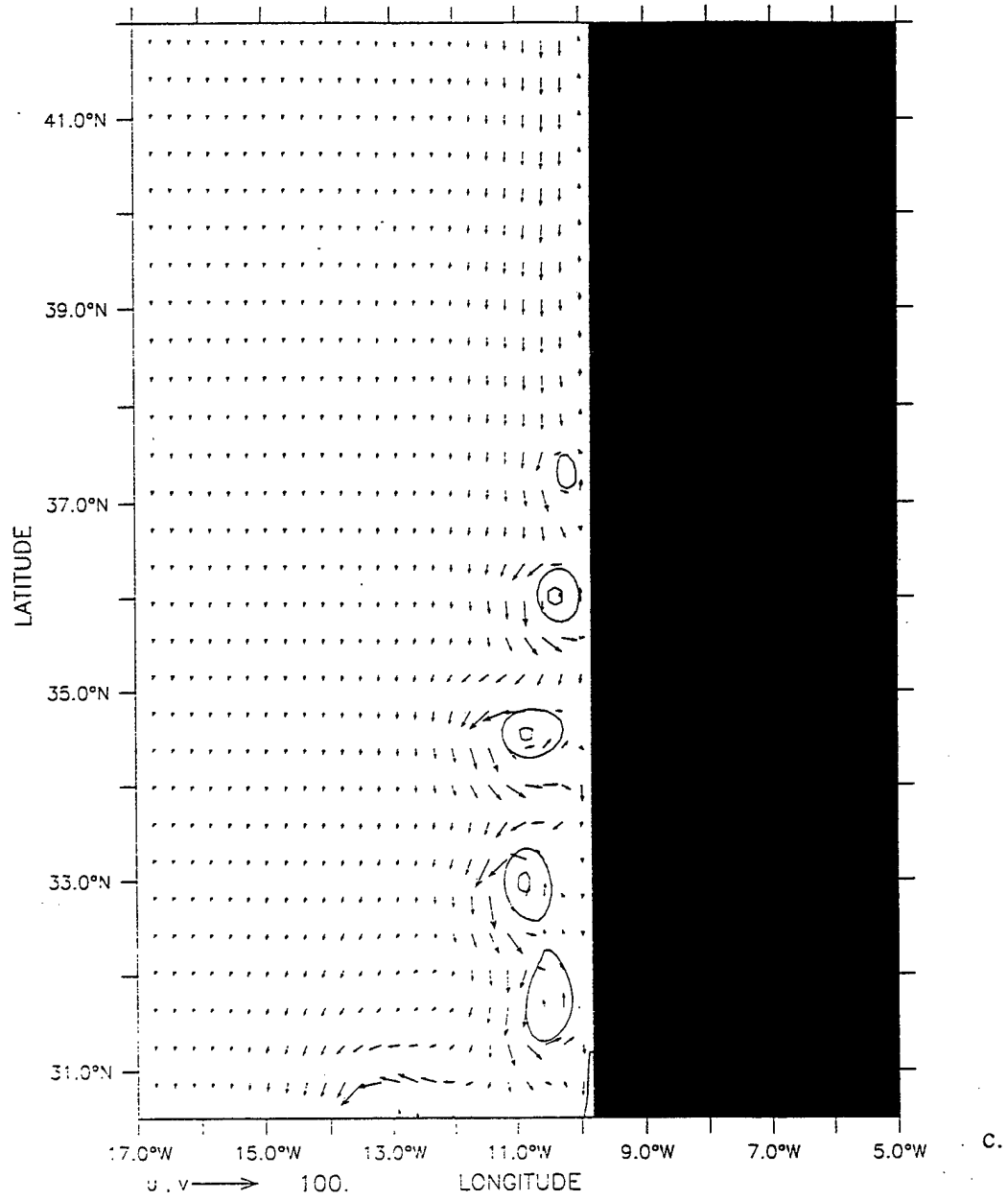
Figure 4. Temperature contours and velocity vectors for Experiment 1 at 30 m depth at days (a) 210, (b) 270, (c) 330 and (d) 621. The contour interval is 1°C. To avoid clutter, the velocity vectors are plotted every third grid point in the cross-shore direction and every fourth grid point in the along-shore direction. Maximum current velocity is 100 cm/s.

DEPTH : 30m  
T : 270

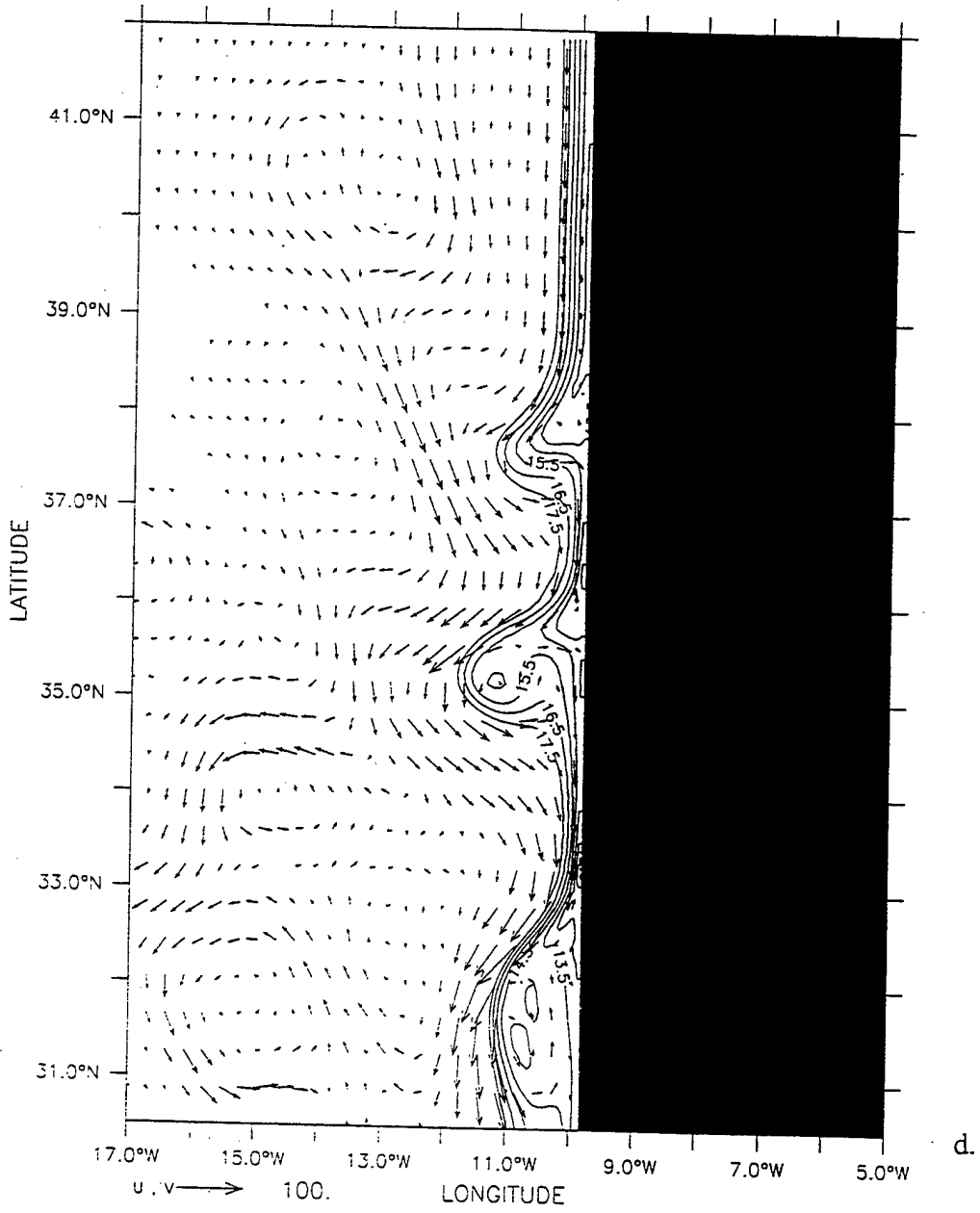


b.

DEPTH : 30m  
T : 330



DEPTH : 30m  
T : 621



LATITUDE : 35.5N  
T : 210

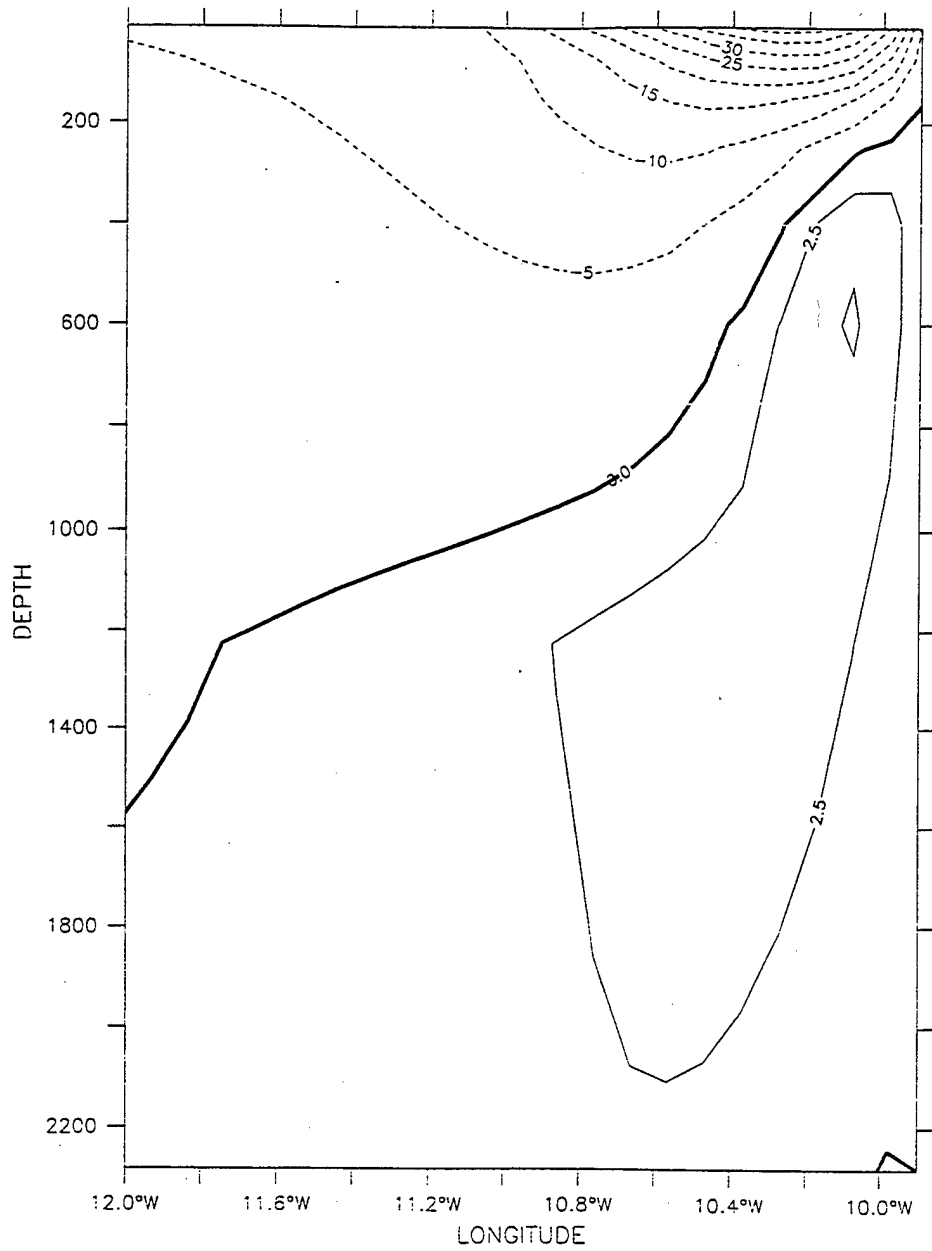


Figure 5. Cross-shore sections of meridional velocity ( $v$ ) for Experiment 1 on day 210 at  $35.5^\circ$  N. Solid lines indicate poleward flow, while dashed lines indicate equatorward flow. The contour interval is 2.5 cm/s for poleward flow and 5 cm/s for equatorward flow.

DEPTH : 30m

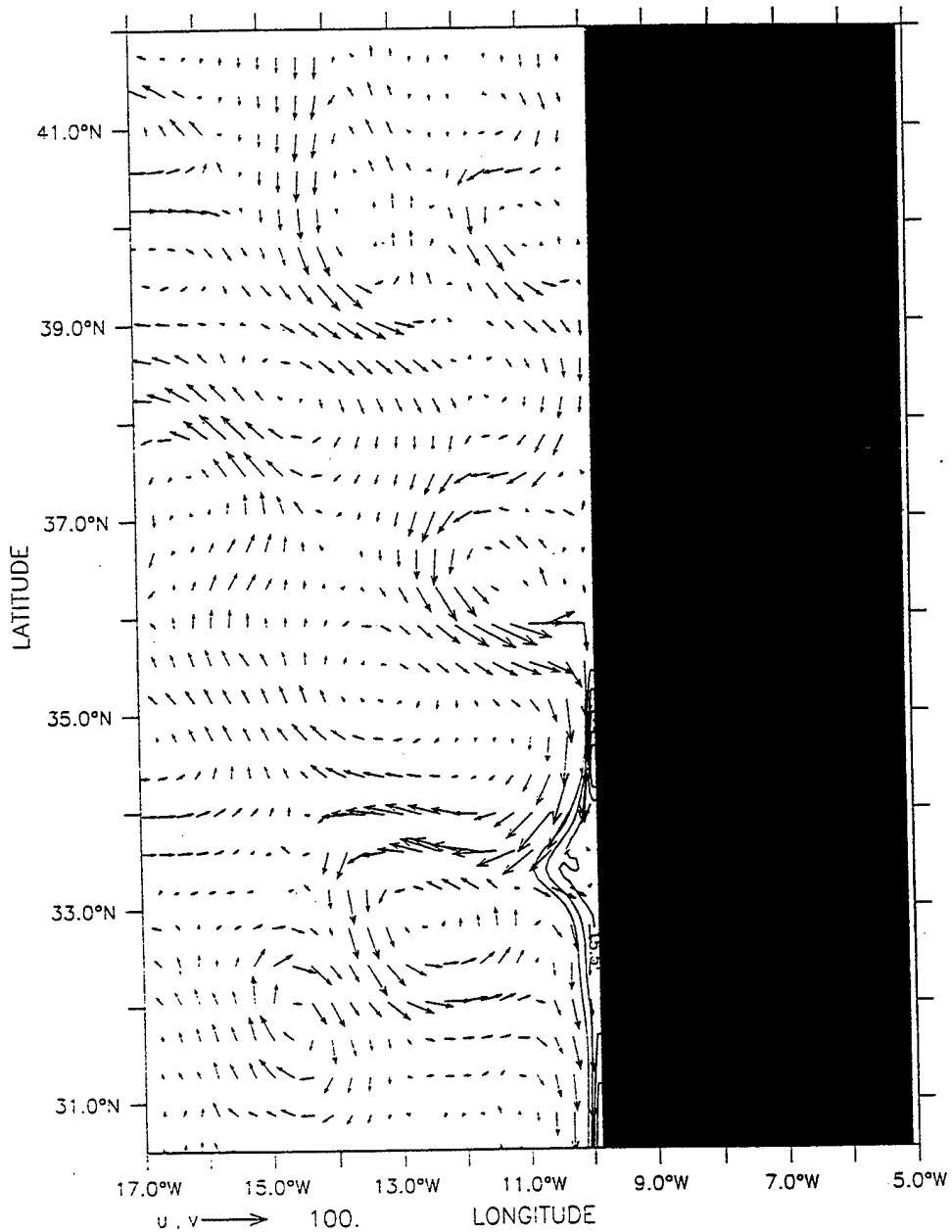
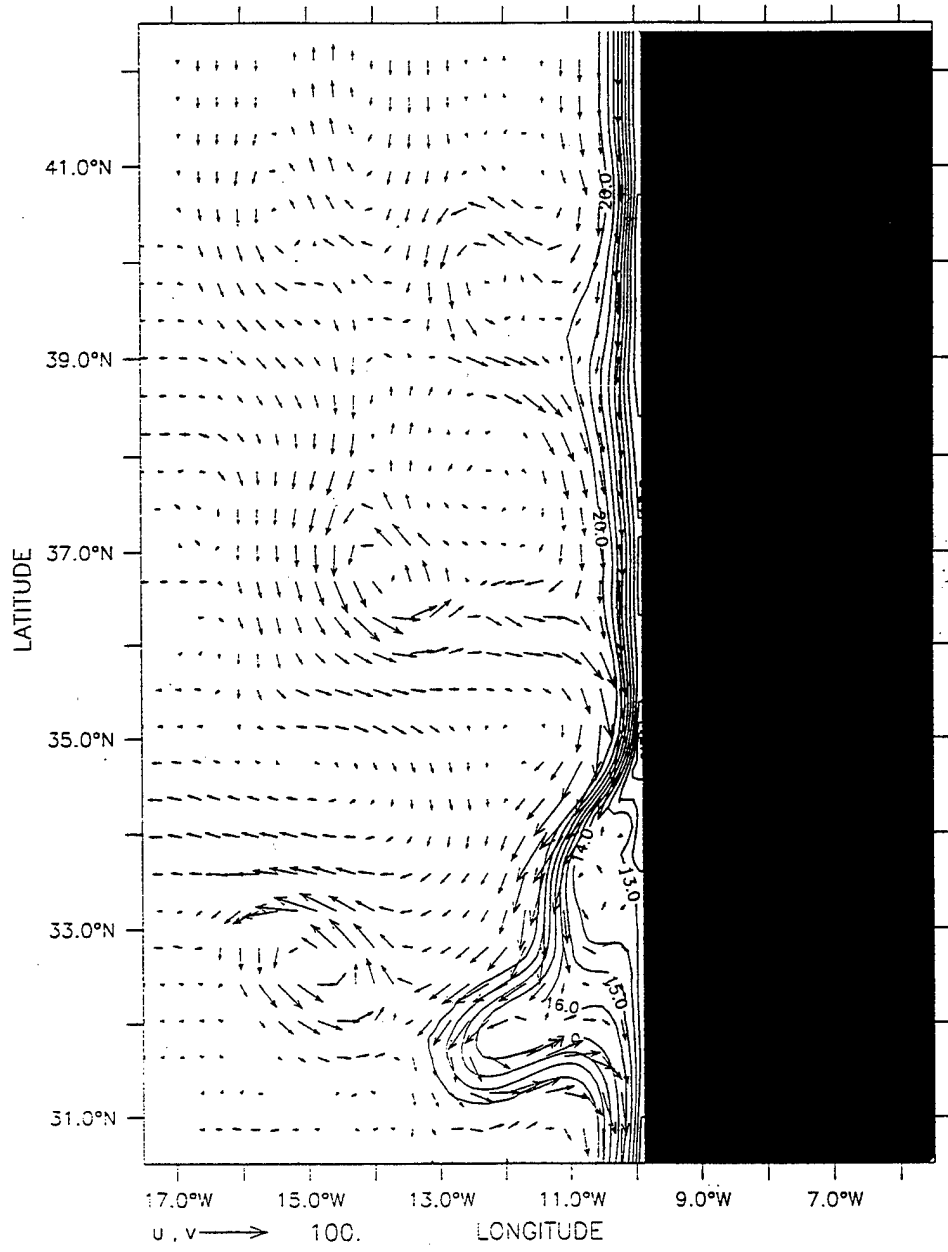


Figure 6. Temperature (a,b) and velocity vectors (a-c) at 30 m depth in the third year of Experiment 1 of the model simulation time-averaged over the months of (a) April, (b) August, (c) December. The contour interval is  $1^{\circ}$  C. Maximum current velocity is 100 cm/s.

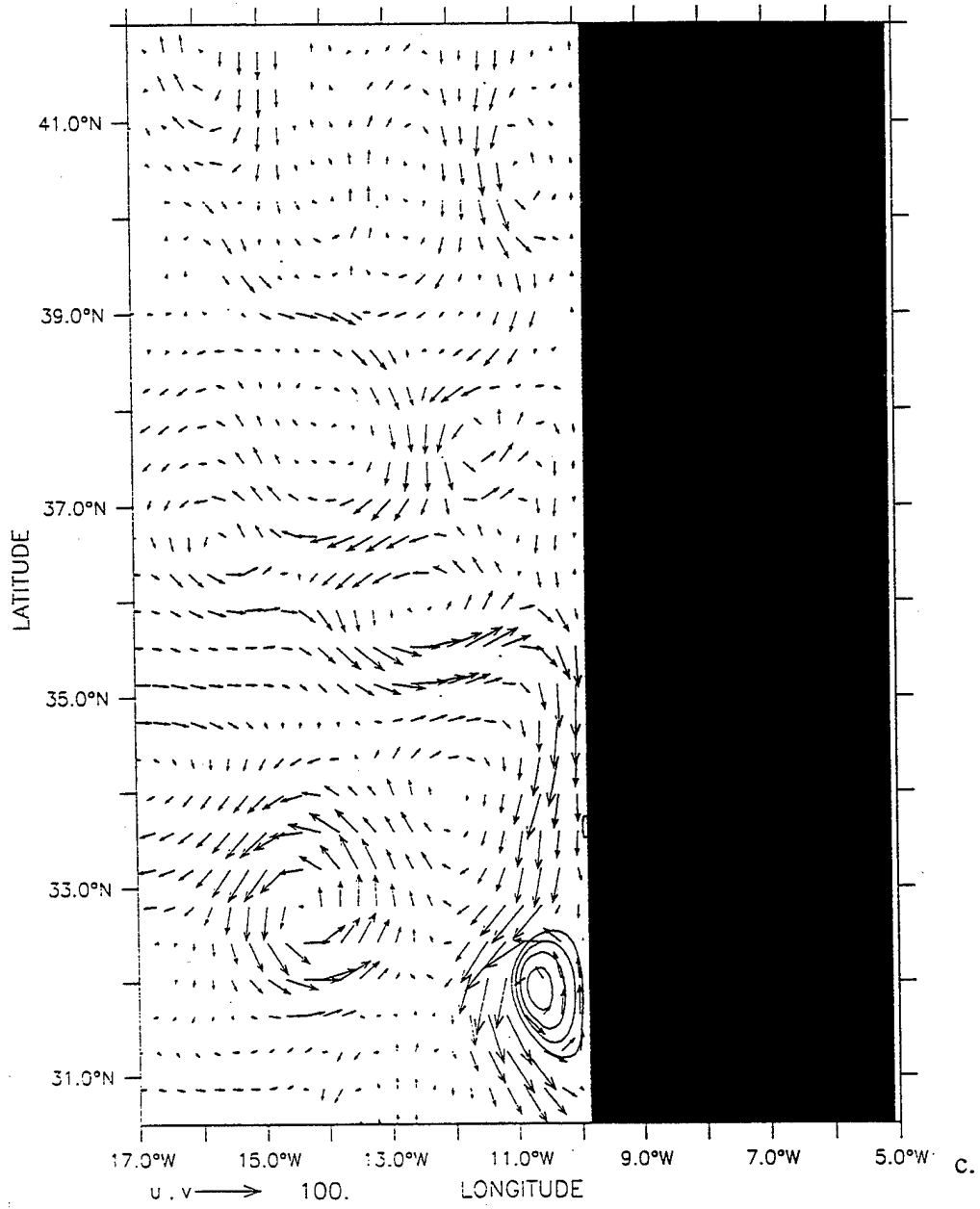


DEPTH : 30m

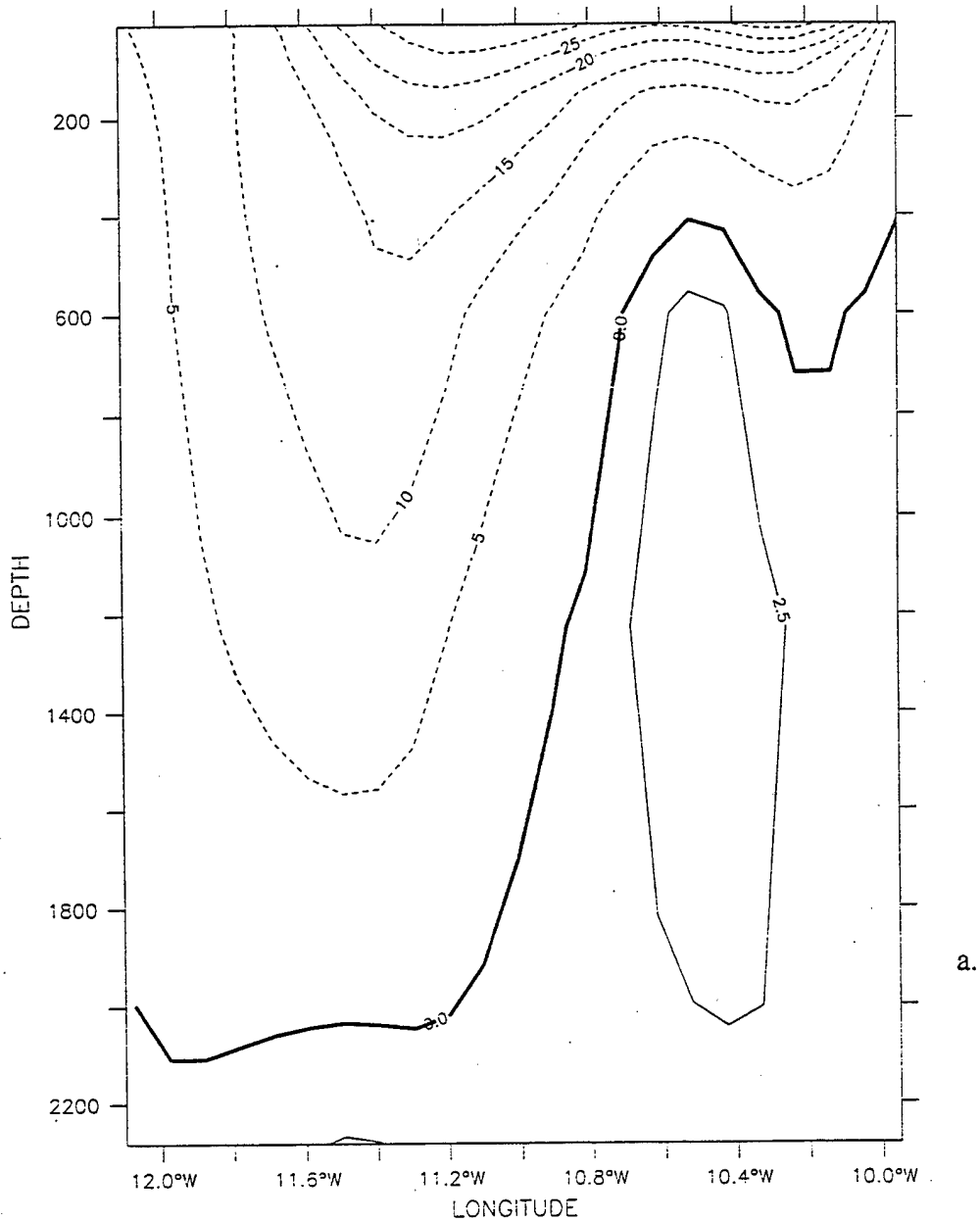


b.

DEPTH : 30m



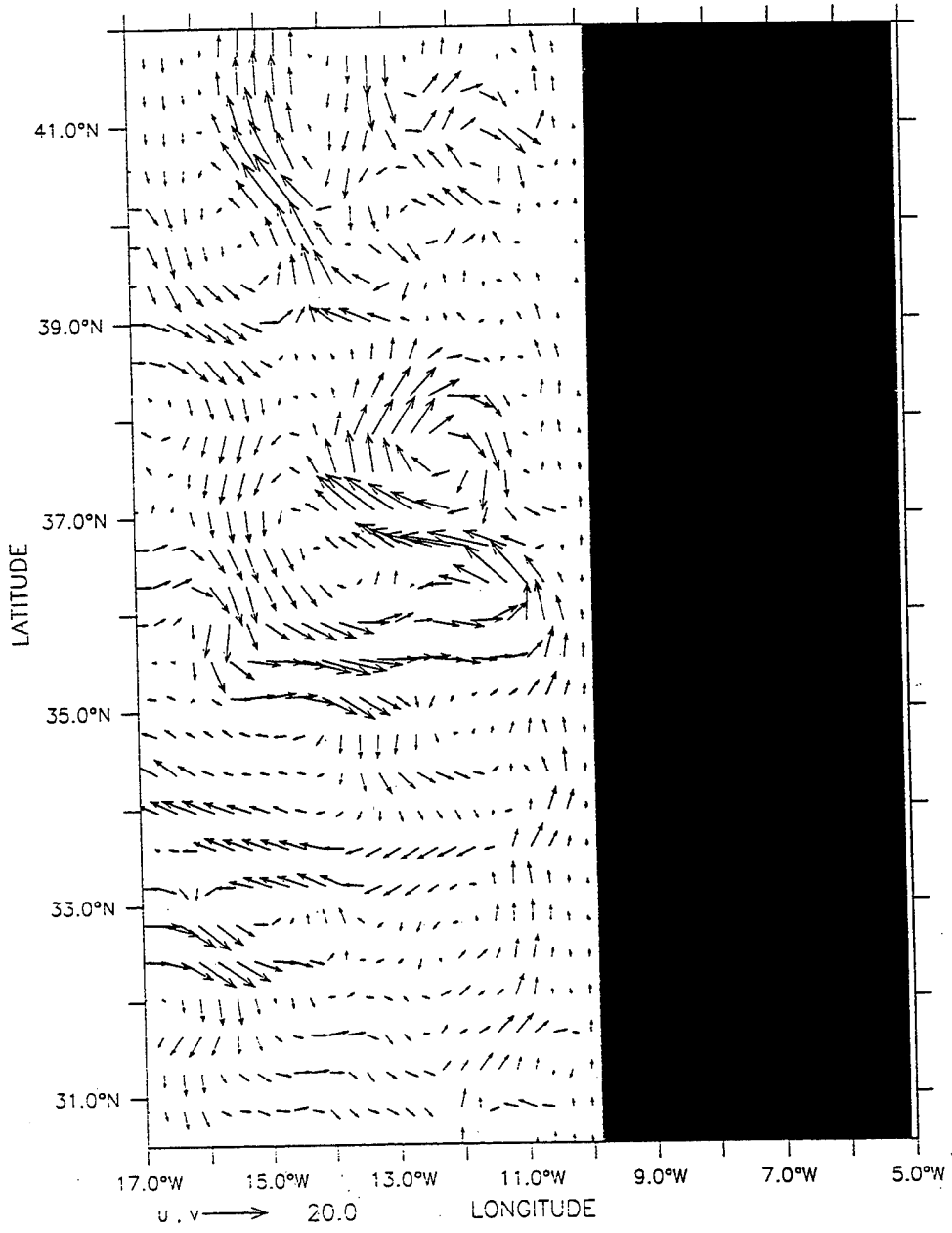
LATITUDE : 38N



a.

Figure 7. Time-averaged plots (Experiment 1) for the peak upwelling season (July-September) of a cross-shore section of mean meridional velocity( $v$ ) in (a) at  $38^\circ$  N, and velocity vectors (b) at 1226 m. In (a) solid lines indicate poleward flow, while dashed lines indicate equatorward flow. The contour interval for poleward flow is 2.5 cm/s. The contour interval for equatorward flow is 5 cm/s in (a). The maximum current velocity is 20 cm/s in (b).

DEPTH : 1226m



b.

DEPTH : 30m  
T : 270

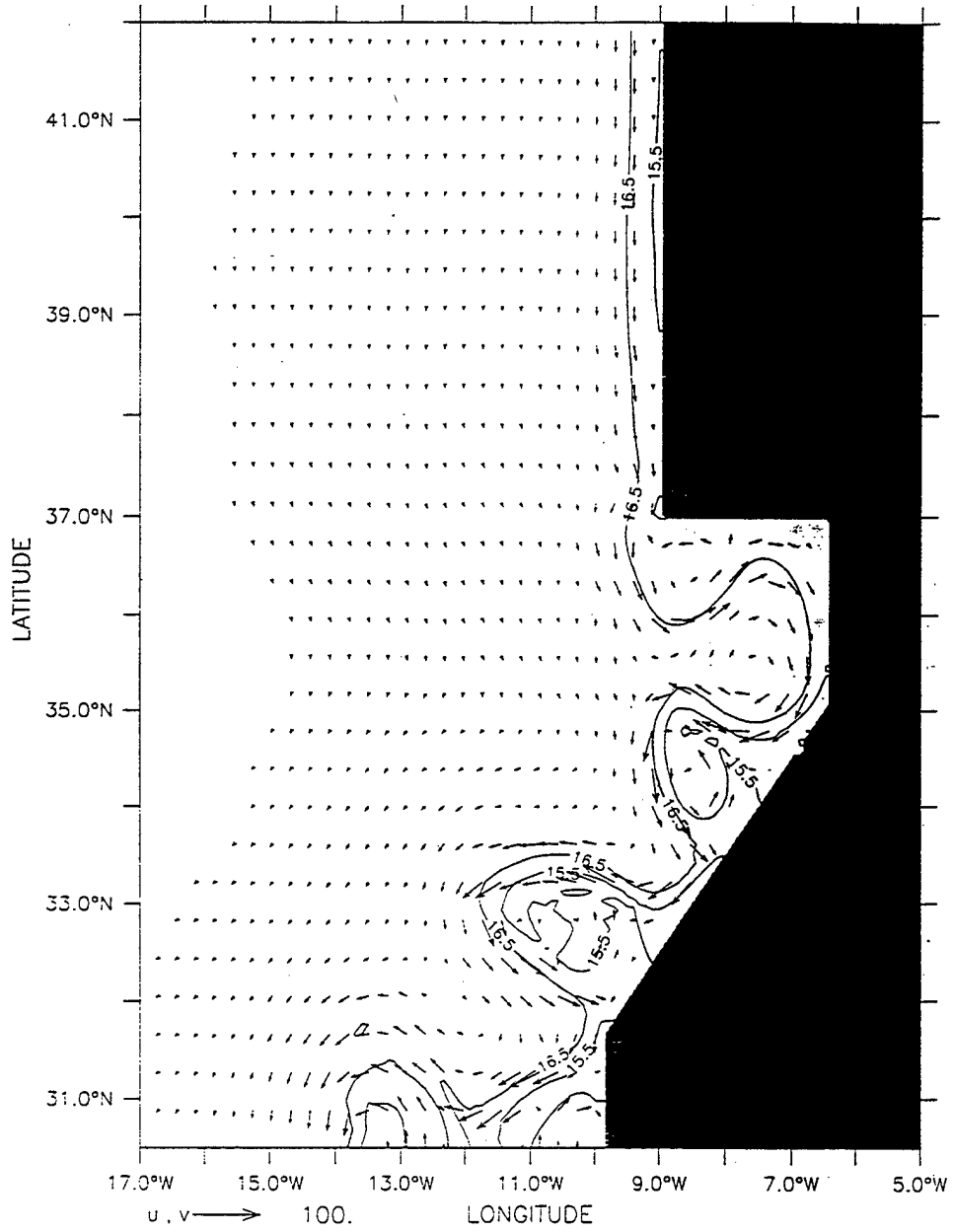


Figure 8. Temperature contours and velocity vectors for Experiment 2 at 30 m depth at day 270. Maximum current velocity is 100 cm/s.

DEPTH : 30m

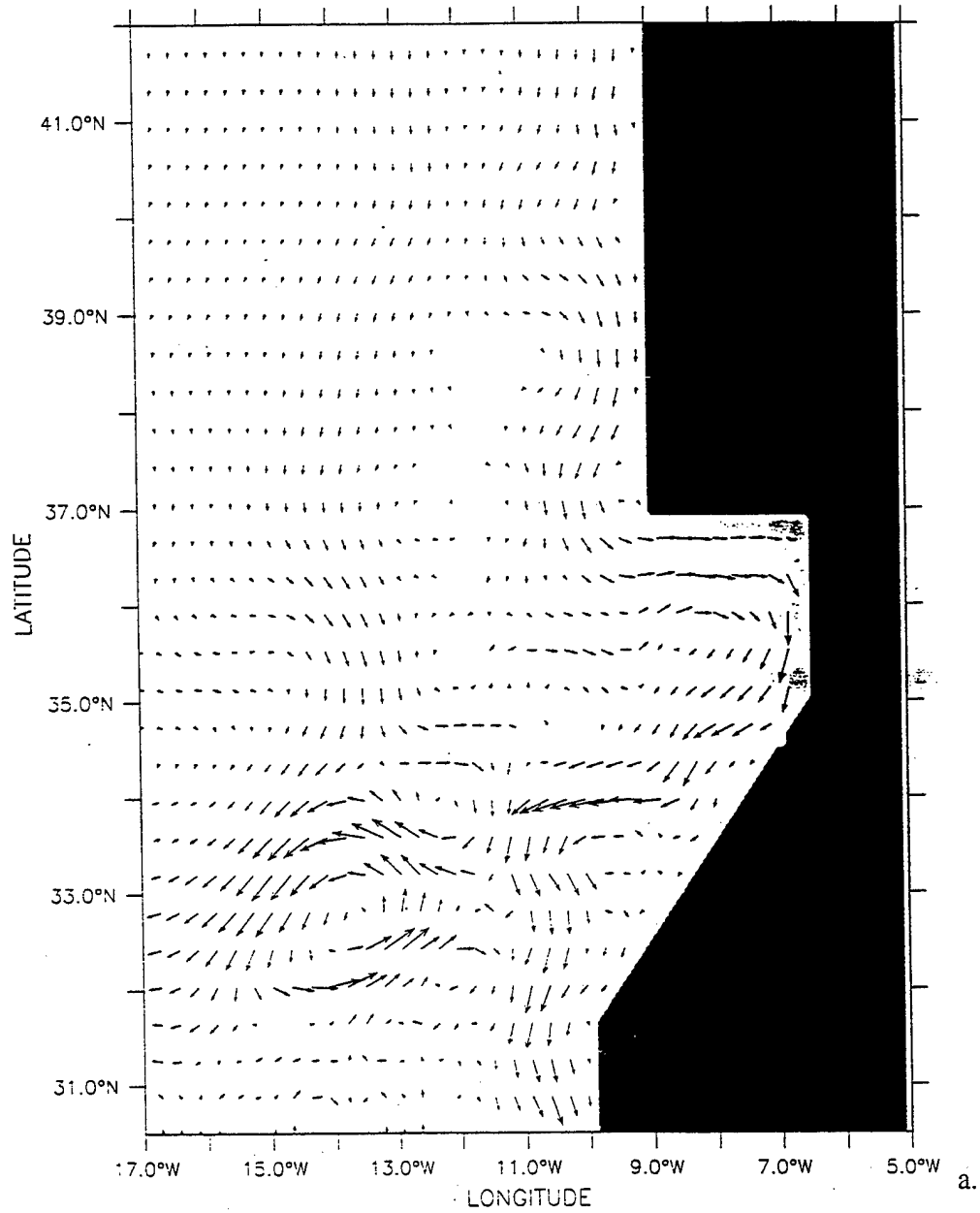
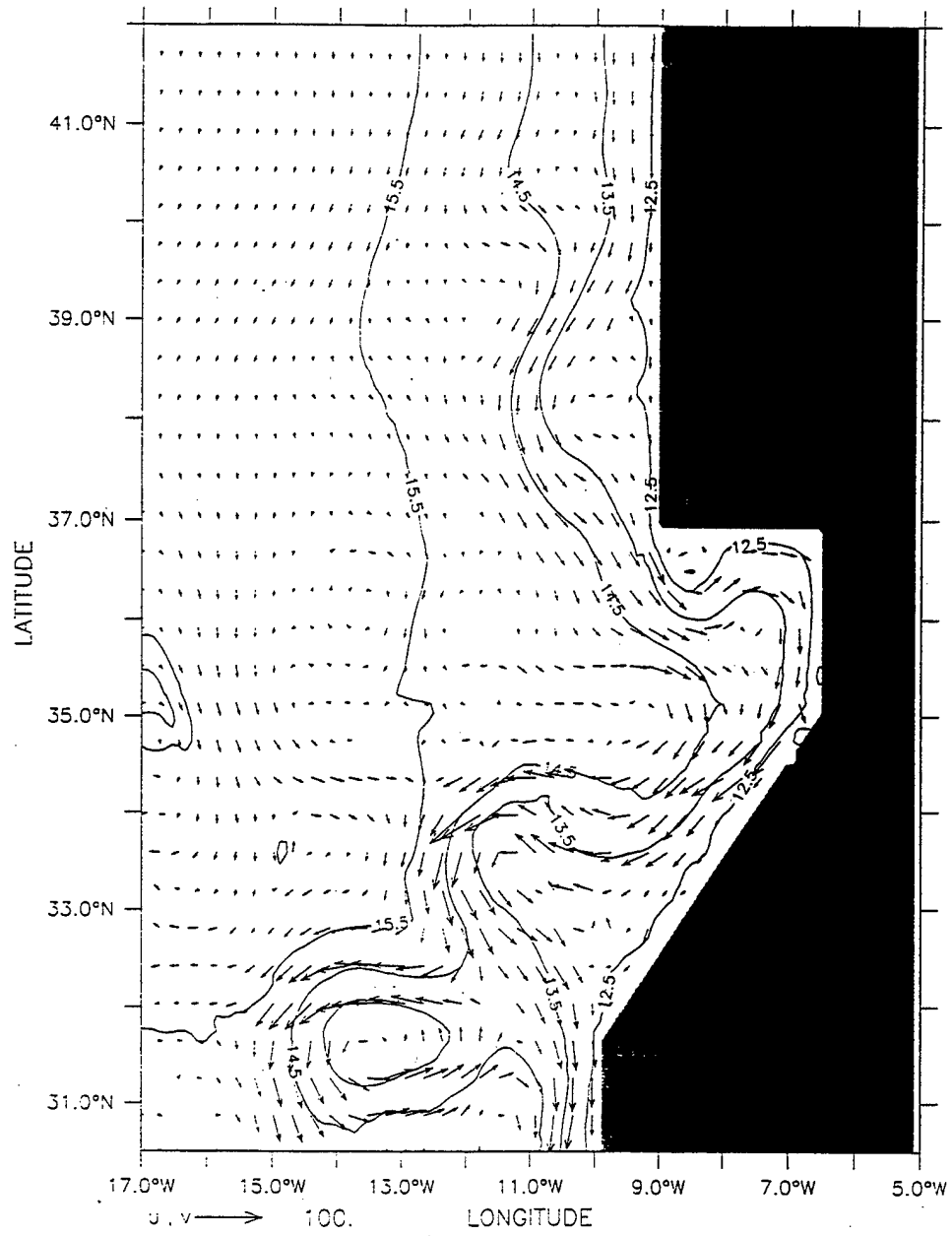


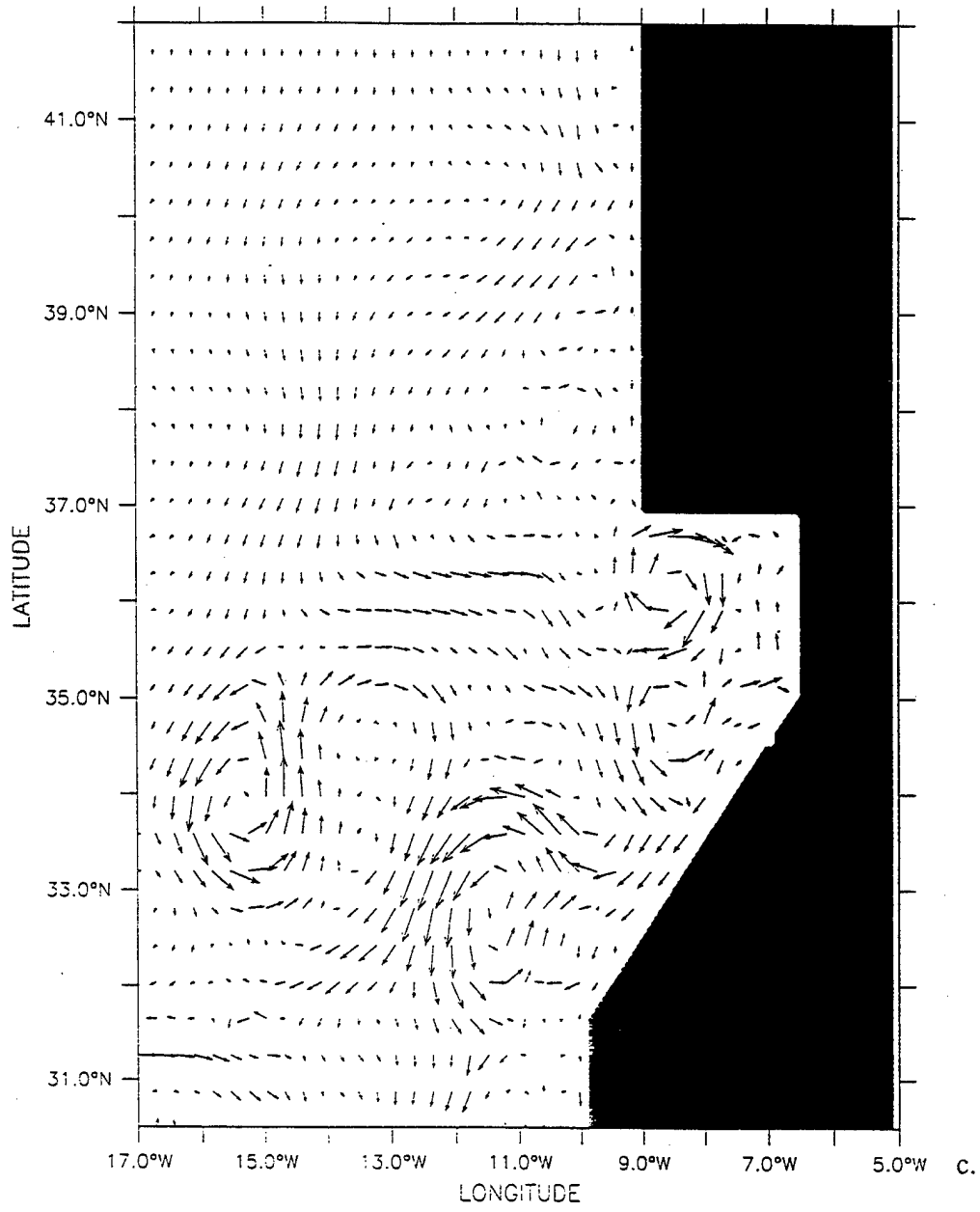
Figure 9. Time-averaged plots (Experiment 2) of temperature (b) and velocity vectors (a-c) at 30 m in the third year for April (a), August (b), December (c). The contour interval is  $1^{\circ}\text{C}$ . The maximum current velocity is 100 cm/s.

DEPTH : 30m



b.

DEPTH : 30m





DEPTH : 30m  
T : 210

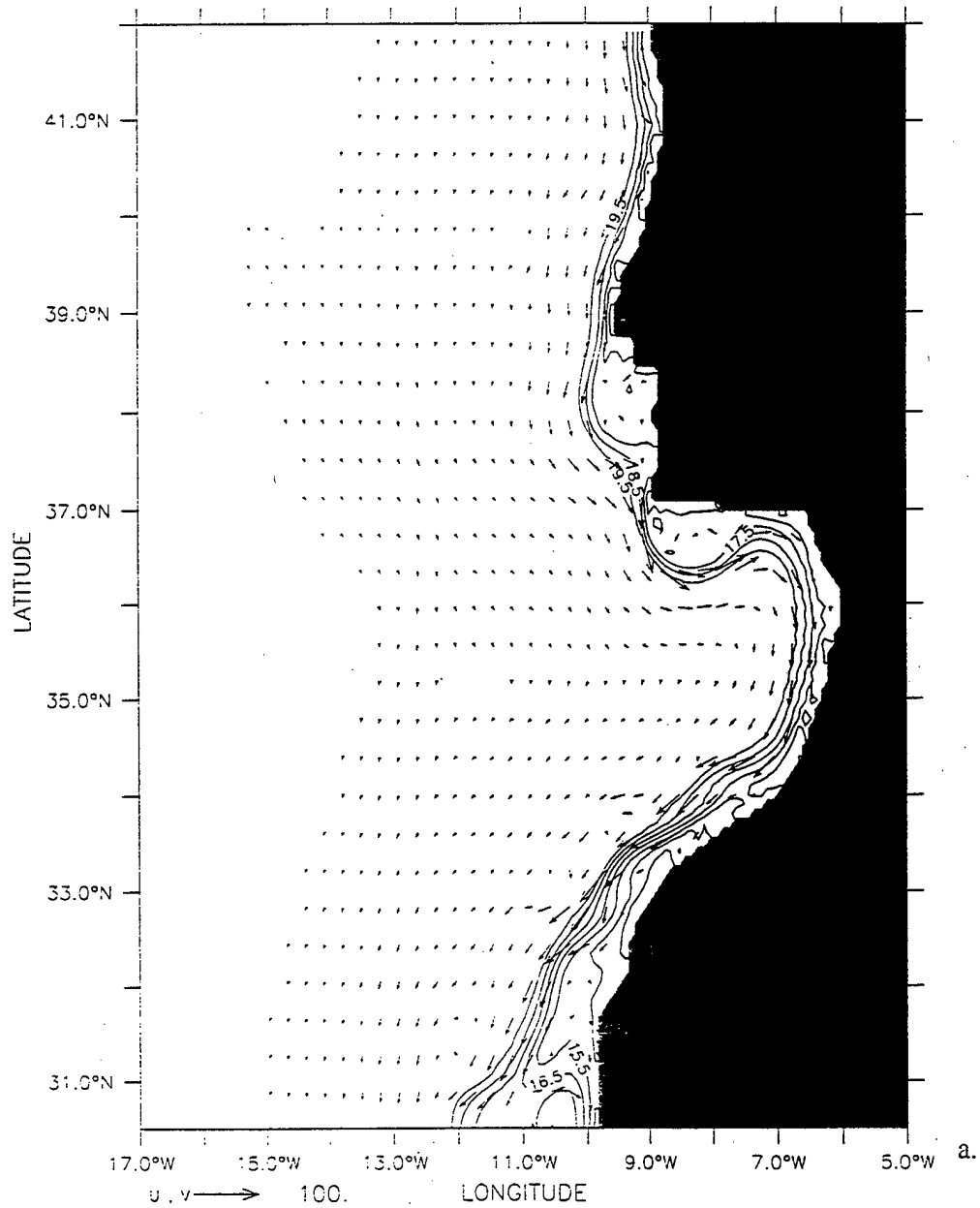
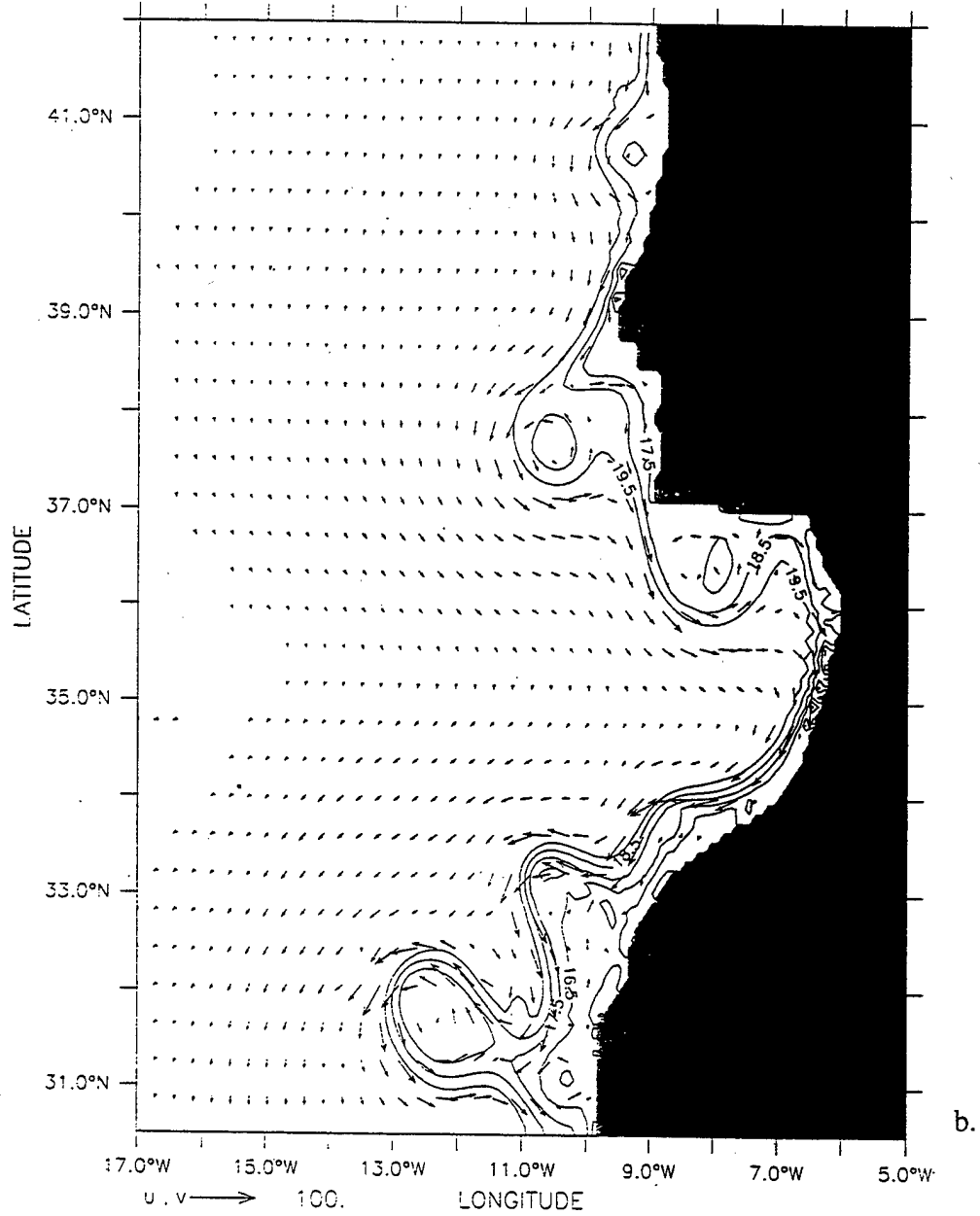
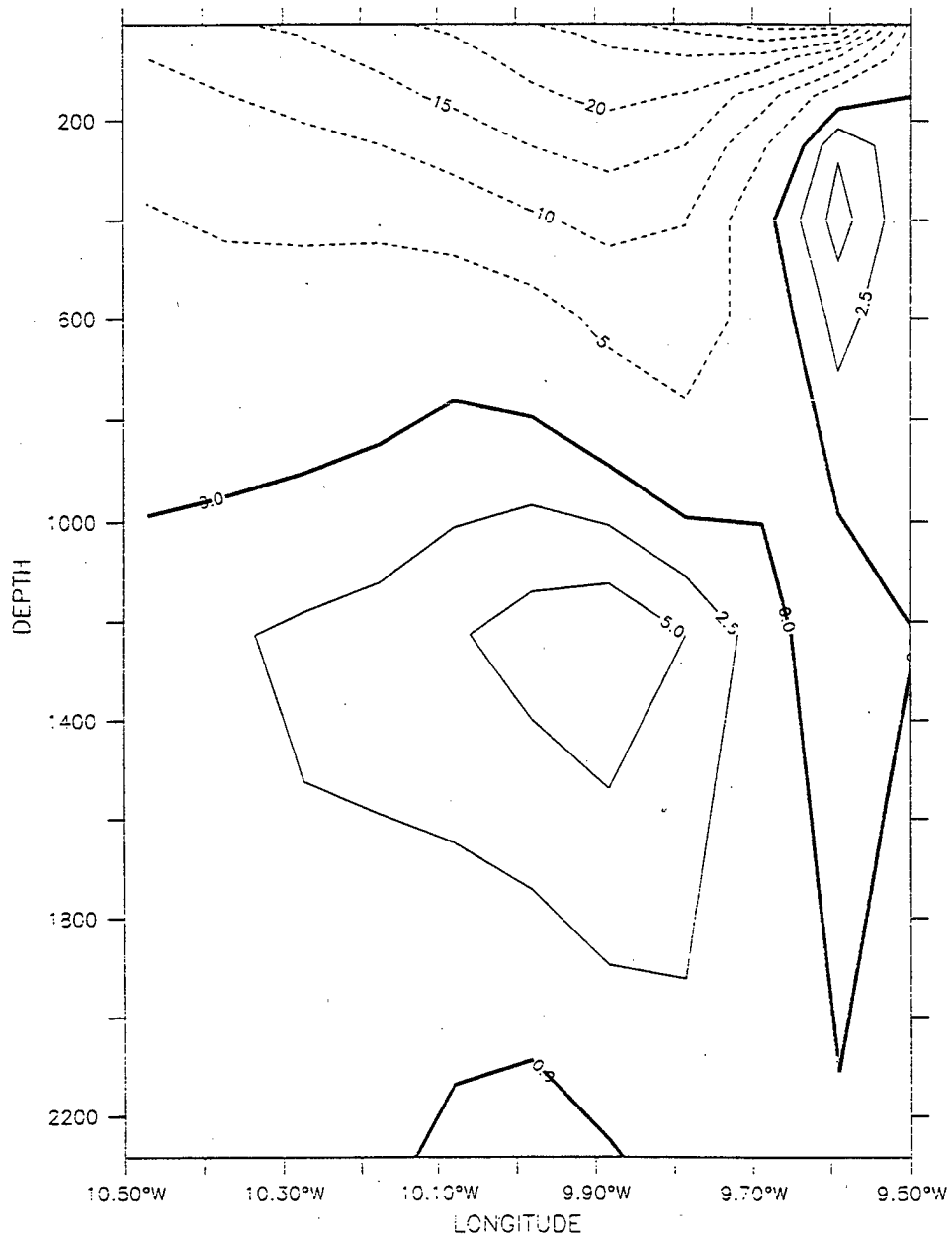


Figure 10. Temperature contours and velocity vectors for Experiment 3 at 30 m depth at days (a) 210 and (b) 285. The contour interval is 1°C. Maximum current velocity is 100 cm/s. The abbreviations used to denote the different capes are as follows: CR (Cabo da Roca), CS (Cabo de Sines), CSV (Cabo de Sao Vicente), CSM (Cabo de Santa Maria), CB (Cape Beddouzza), CG (Cape Ghir).

DEPTH : 30m  
T : 285



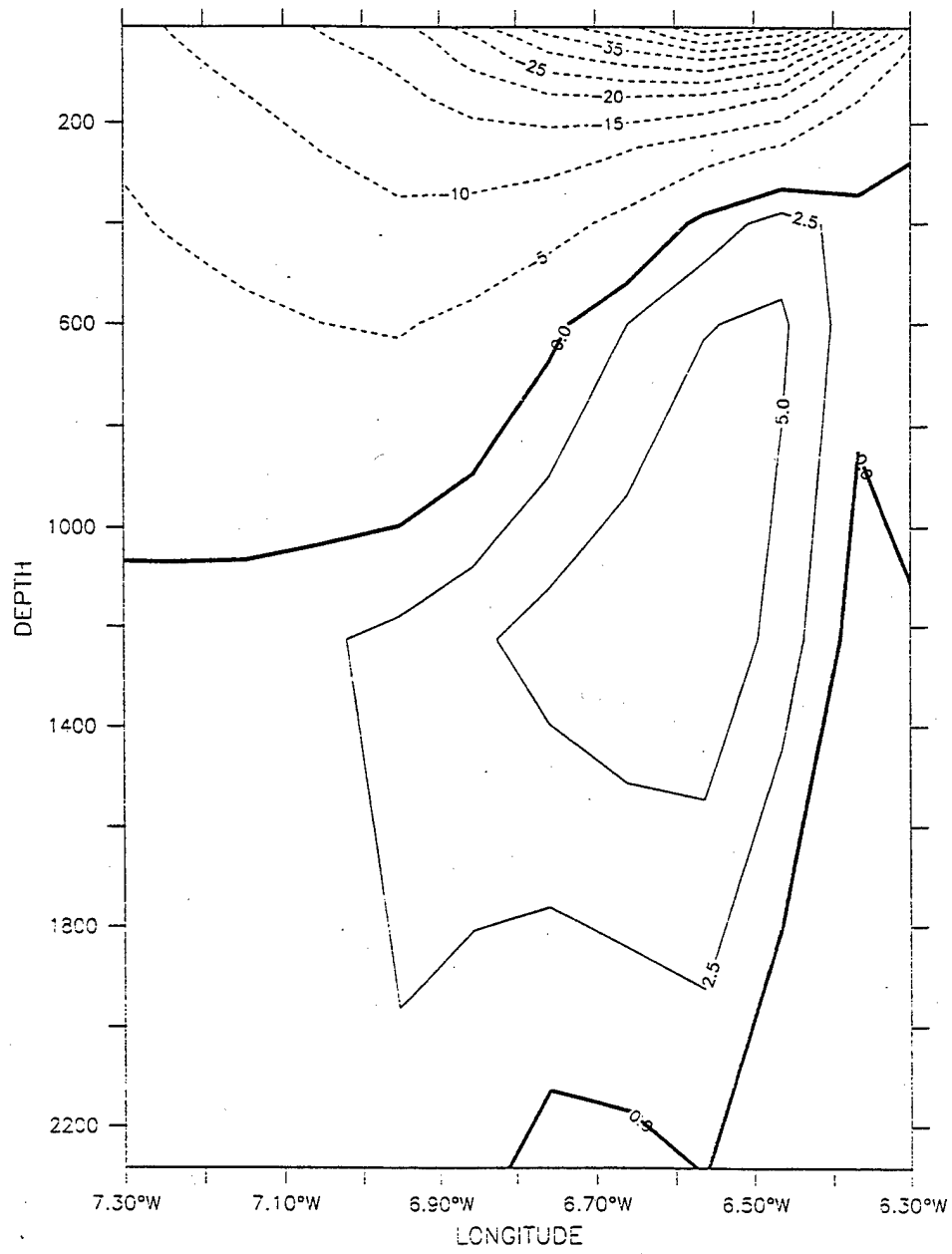
LATITUDE : 39.5N  
T : 240



a.

Figure 11. Cross-shore sections of meridional velocity ( $v$ ) for Experiment 3 on day 240 at  $39.5^\circ\text{N}$  (a) and at  $35.5^\circ\text{N}$  (b). Solid lines indicate poleward flow, while dashed lines indicate equatorward flow. The contour interval is 2.5 cm/s for poleward flow and 5 cm/s for equatorward flow.

LATITUDE : 35.5N  
T : 240



b.

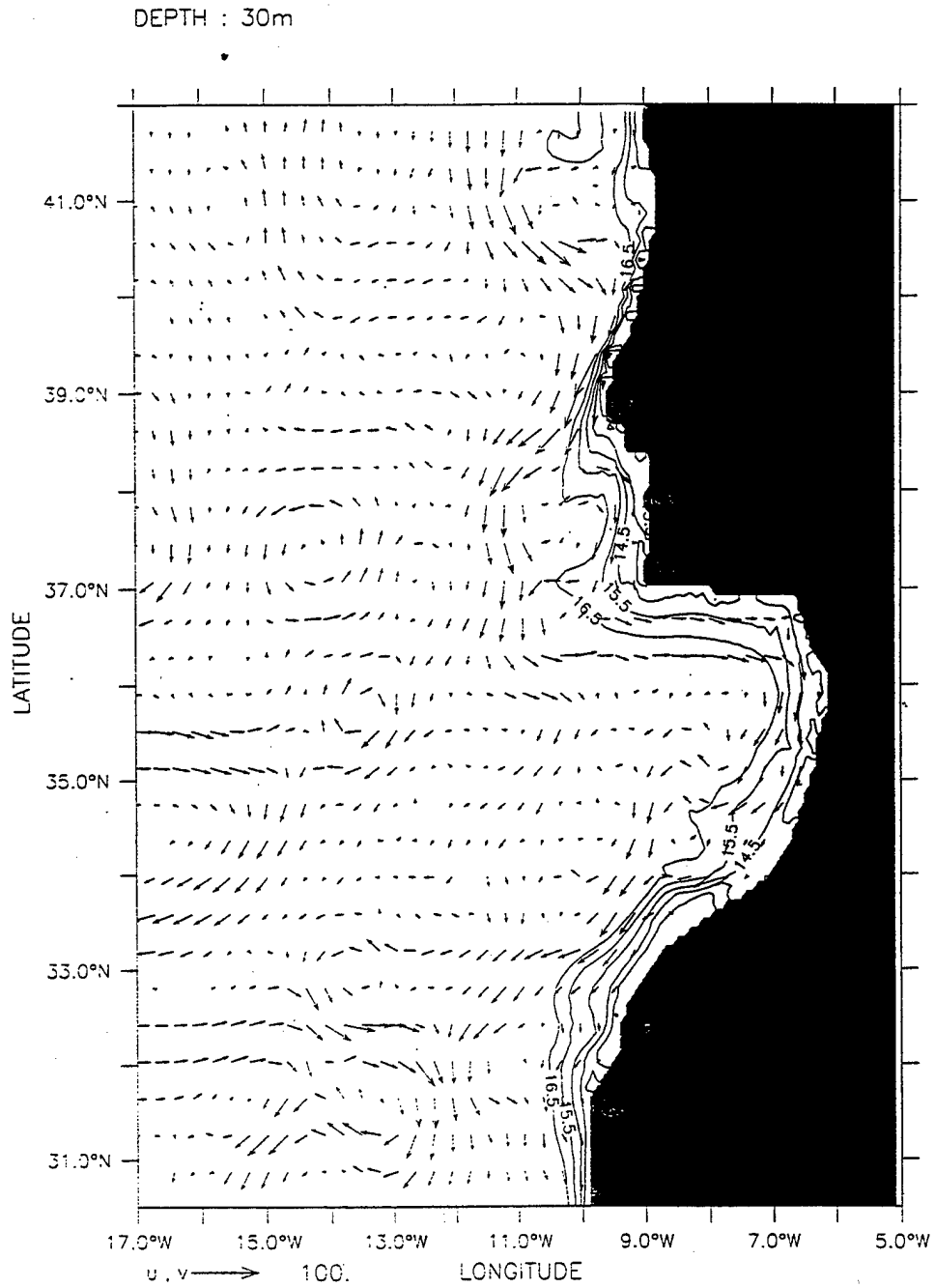


Figure 12. Time-averaged plot of temperature contours and velocity vectors for Experiment 3 at 30 m in the third year for August. The contour interval is  $1^{\circ}\text{C}$ . The maximum current velocity is 100 cm/s.

LATITUDE : 37.5N

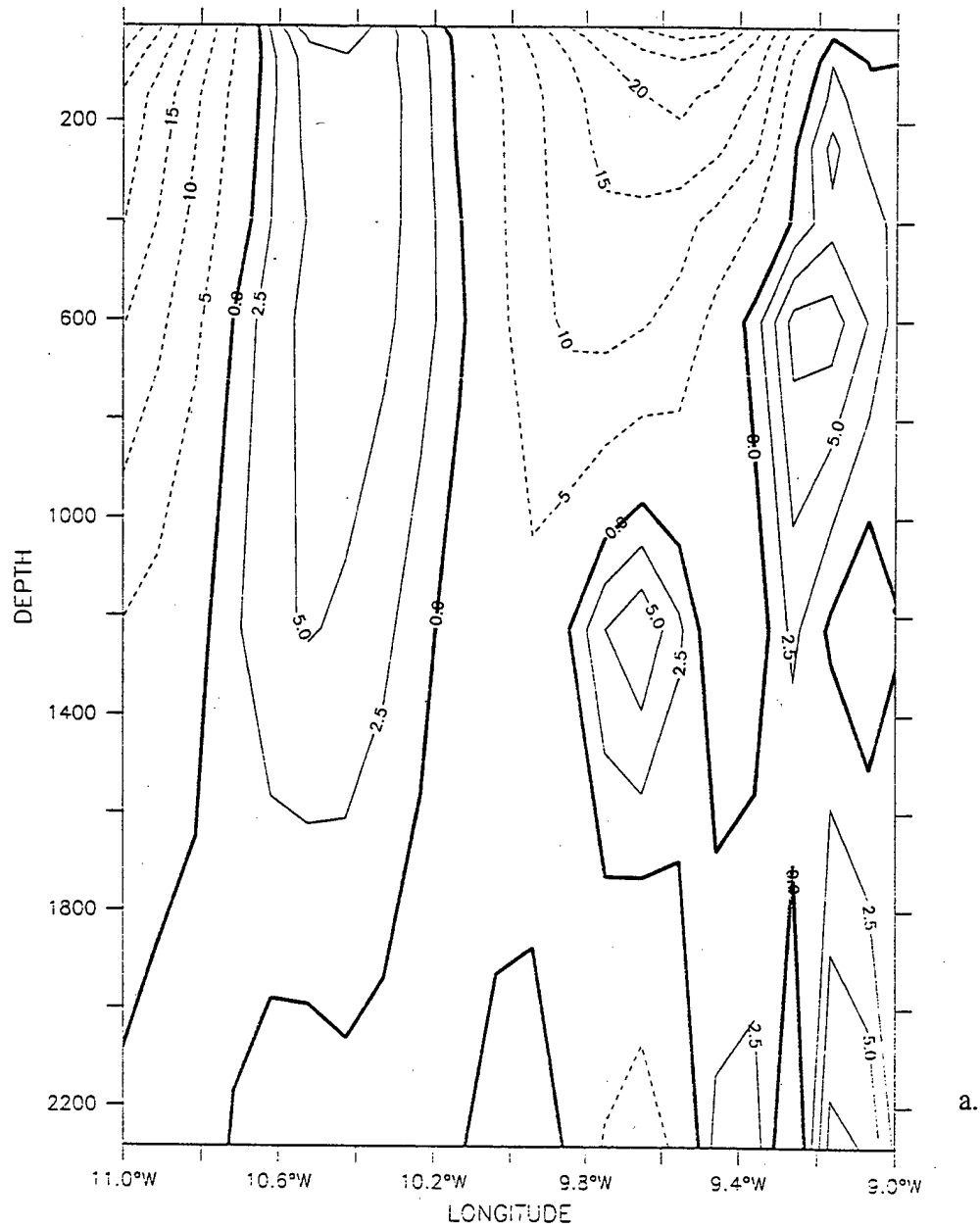
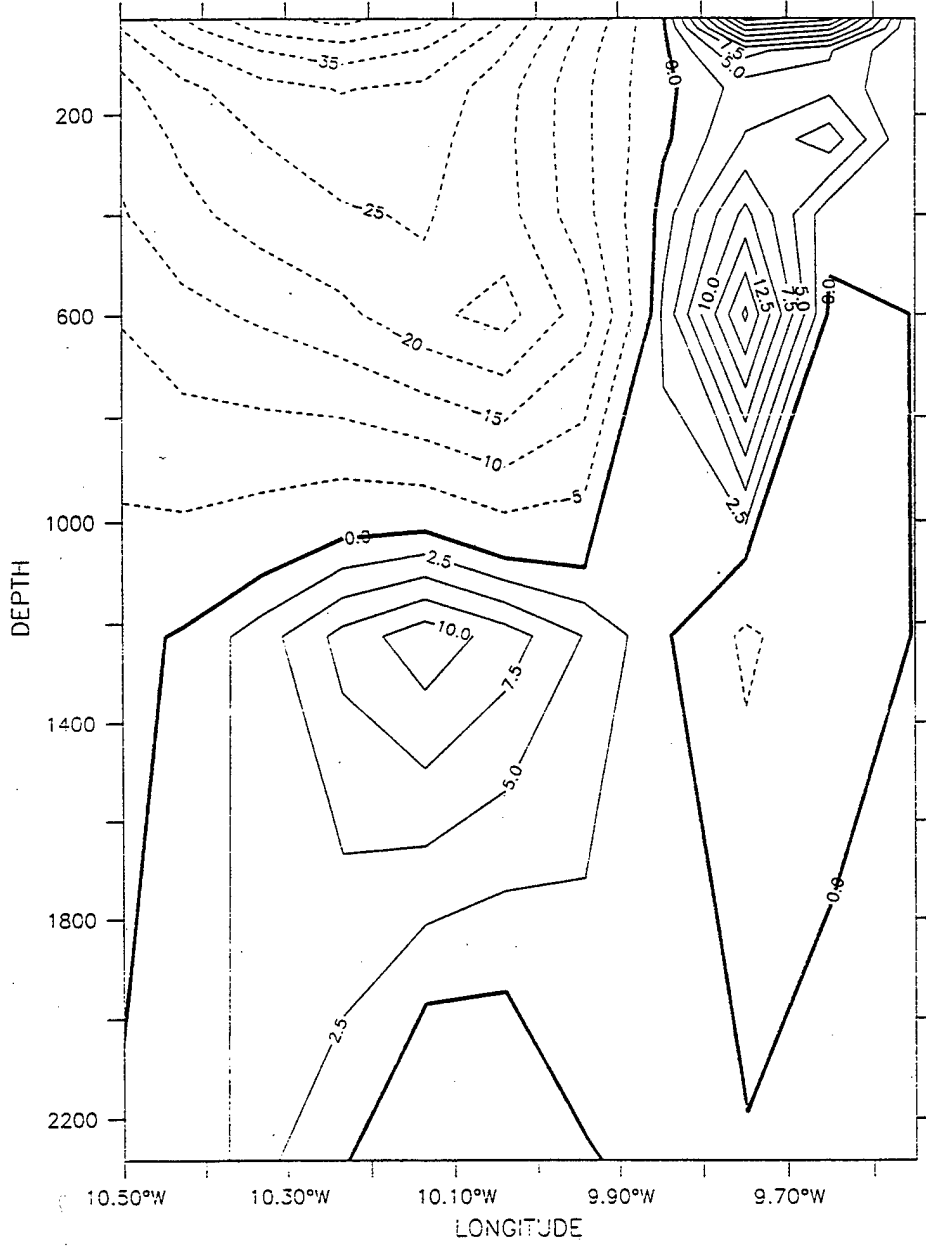


Figure 13. Time-averaged plots (Experiment 3) for cross-shore sections of mean meridional velocity in August at 37.5° N (a) and in January at 39.4° N (b). Solid lines indicate poleward flow, while dashed lines indicate equatorward flow. The contour interval is 2.5 cm/s for poleward flow and 5 cm/s for equatorward flow.

LATITUDE : 39.4N



b.

DEPTH : 30m  
T : 30

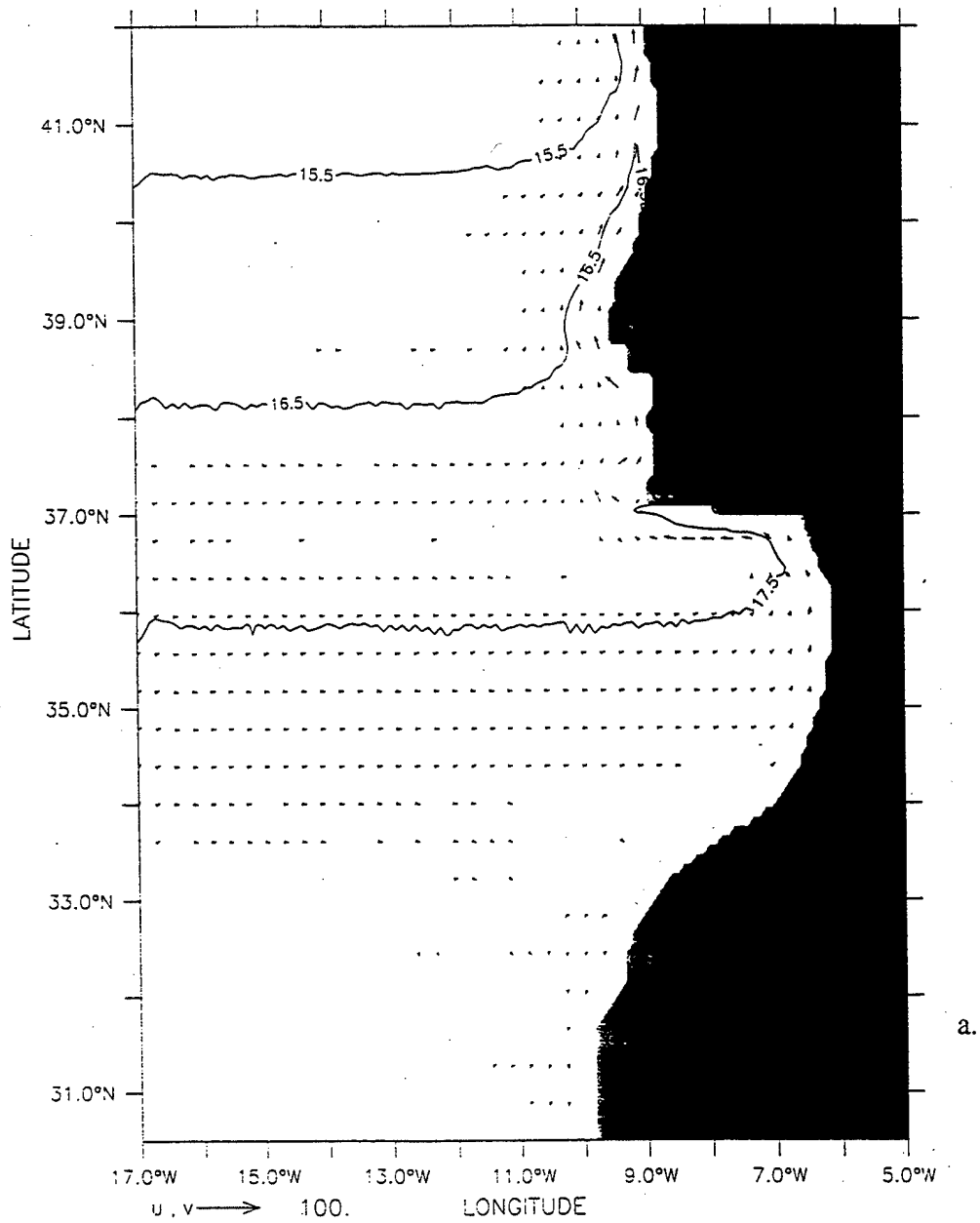
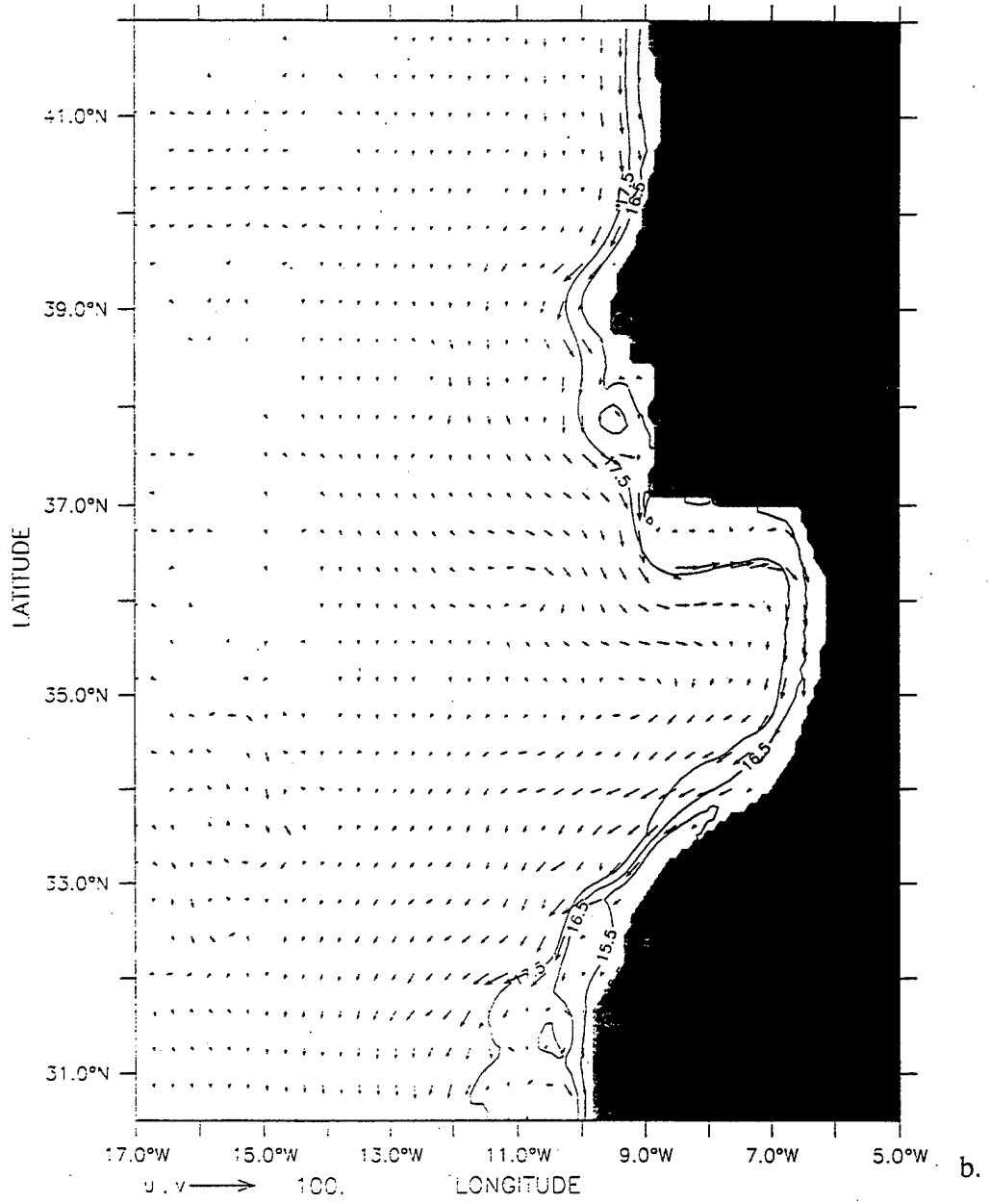


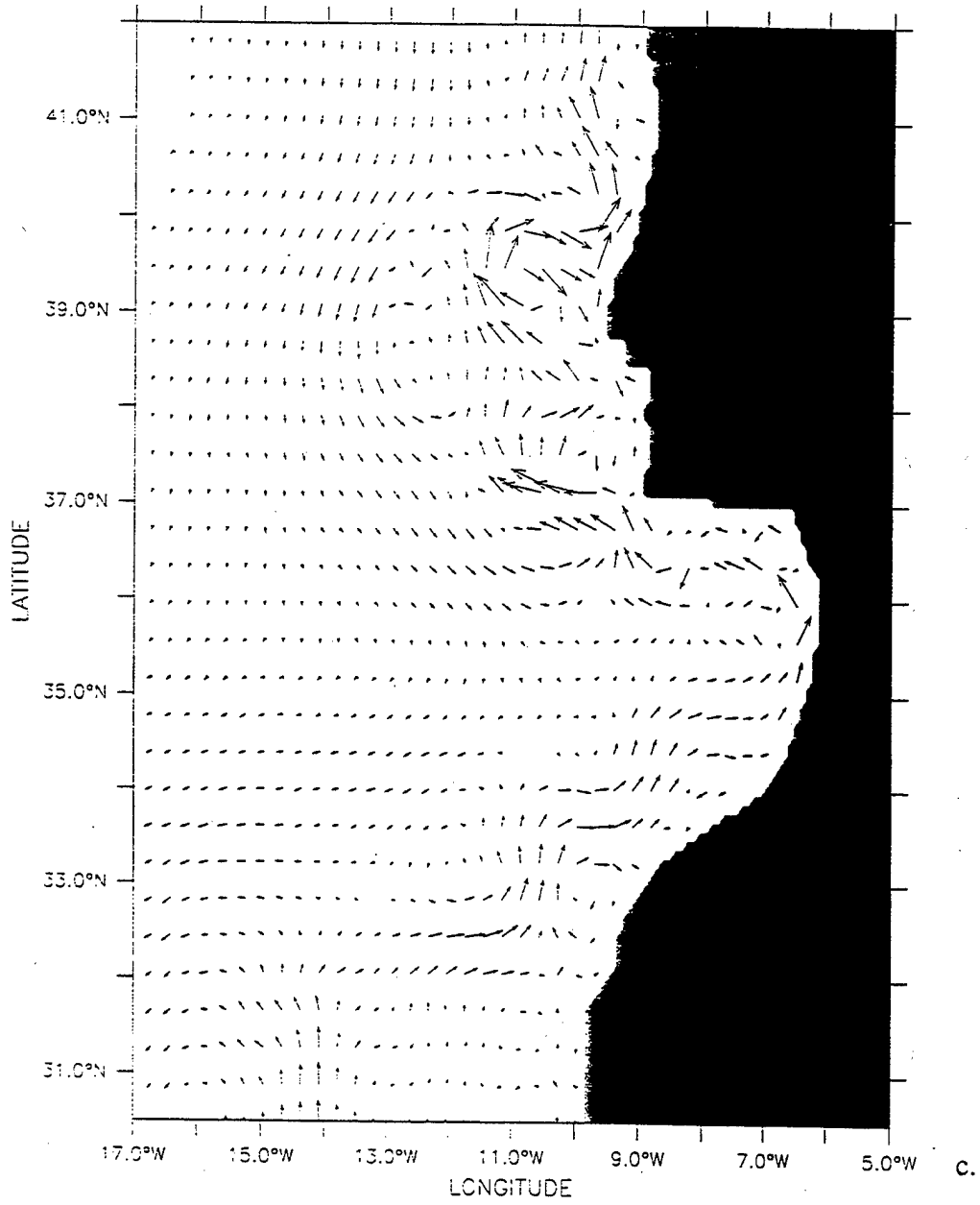
Figure 14. Temperature contours (a,b) and velocity vectors (a-c) for Experiment 4 at 30 depth on day (a) 30, (b) 255, (c) 363. The contour interval is  $1^{\circ}$  C. Maximum velocity is 100 cm/s in (a,b) and 20 cm/s in (c).



DEPTH : 30m  
T : 255



DEPTH : 1226m  
T : 363



LATITUDE : 37.5N  
T : 210

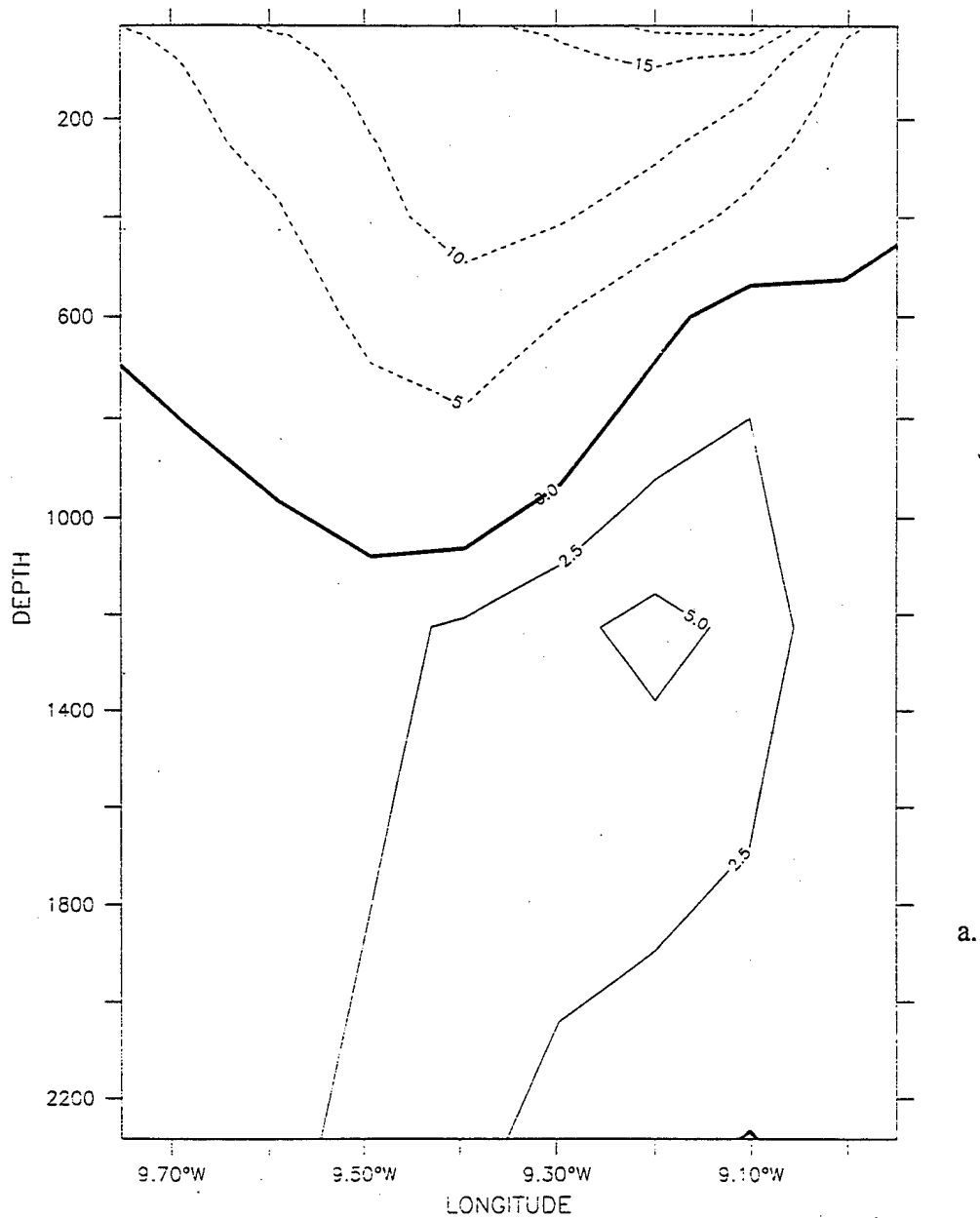
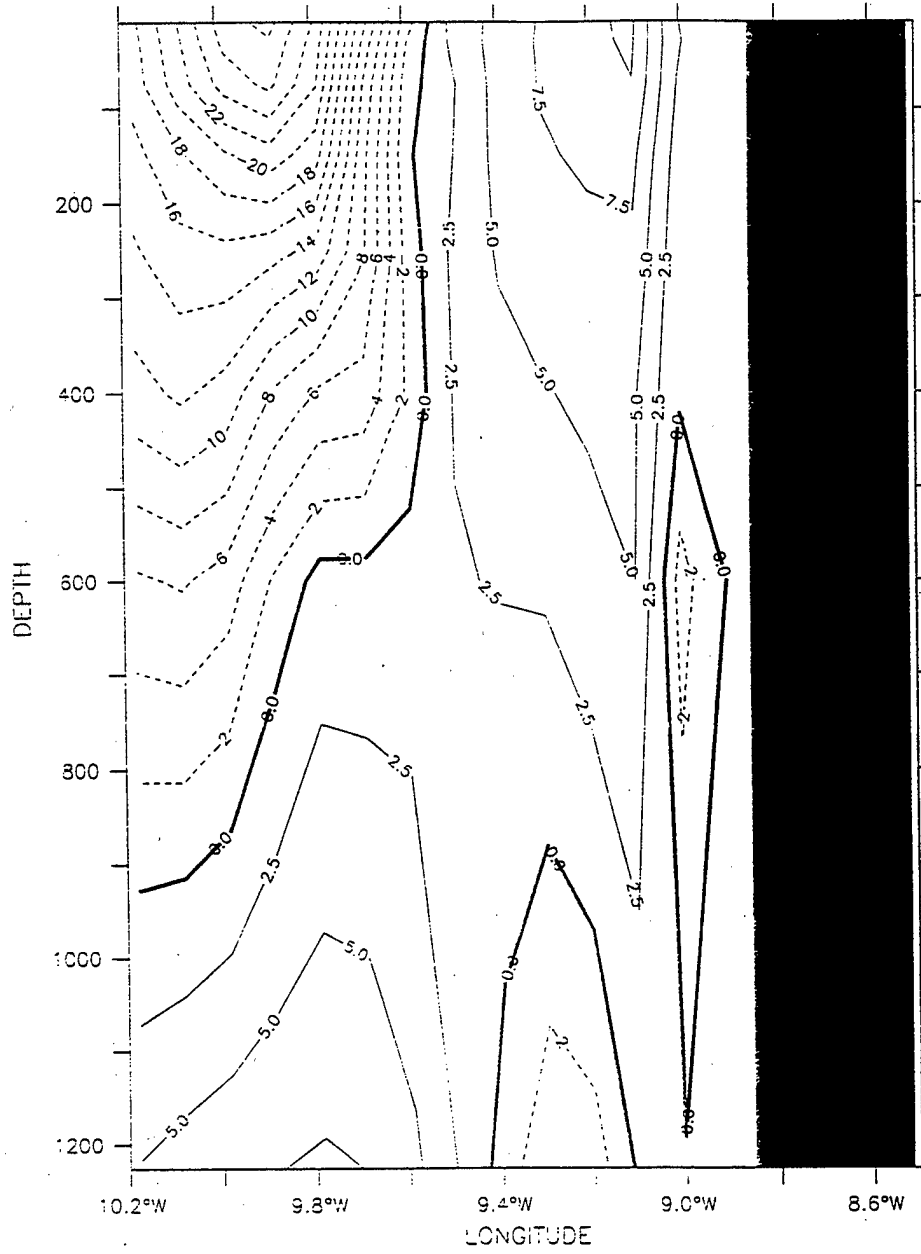


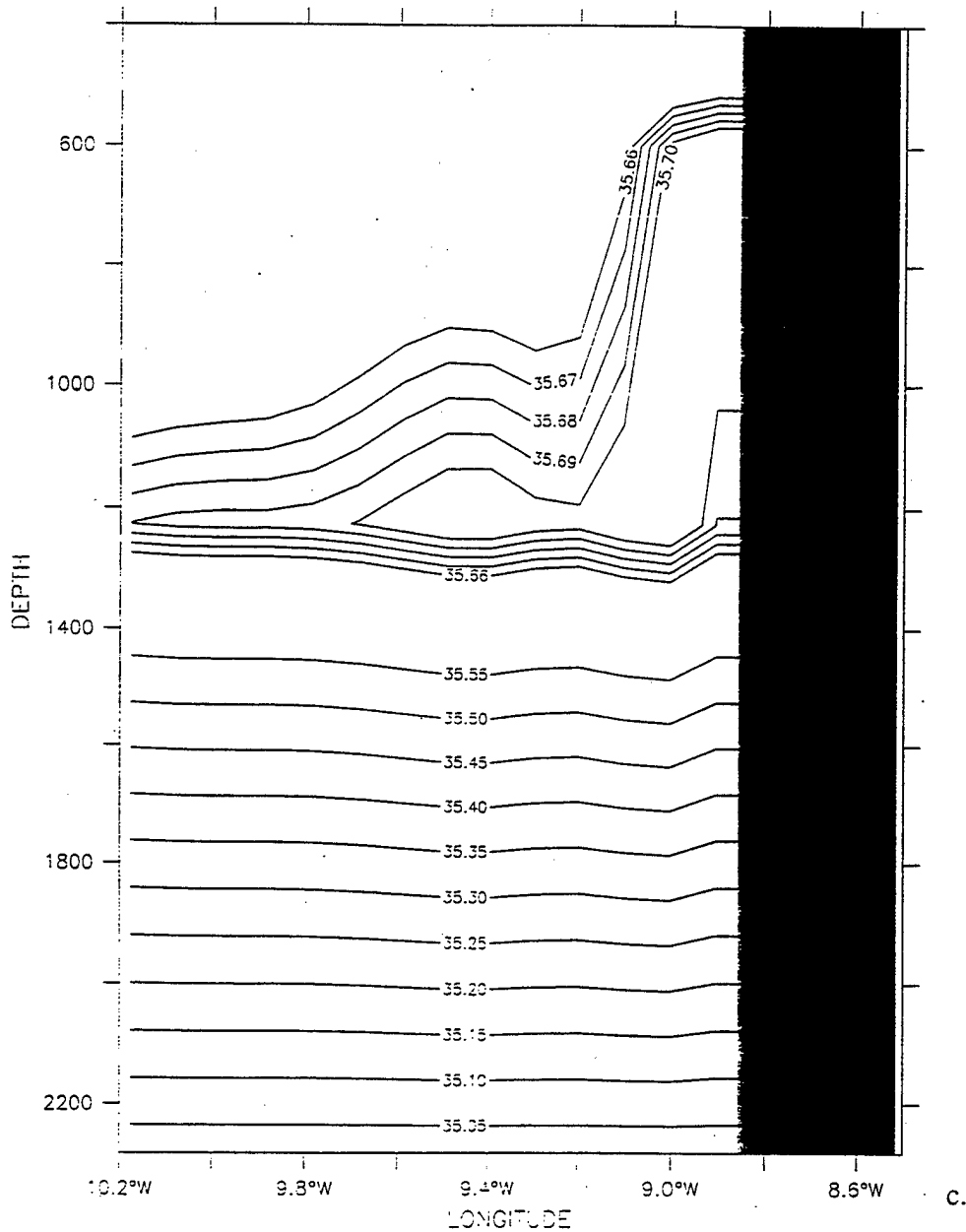
Figure 15. Cross-shore sections of meridional velocity ( $v$ ) (a-b) and salinity ( $S$ ) (c) for Experiment 4 on day 210 at  $37.5^\circ$  N (a) and on day 363 at  $41.5^\circ$  N (b-c). The contour interval for  $v$  is 2.5 cm/s for the poleward flow in (a,b), and 5 cm/s for equatorward flow in (a) and 2 cm/s in (b). The contour interval for  $S$  is 0.01 (0.05) above (below) 1400 m depth.

LATITUDE : 41.5N  
T : 363



b.

LATITUDE : 41.5N  
T (DAY) : 363



DEPTH : 30m

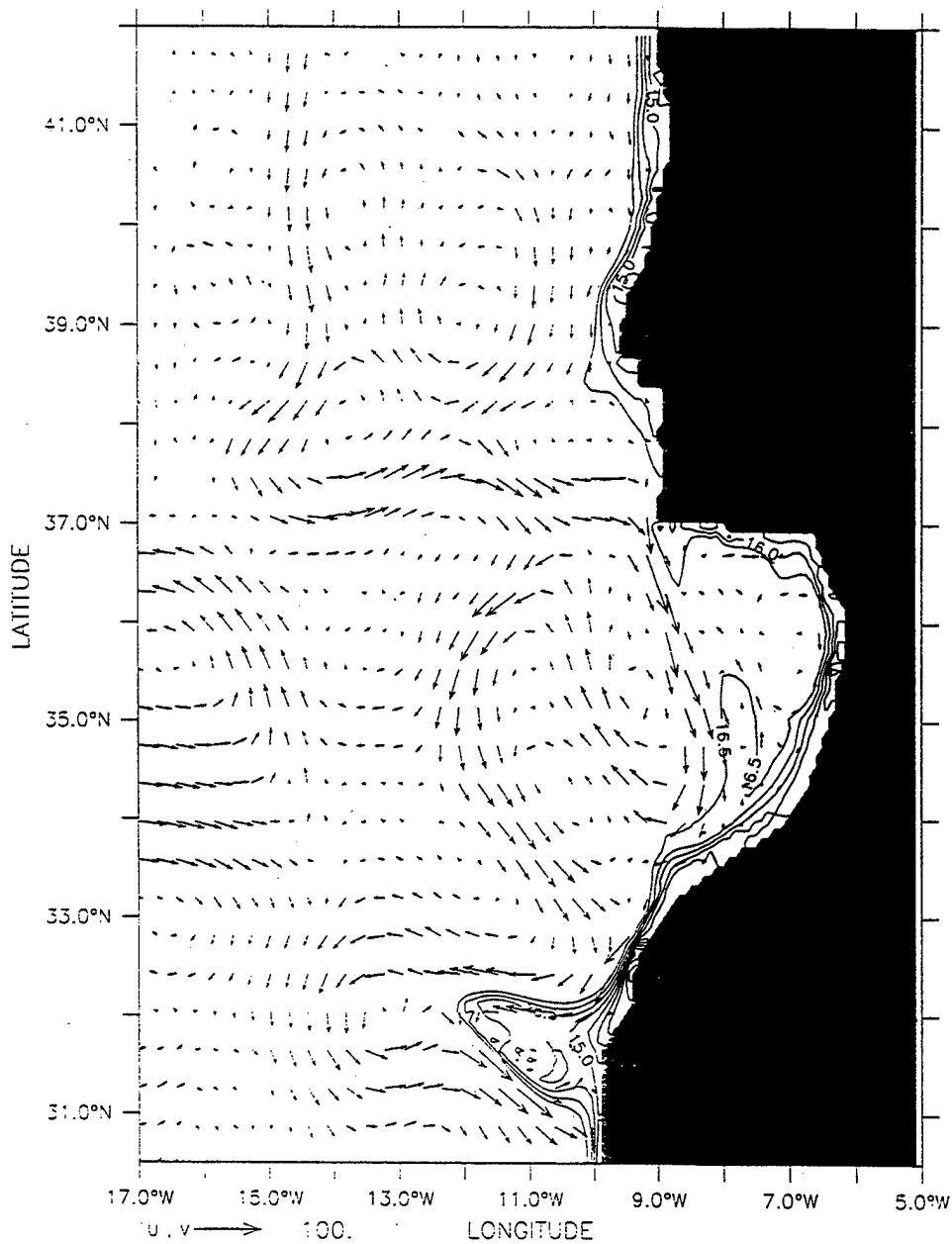


Figure 16. Time-averaged plot of temperature contours and velocity vectors for Experiment 4 at 30 m in the third year for August. The contour interval is 1° C. The maximum current velocity is 100 cm/s.

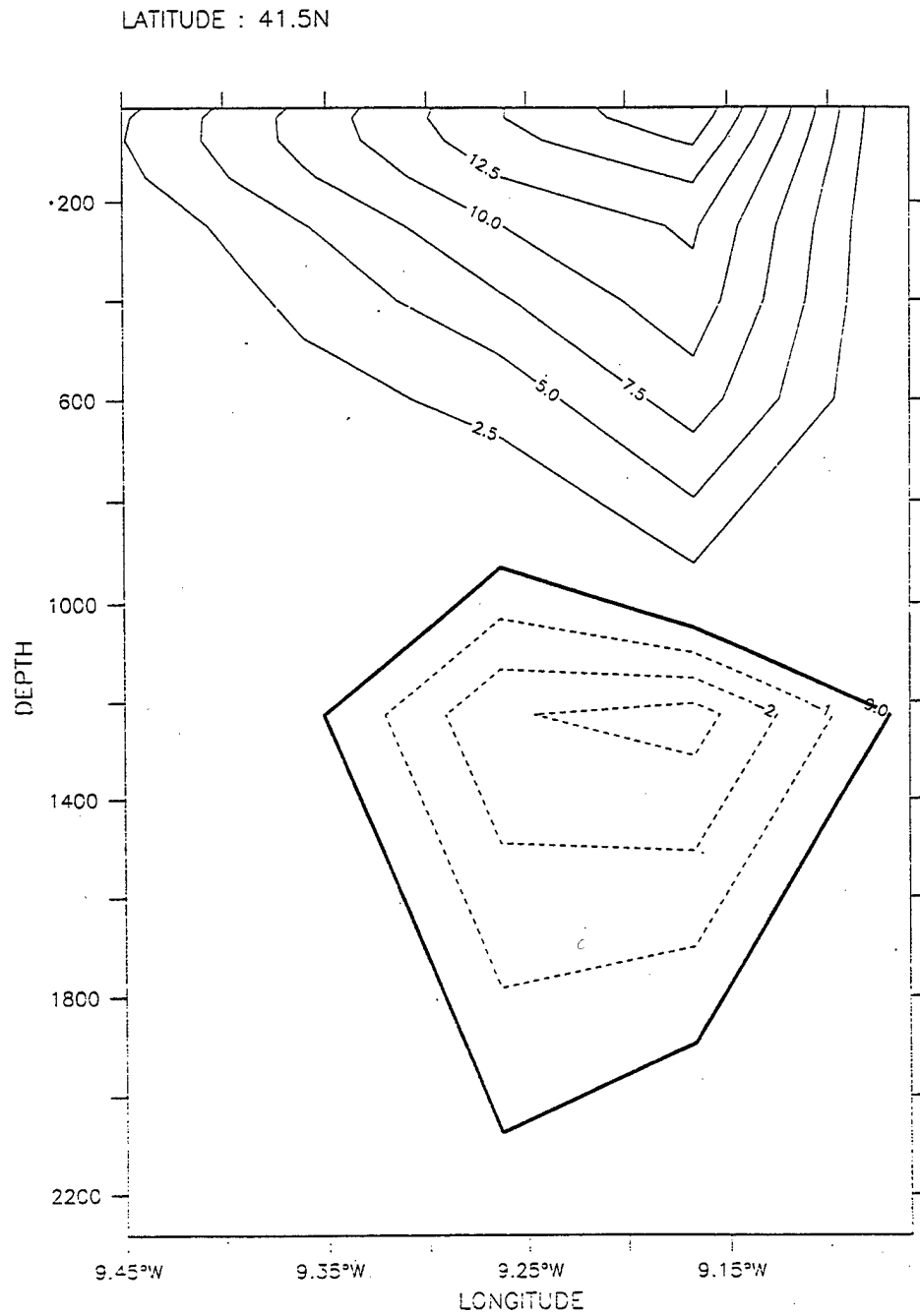


Figure 17. Time-averaged plot for Experiment 4 of cross-shore sections of meridional velocity ( $v$ ) in the third year for December. The contour interval is 2.5 cm/s for poleward flow and 1 cm/s for equatorward flow.

LATITUDE : 38N  
T (DAY) : 999

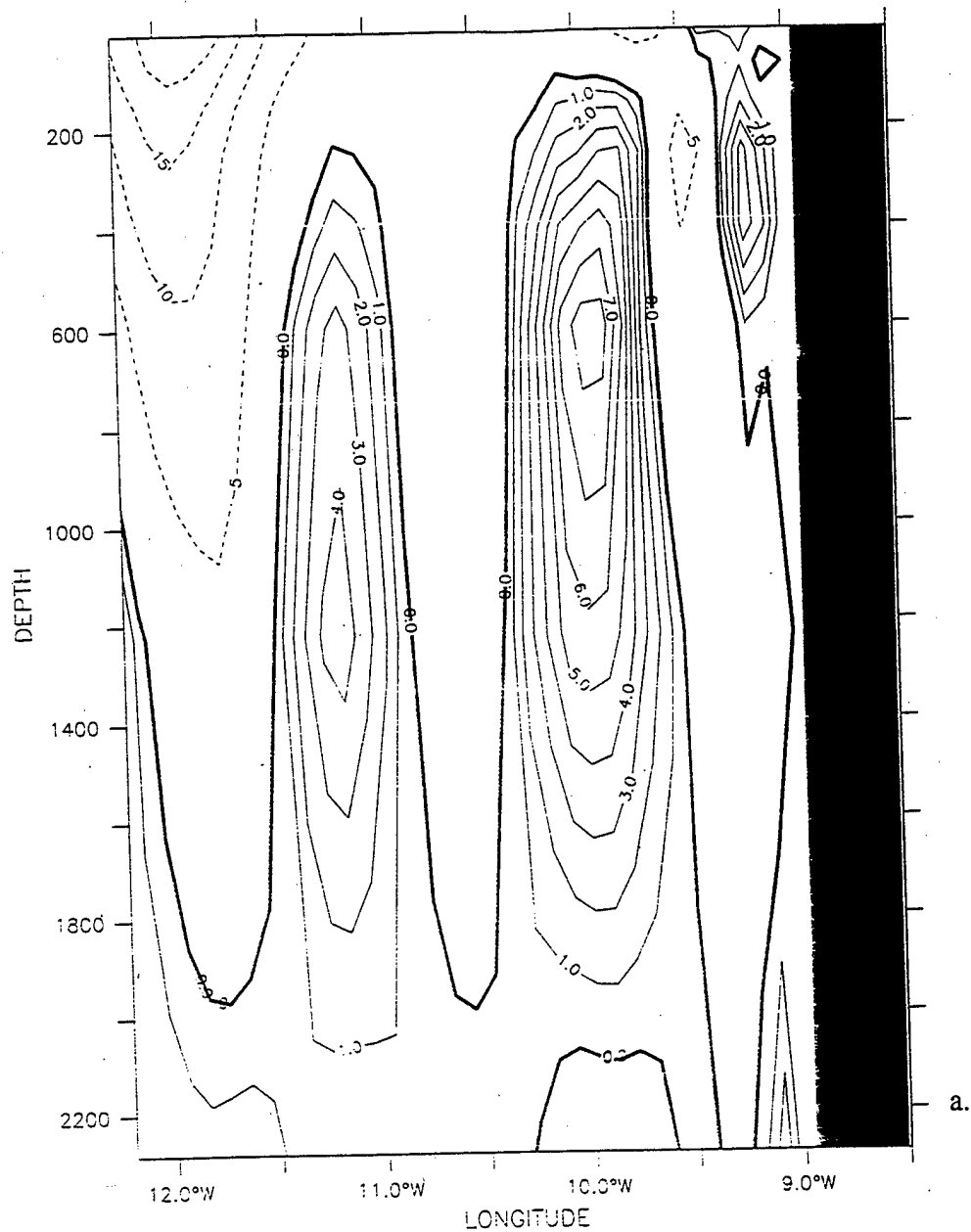
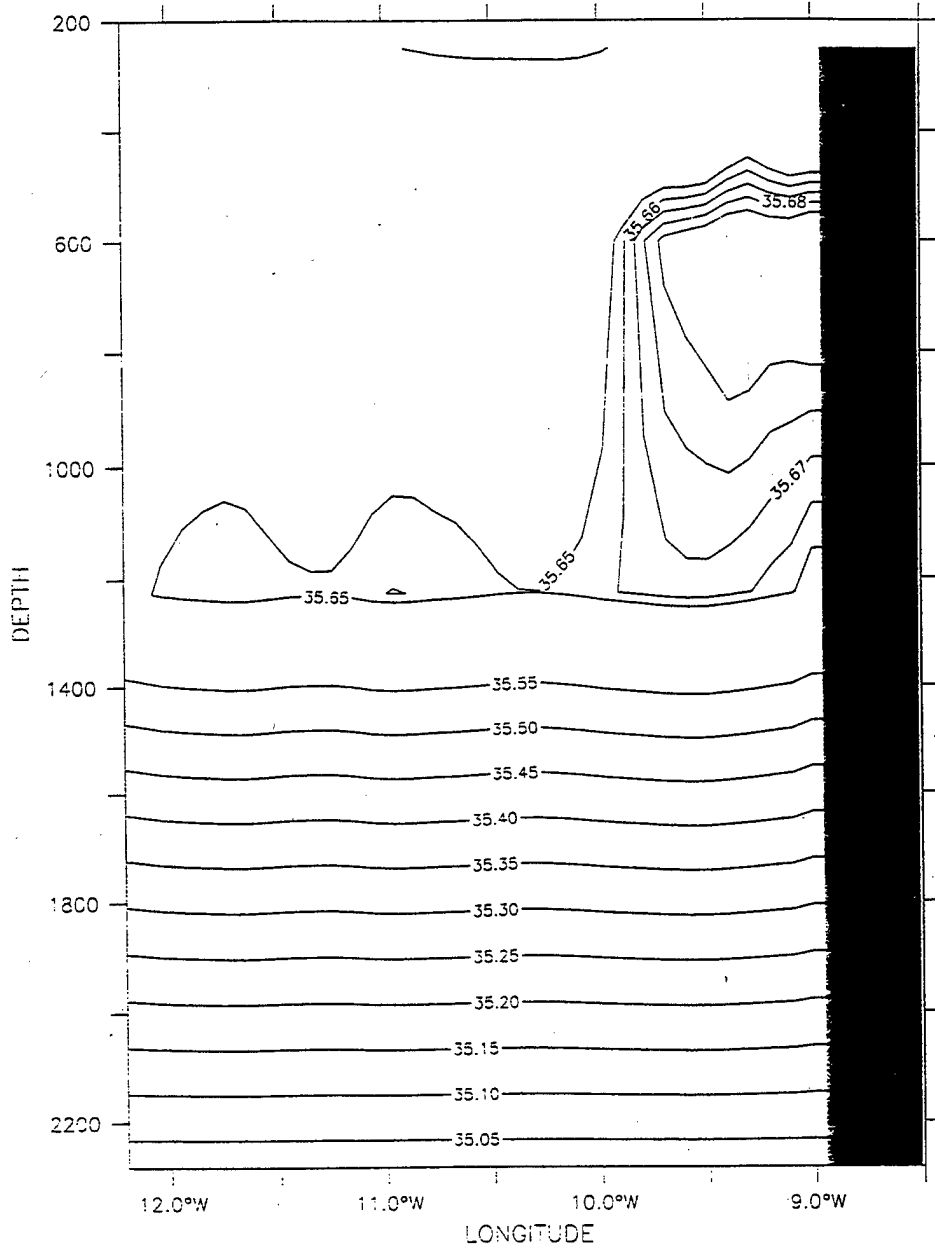


Figure 18. Cross-shore sections for Experiment 4 for day 999 (end of September) at 38° N of meridional velocity ( $v$ ), and salinity ( $S$ ) (b). The contour interval for  $v$  is 1 cm/s for poleward flow and 5 cm/s for equatorward flow. The contour interval for  $S$  is 0.01 (0.05) above (below) 1300 m depth.



LATITUDE : 38N  
T (DAY) : 999



DEPTH : 1226m

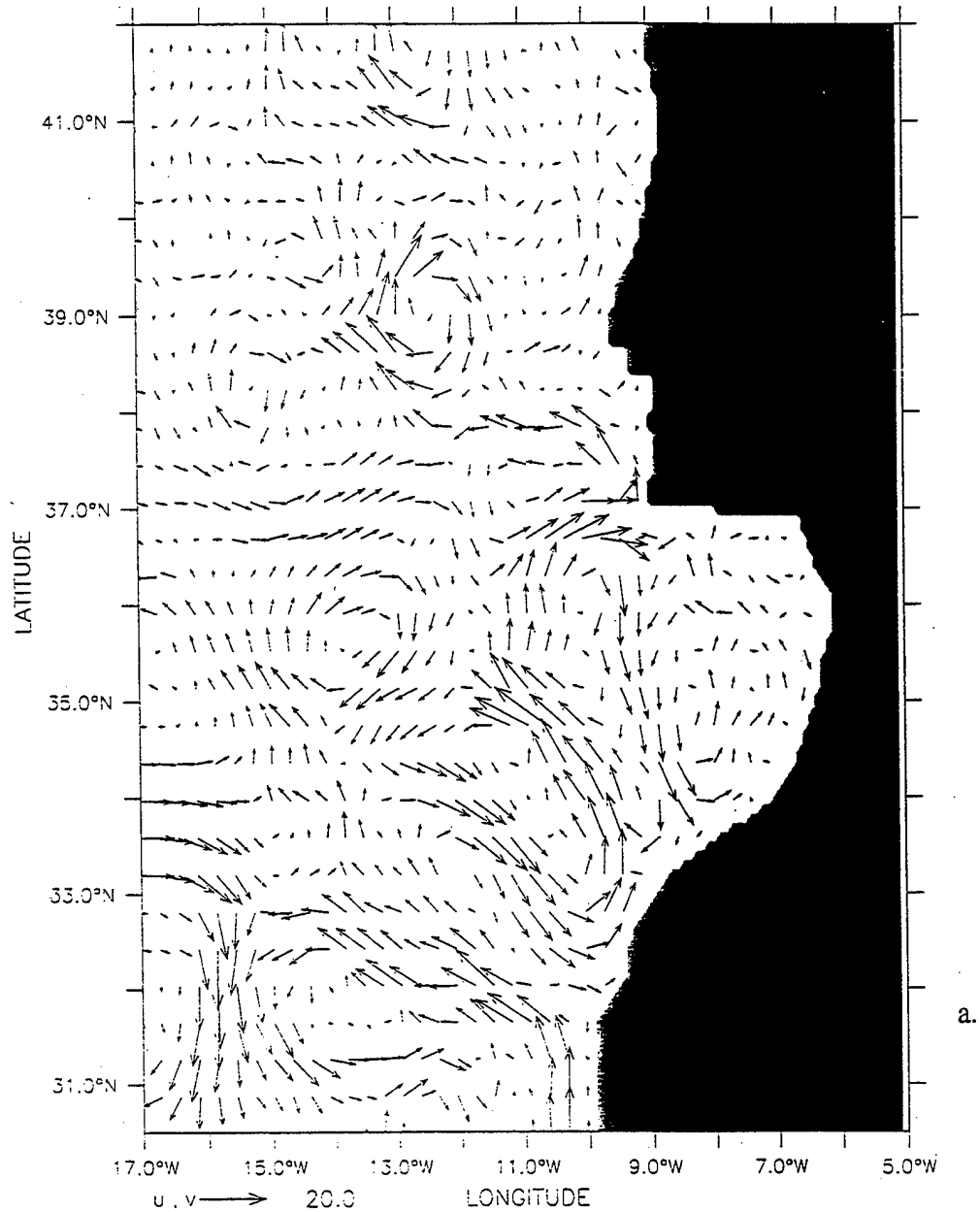
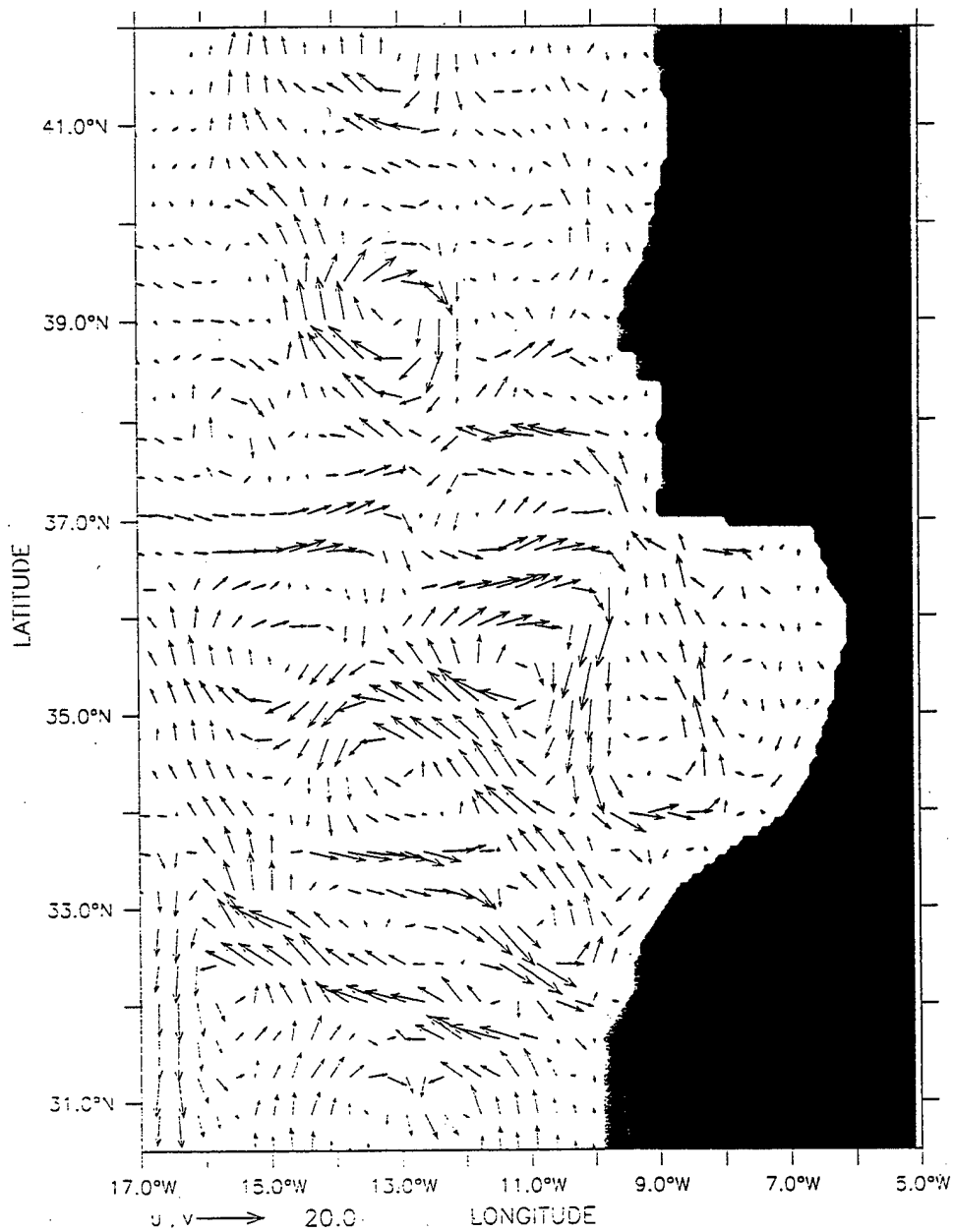


Figure 19. Time-averaged plots of velocity vectors for Experiment 4 at 1226 m depth in the third year of the model for September (a) and of November (b). Maximum current velocity is 20 cm/s.

DEPTH : 1226m

DATA SET: case4c\_mave\_novyr3



b.

LATITUDE : 36N  
T (DAY) : 1059

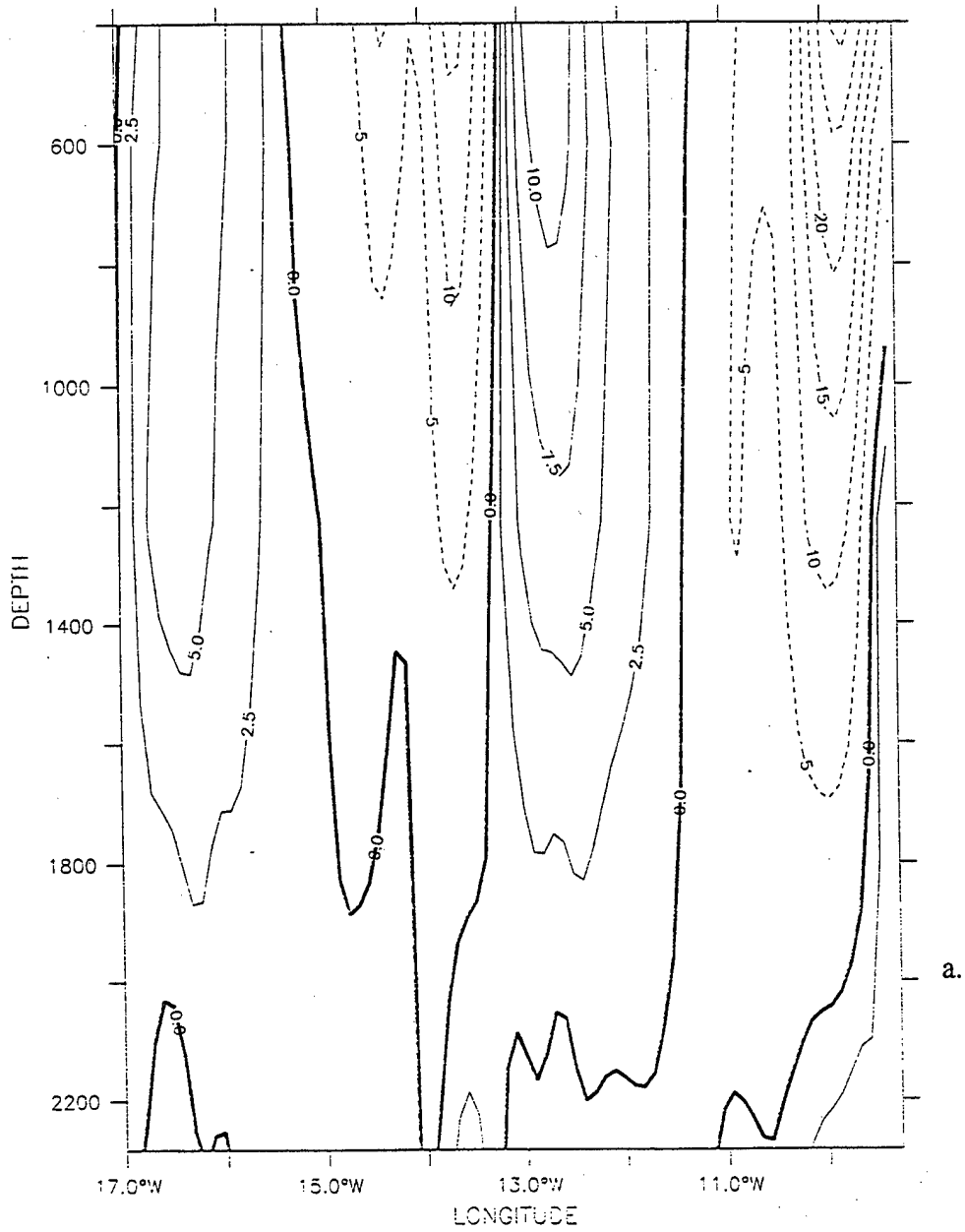
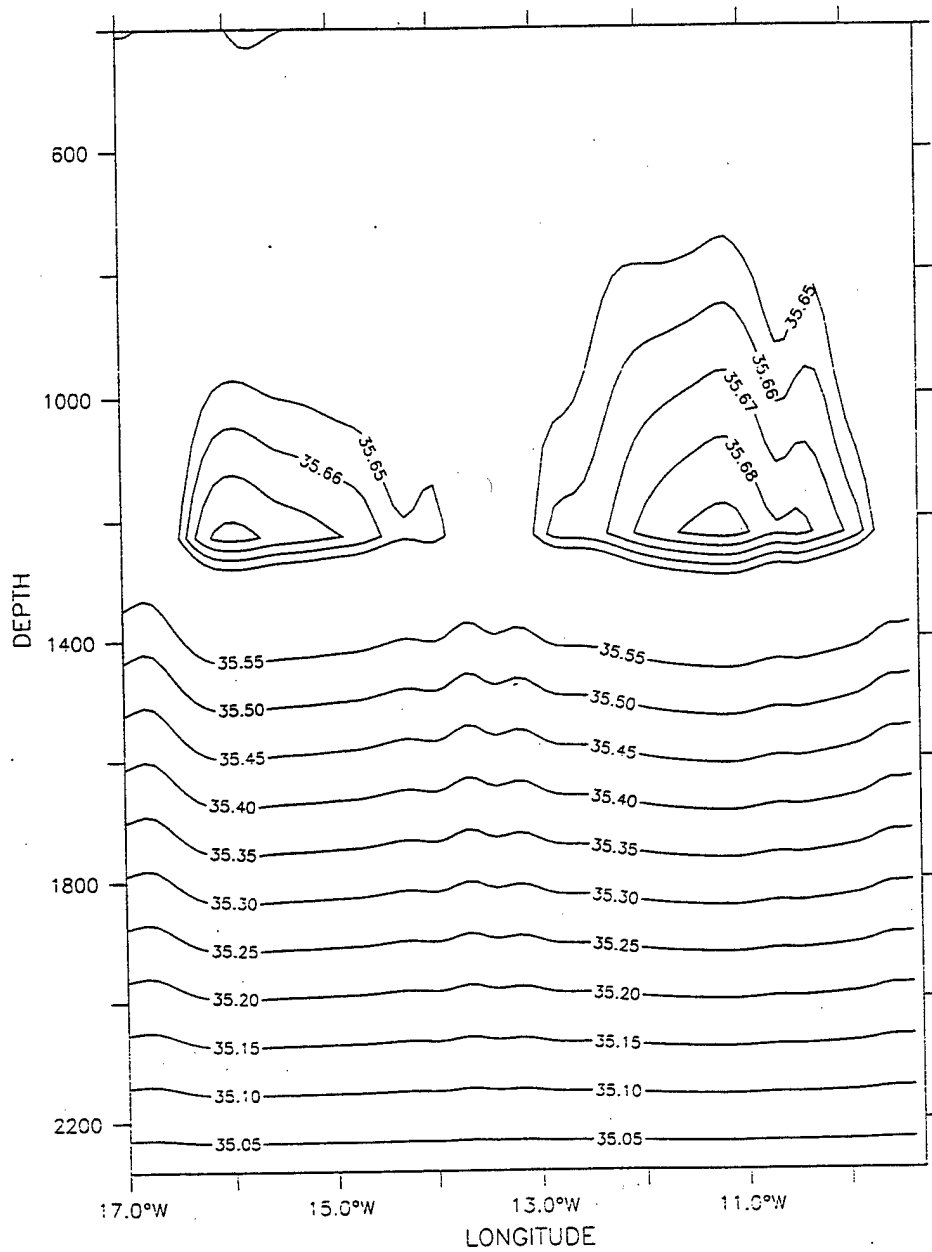


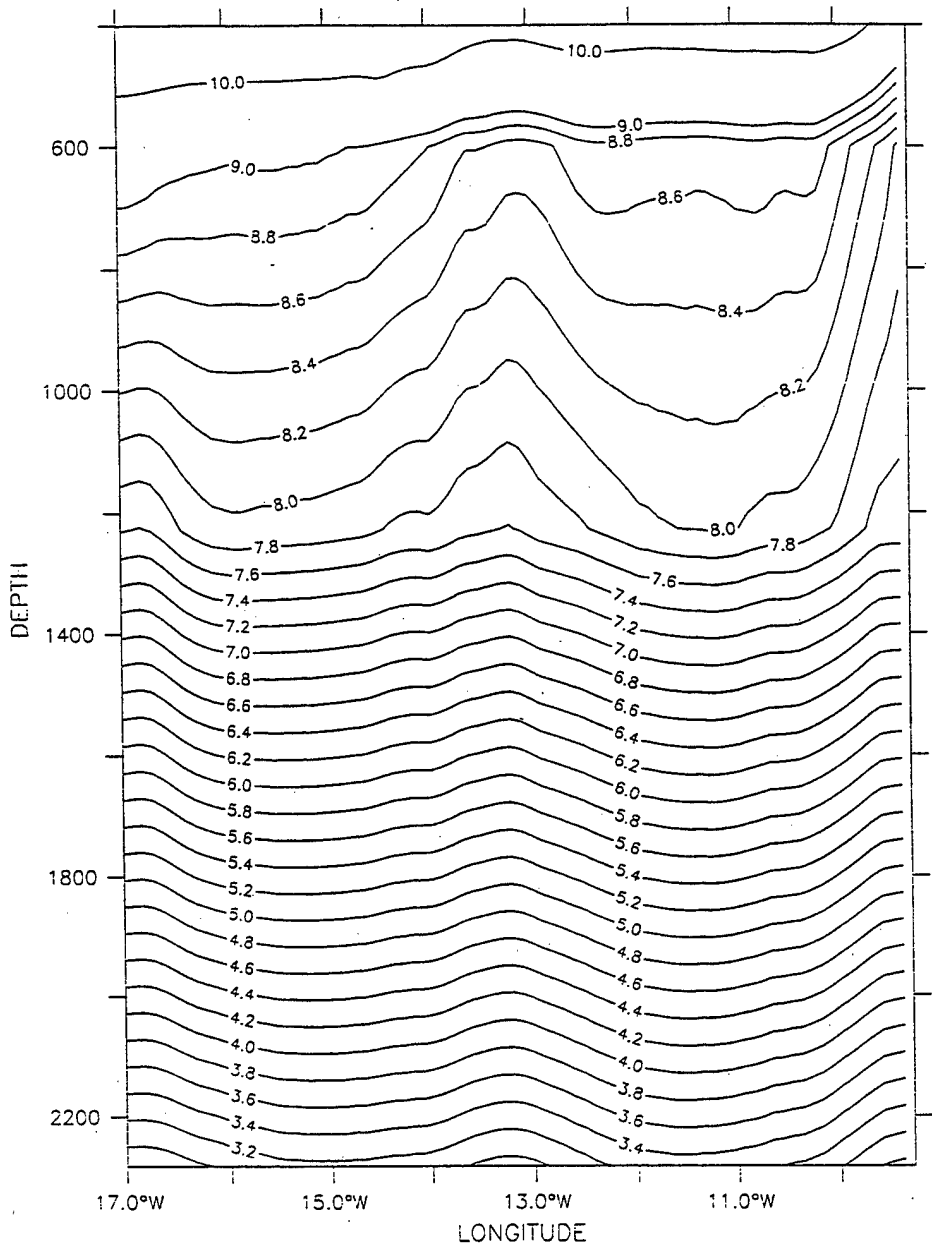
Figure 20. Cross-shore sections for Experiment 4 on day 1059 (end of November) at 36° N of meridional velocity (v) (a), temperature (T) (b), and and salinity (S) (c). The contour interval for v is 2.5 cm/s for poleward flow and 5 cm/s for equatorward flow. The contour interval for T is 0.2 (1.0) above (below) 600 m depth. The contour interval for S is 0.01 (0.05) above (below) 1300 m depth.

LATITUDE : 36N  
T (DAY) : 1059



b.

LATITUDE : 36N  
T (DAY) : 1059



C.



**Table 1. Summary of specific experimental design.**

<b>Cases</b>	<b>Type of coastline</b>	<b>Mediterranean Outflow and Thermohaline Forcing</b>
1	Straight	NO
2	Ideal Irregular	NO
3	Realistic Irregular	NO
4	Realistic Irregular	YES



**Table 2. Values of Constants Used in the Model**

<b>Constant</b>	<b>Value</b>	<b>Definition</b>
$T_0$	278.2°K	Constant Reference Temperature
$S_0$	34.7	Constant Reference Salinity
$\rho_0$	1.0276 gm cm <sup>3</sup>	Density of Sea Water At $T_0$ and $S_0$
$\alpha$	$2.4 \times 10^{-4}$ (°K) <sup>-1</sup>	Thermal Expansion Coefficient
$\beta$	$7.5 \times 10^{-4}$	Saline Expansion Coefficient
$K$	10	Number of Levels In Vertical
$\Delta x$	$9.0 \times 10^5$ cm	Cross-Shore Grid Spacing
$\Delta y$	$1.1 \times 10^6$ cm	Alongshore Grid Spacing
$H$	$4.5 \times 10^5$ cm	Total Ocean Depth
$\Delta t$	800 s	Time Step
$f_0$	$0.86 \times 10^4$ s <sup>-1</sup>	Mean Coriolis Parameter
$g$	980 cm s <sup>2</sup>	Acceleration of Gravity
$A_M$	$2 \times 10^{17}$ cm <sup>4</sup> s <sup>-1</sup>	Biharmonic Momentum Diffusion Coefficient
$A_H$	$2 \times 10^{17}$ cm <sup>4</sup> s <sup>-1</sup>	Biharmonic Heat Diffusion Coefficient
$K_M$	0.5 cm <sup>2</sup> s <sup>-1</sup>	Vertical Eddy Viscosity
$K_H$	0.5 cm <sup>2</sup> s <sup>-1</sup>	Vertical Eddy Conductivity

**Table 3: Salinity profiles**

<b>Layer</b>	<b>(Depth in meters)</b>	<b>Salinity (psu)</b>
1	10	36.07
2	30	36.05
3	75	36.05
4	150	36.05
5	250	36.05
6	400	35.75
7	600	35.75
8	1226	36.25
9	2283	35.25
10	3656	34.70



## LIST OF REFERENCES

- Ambar, I., Mediterranean influence off Portugal, in *Actual problems of oceanography in Portugal*, Junta Nacional de Investigacao Cientifica e Tecnologica, Lisboa, 73-87, 1982.
- Ambar, I., and M.R. Howe. Observations of the Mediterranean outflow – 1. Mixing in the Mediterranean outflow. *Deep-Sea Res.*, 26, 535-554, 1979.
- Arakawa, A. and V. R. Lamb, Computational design of the basic dynamical processes of the UCLA general circulation model, *Methods Comput. Phys.*, 17, 173-265, 1977.
- Bakun, A. and Nelson, C.S. The seasonal cycle of wind stress curl in subtropical eastern boundary current regions. *J. Phys. Oceanogr.*, 21, 1815-1834, 1991.
- Barton, E. D., A filament program in the Iberian upwelling region, *Coastal Transition Zone Newsletter*, 1, 2-5, 1986.
- Batteen, M. L., Wind-forced modeling studies of currents, meanders, and eddies in the California Current System, *J. Geophys. Res.*, 102, 985-1009, 1997.
- Batteen, M. L. and Y. -J. Han, On the computational noise of finite difference schemes used in ocean models, *Tellus*, 33, 387-396, 1981.
- Batteen, M. L., C. N. Lopes da Costa, and C. S. Nelson, A numerical study of wind stress curl effects on eddies and filaments off the Northwest coast of the Iberian Peninsula, *J. Mar. Systems*, 3, 249-266, 1992.
- Batteen, M. L., N. J. Cipriano, and J. T. Monroe, A large-scale modeling study of the California Current System, *Deep-Sea Res.*, submitted, 1998.

Batteen, M. L., and P. W. Vance, Modeling studies of the effects of wind forcing and thermohaline gradients in the California Current System, *Deep-Sea Res. II*, 45, 1507-1556, 1998.

Batteen, M. L., R. L. Haney, T. A. Tielking, and P. G. Renaud, A numerical study of wind forcing of eddies and jets in the California Current System, *J. Mar. Res.*, 47, 493-523, 1989.

Camerlengo, A. L. and J. J. O'Brien, Open boundary conditions in rotating fluids, *J. Comput. Phys.*, 89, 12-35, 1980.

Carton, J. A., Coastal circulation caused by an isolated storm, *J. Phys Oceanogr.*, 14, 114-124, 1984.

Carton, J. A. and S. G. H. Philander, Coastal upwelling viewed as a stochastic phenomena, *J. Phys Oceanogr.*, 14, 1499-1509, 1984.

Defense Mapping Agency Hydrographic/Topographic Center (DMAH/TC), *Sailing Directions (Planning Guide) for the North Atlantic*, DMA Pub. No. 140, Washington D. C., 390 pp., 1988.

Fiuza, A. F. de G., The Portuguese coastal upwelling system, in *Actual problems of oceanography in Portugal*, Junta Nacional de Investigacao Cientifica e Tecnologica, Lisboa, 45-71, 1982.

Fiuza, A. F. de G., M. E. de Macedo, M. R. Guerreiro, Climatological space and time variation of the Portuguese coastal upwelling, *Oceanologica Acta*, Vol. 5, No. 1, 31-40, 1982.

Fiuza, A. F. de G., Upwelling patterns off Portugal, in E. Suess and J. Thiede (Editors), Coastal Upwelling. Its Sediment Record. Plenum Press, New York, pp. 85-97, 1983.

Fiuza, A. F. de G., Hidrologia e dinamica das Aguas costeiras de Portugal. Dissertacao apresentada a Universidade de Lisboa para obtencao do grau de Doutor em Fisica, especializacao em Ciencias Geofisicas. Univ Lisboa, 294pp., 1984.

Fiuza, A. F. de G. and F. M. Sousa, Preliminary results of a CTD survey in the Coastal Transition Zone off Portugal during 1-9 September 1988, *Coastal Transition Zone Newsletter*, 4, 2-9, 1989.

Folkard, A. M., P. A. Davis, A. F. de G. Fiuza, and I. Ambar, Remotely sensed sea surface thermal patterns in the Gulf of Cadiz and the Strait of Gibraltar: Variability, correlations, and relationships with the surface wind field, *J. Geophys. Res.*, 102, 5669-5683, 1997.

Frouin, R., A. F. G. Fiuza, I. Ambar, and T. J. Boyd, Observations of a poleward surface current off the coasts of Portugal and Spain during Winter, *J. Geophys. Res.*, 95, 679-691, 1990.

Hagen, E., C. Zulicke, and R. Feistel, Near-surface structures in the Cape Ghir filament off Morocco, *Oceanol. Acta*, 19, 6, 577-598, 1996.

Haidvogel, D. B., A. Beckmann, and K. S. Hedstrom, Dynamical simulation of filament formation and evolution in the coastal transition zone, *J. Geophys. Res.*, 96, 15,017-15,040, 1991.

Haynes, R. and E. D. Barton, A poleward flow along the Atlantic coast of the Iberian Peninsula, *J. Geophys. Res.*, 95, 11425-11441, 1990.

Hickey, B.M., The California Current System – Hyptheses and facts. *Prog. Oceanogr.* 8, 191-279, 1979.

Hickey, B.M., Western North America, Tip of Baja California to Vancouver Island. In: Robinson, A. R. and K. H. Brink, *The Sea*, Wiley, New York, 345-393, 1998.

Holland, W. R., The role of mesoscale eddies in the general circulation of the ocean- Numerical experiments using a wind-driven quasi-geostrophic model, *J. Phys. Oceanogr.*, 8, 363-392, 1978.

Holland, W. R. and M. L. Batteen, The parameterization of subgrid scale heat diffusion in eddy-resolved ocean circulation models, *J. Phys. Oceanogr.*, 16, 200-206, 1986.

Ikeda, M., W. J. Emery, and L. A. Mysak, Seasonal variability in meanders of the California Current system off Vancouver Island, *J. Geophys. Res.*, 89, 3487-3505, 1984a.

Ikeda, M., L. A. Mysak, and W. J. Emery, Observations and modeling of satellite-sensed meanders and eddies off Vancouver Island, *J. Phys. Oceanogr.*, 14, 3-21, 1984b.

Kase, R.H., A. Beckmann, and H.H. Hinrichsen, Observational evidence of salt lens formation in the Iberian Peninsula, *J Geophys. Res.*, 94, 4905-4912, 1989.

Levitus, S., and T. P. Boyer, World ocean atlas 1994, Vol. 4: Temperature, *NOAA Atlas NESDI 4*, 117 pp., U. S. Dept. of Commerce, Washington, D.C., 1994.

Levitus, S., R. Burgett, and T.P. Boyer, World ocean atlas, 1994, Vol. 3: Salinity, *NOAA Atlas NESDI 3*, 99 pp., U.S. Dept. of Commerce, Washington, D.C., 1994.

McClain, C. R., S. Chao, L. P. Atkinson, J. O. Blanton, and F. Castillejo, Wind-driven upwelling in the vicinity of Cape Finisterre, Spain, *J. Geophys. Res.*, 91, 8470-8486, 1986.

McCreary, J. P., Y. Fukamachi, and P. K. Kundu, A numerical investigation of jets and eddies near an eastern ocean boundary, *J. Geophys. Res.*, 92, 2515-2534, 1991.

McCreary, J. P., P. K. Kundu, and S. Y. Chao, On the dynamics of the California Current system, *J. Mar. Res.*, 45, 1-32, 1987.

Meincke, J., G. Siedler, and W. Zenk., Some current observations near the continental slope off Portugal. *"Meteor" Forsch.-Ergebn.*, A, 16, 15-22, 1975.

Nelson, C. S., Wind stress and wind stress curl over the California Current, NOAA Tech Rep. NMFS SSFR-714, U. S. Dept. Commerce, 87 pp., 1977.

Pares-Sierra, A., W. B. White, and C. -K. Tai, Wind-driven coastal generation of annual mesoscale eddy activity in the California Current system: A numerical model, *J. Phys Oceanogr.*, 23, 1110-1121, 1993.

Parrish, R.H., C. S. Nelson, and A. Bakun, Transport mechanisms and reproductive success of fishes in the California Current, *Biol. Oceanogr.*, 1, 175-203, 1981.

Pedlosky, J., Longshore currents, upwelling, and bottom topography, *J. Phys Oceanogr.*, 4, 214-226, 1974.

Philander, S. G. H. and J. H. Yoon, Eastern boundary currents and upwelling, *J. Phys Oceanogr.*, 12, 862-879, 1982.



Richardson, P. L., and A. Tychensky, Meddy trajectories in the Canary Basin measured during the SEMAPHORE experiment, 1993-1995, *J. Geophys. Res.*, 103, 25,029-25,045, 1998.

Richardson, P. L., D. Walsh, L. Armi, M. Schroder, and J.F. Price, *J. Phys Oceanogr.*, 19, 371-383, 1989.

Tomczak, M. and J. S. Godfrey, *Regional Oceanography: An Introduction*, Pergamon Press, New York, 422 pp., 1994.

Trenberth, K. E., W. G. Large, J. G. Olsen, The mean annual cycle in global ocean wind stress, *J. Phys Oceanogr.*, 20, 1742-1760, 1990.

Van Camp, L., L. Nykjaer, E. Mittelstaedt, and P. Schlittenhardt, Upwelling and boundary circulation off Northwest Africa as depicted by infrared and visible satellite observations, *Prog. Oceanog.*, 26, 357-402, 1991.

Weatherly, G. L., A study of the bottom boundary layer of the Florida Current, *J. Phys Oceanogr.*, 2, 54-72, 1972.

Wooster, W. S. and J. L. Reid, Jr., Eastern Boundary Currents in *The Sea, Vol. 2*, M. N. Hill, Ed., Wiley International, New York, 253-280, 1963.

Wooster, W. S., A. Bakun, and D. R. McLain, The seasonal upwelling cycle along the eastern boundary of the North Atlantic, *J. Mar. Res.*, 34, 131-140, 1976.

## INITIAL DISTRIBUTION LIST

	No. Copies
1. Defense Technical Information Center..... 8725 John J. Kingman Rd, STE 0944 Ft. Belvoir, VA 22060-6218	2
2. Dudley Knox Library..... Naval Postgraduate School 411 Dyer Rd Monterey, CA 93943-5101	2
3. Chairman (Code OC/Bf) ..... Department of Oceanography Naval Postgraduate School Monterey, CA 93943-5122	1
4. Chairman (Code MR/Wx)..... Department of Meteorology Naval Postgraduate School Monterey, CA 93943-5114	1
5. Dr. Mary L. Batteen (Code OC/Bv) ..... Department of Oceanography Naval Postgraduate School Monterey, CA 93943-5122	4
6. Dr. Curtis A. Collins (Code OC/Co)..... Department of Oceanography Naval Postgraduate School Monterey, CA 93943-5122	1
7. Dr. Tom Kinder ..... Physical Oceanography Division Office of Naval Research 800 N. Quincy Street Arlington, VA 22217	1
8. LT Johnny R. Martinez..... 5977 South Gallup St. Apt. 101 Littleton, Co 80120	3